STRUCTURAL AND FUNCTIONAL STUDIES ON HUMAN MITOCHONDRIAL IRON-SULFUR CLUSTER BIOSYNTHESIS

A Dissertation

by

CHI-LIN TSAI

Submitted to the Office of Graduate Studies of
Texas A&M University
in partial fulfillment of the requirements for the degree of

DOCTOR OF PHILOSOPHY

May 2011

Major Subject: Chemistry

Structural and Functional Studies on Human

Mitochondrial Iron-Sulfur Cluster Assembly Biosynthesis

STRUCTURAL AND FUNCTIONAL STUDIES ON HUMAN MITOCHONDRIAL IRON-SULFUR CLUSTER BIOSYNTHESIS

A Dissertation

by

CHI-LIN TSAI

Submitted to the Office of Graduate Studies of
Texas A&M University
in partial fulfillment of the requirements for the degree of

DOCTOR OF PHILOSOPHY

Approved by:

Chair of Committee,	David P. Barondeau
Committee Members,	Frank M. Raushel
	James C. Sacchettini
	Daniel A. Singleton
Head of Department,	David H. Russell

May 2011

Major Subject: Chemistry

ABSTRACT

Structural and Functional Studies on Human

Mitochondrial Iron-Sulfur Cluster Biosynthesis. (May 2011)

Chi-Lin Tsai, B.S., National Chung Hsing University;

M.S. , National Taiwan University

Chair of Advisory Committee: Dr. David P. Barondeau

Iron-sulfur (Fe-S) clusters are critical protein cofactors found in all life forms. In eukaryotes, a well-conserved biosynthetic pathway located in the mitochondria is used to assemble Fe-S clusters. Although proteins required for Fe-S cluster biosynthesis have been identified, their precise function and mechanism remain elusive. In this study, biochemical and biophysical methods are applied to understand molecular details for the core components of the human Fe-S cluster biosynthesis: Nfs1, Isd11, Isu2, and frataxin (Fxn). Nfs1 is a cysteine desulfurase that converts cysteine into alanine and transfers the sulfur to a scaffold protein Isu2 for Fe-S clusters. Fxn depletion is associated with the neurodegenerative disease Friedreich's ataxia (FRDA), and results in a complicated phenotype that includes loss of Fe-S clusters.

The results presented here provide the first *in vitro* evidence for a stable protein complex that exists in at least two forms: an inactive complex with Nfs1, Isd11, and Isu2 (SDU) components and an active form that also includes Fxn (SDUF). Fxn binding dramatically changes the catalytic efficiency (k_{cat}/K_M) of Nfs1 from 25 to 10,100 $M^{-1}s^{-1}$

and enhances the rate of Fe-S cluster biosynthesis 25 fold. Oxidizing conditions diminish the levels of both complex formation and Fxn-based activation, whereas Fe^{2+} further stimulates Nfs1 activity. Mutagenesis coupled to enzyme kinetics indicate that one of the three conserved cysteines (C104) on Isu2 accepts the sulfane sulfur from Nfs1 and that this transfer event likely requires prior binding of Fxn. *In vitro* interrogation of FRDA I154F and W155R and related Fxn variants revealed the binding affinity to SDU followed the trend Fxn ~ I154F > W155F > W155A ~ W155R. The Fxn variants also have diminished ability to facilitate both sulfur transfer and Fe-S cluster assembly. Fxn crystallographic structures reveal specific rearrangements associated with the loss of function. Importantly, the weaker binding and lower activity of the W155R variant compared to I154F explains the earlier onset and more severe disease progression. Finally, these experimental results coupled with computational docking studies suggest a model for how human Fxn functions as an allosteric activator and triggers sulfur transfer and Fe-S cluster assembly.

DEDICATION

This dissertation is dedicated to my father (Chung-Ming Tsai) and mother (Shuen Tsai-Wang) for their acceptance and encouragement, their spiritual and financial support, and their patience and love.

ACKNOWLEDGEMENTS

The first person I would like to thank is my advisor, Dr. David Barondeau. He taught me how to discover the new projects, to design the new experiments, to write the manuscripts and proposals, to think about science logically, and to become a better person. He went through the dissertation, proposals, and manuscripts with me, and gave me a lot of feedback. He is an outstanding advisor and also a very good friend. I also would like to thank my committee members, Dr. Frank Raushel, Dr. James Sacchettini, and Dr. Daniel Singleton, for their good suggestions and support of my research and dissertation. I also want to thank Dr. Paul Fitzpatrick for his guidance on enzyme kinetics in my earlier Ph.D. career.

I would like to thank my colleagues, Jennifer Bridwell-Rabb, Nicholas Fox, Michaella Levy, Darrell Martin, Hong-Li Sheu, Melissa Thorstad , Melissa James Vranish, and Andrew Winn, for making my life more entertaining, and for their support and encouragement on my research. Specifically, I would like to thank Jen for her great work on Isu2 and Fxn mutant projects. This dissertation would not have been completed without her. She makes my day, every day. I can't stop laughing when she is around. She is such a spirit-motivating cheerleader. Also, I want to thank my roommate, Nick, for the encouragement when I was down, and the kindness for sparing a bedroom for me to stay during my late Ph.D. period. Thanks to Michaella Levy for giving me the suggestions for my experiments. I won't forget the trip with her to ALS to collect the SAXS data. Thanks to James Vranish for some clever ideas in my research. I really enjoyed having

the discussions with him. Thanks to Andrew Winn for his hard work on making Fxn and Isu2 mutants and purifying proteins. I feel so lucky to have these amazing colleagues.

I would like to thank Dr. Christos Savva and Dr. Andreas Holzenburg for collecting EM data. Thanks to Stanford Synchrotron Radiation Laboratory (SSRL), Advanced Light Source (ALS), Advanced Photon Source (APS), and Oak Ridge National Laboratory (ORNL) for providing the opportunities to use their synchrotron and neutron facilities for protein crystallography and small-angle x-ray scattering (SAXS) studies. Thanks to Dr. Silke Leimkühler and Mr. Zvonimir Marelja for providing Nfs1-Isd11 plasmid DNA. My research could not move forward as fast without their kindly support. Thanks to Dr. James Sacchettini for allowing me to use his Robot and Rigaku x-ray equipment for setting up crystal trays and crystal screening for cryo-protecting conditions.

I would like to thank my friends, Peter, Vivian, Jerick, Karen, Kang-Shyang, Calvin, Erin, Yung-Yih, and Ching-Hua, for their great support. They help make my life go forward. Their friendship is very important to me in my Ph.D. life.

Finally, I would like to thank Ching-Wen (Yvette) for her love and understanding, and for motivating me to finish my Ph.D.

NOMENCLATURE

A. vinelandii	*Azotobacter vinelandii*
A. aeolicus	*Aquifex aeolicus*
AUC	Analytical ultracentrifugation
CBTP	Citric acid/Bis-tris propane
CD	Circular dichroism
DPD	*N*,*N*-Dimethyl-*p*-phenylenediamine
DTT	Dithiothreitol
E. coli	*Escherichia coli*
EM	Electron microscopy
Fxn	Frataxin
IPTG	Isopropyl β-D-thiogalatopyranoside
IRE	Iron responsive element
IRP	Iron regulatory protein
NMR	Nuclear magnetic resonance
SAXS	Small-angle x-ray scattering
S. cerevisiae	*Saccharomyces cerevisiae*
SD	Nfs1 and Isd11 protein complex
SDF	Nfs1, Isd11, and Fxn protein complex
SDU	Nfs1, Isd11, and Isu2 protein complex
SDUF	Nfs1, Isd11, Isu2, and Fxn protein complex

S. pyogenes	*Streptococcus pyogenes*
SRF	Serum response factor (transcription factor)
TCEP	Tris(2-carboxyethyl)Phosphine
T. maritima	*Thermotoga maritima*
TRAP2	Transcription factor AP2

TABLE OF CONTENTS

CHAPTER Page

LIST OF FIGURES

FIGURE Page

FIGURE Page

FIGURE Page

FIGURE Page

FIGURE Page

LIST OF TABLES

CHAPTER I

INTRODUCTION

Iron-Sulfur clusters (Fe-S) are ubiquitous in all life forms and functions as one of the most important protein cofactors in both prokaryotic and eukaryotic cells. Early studies on photosynthetic organisms (*1*) and nitrogen-fixing bacteria (*2*) revealed proteins that were critical for oxidoreduction. These proteins were shown to contain complexes of iron and sulfide in the form of two- and four-iron clusters. Several different forms of Fe-S clusters have since been discovered in biological systems, including $[Fe_2S_2]$, $[Fe_3S_4]$, $[Fe_4S_4]$, $[NiFe_4S_4]$, $[Fe_8S_7]$, and $[Fe_7S_9Mo]$ complexes (*3*). The most common Fe–S clusters found in nature are rhombic, $[Fe_2S_2]$, or cubic, $[Fe_4S_4]$, clusters that are usually coordinated to cysteine ligands in the proteins (Figure 1-1). Due to their chemical geometry and electronic features, Fe-S clusters play several different functions such as electron transfer, coupled proton/electron transfer, substrate binding/activation, regulation of gene expression, and sulfur donor (*4*). Fe-S clusters self-assemble in solution from ferrous iron and sulfide and may go through a $[Fe_2S_2]$ intermediate in forming more complex clusters (*5*). Since ferrous iron and sulfide are toxic molecules to the cell, biological systems utilize complex Fe–S cluster assembly machinery to sequester and control the reactivity of these molecules.

This dissertation follows the style of *Biochemistry*.

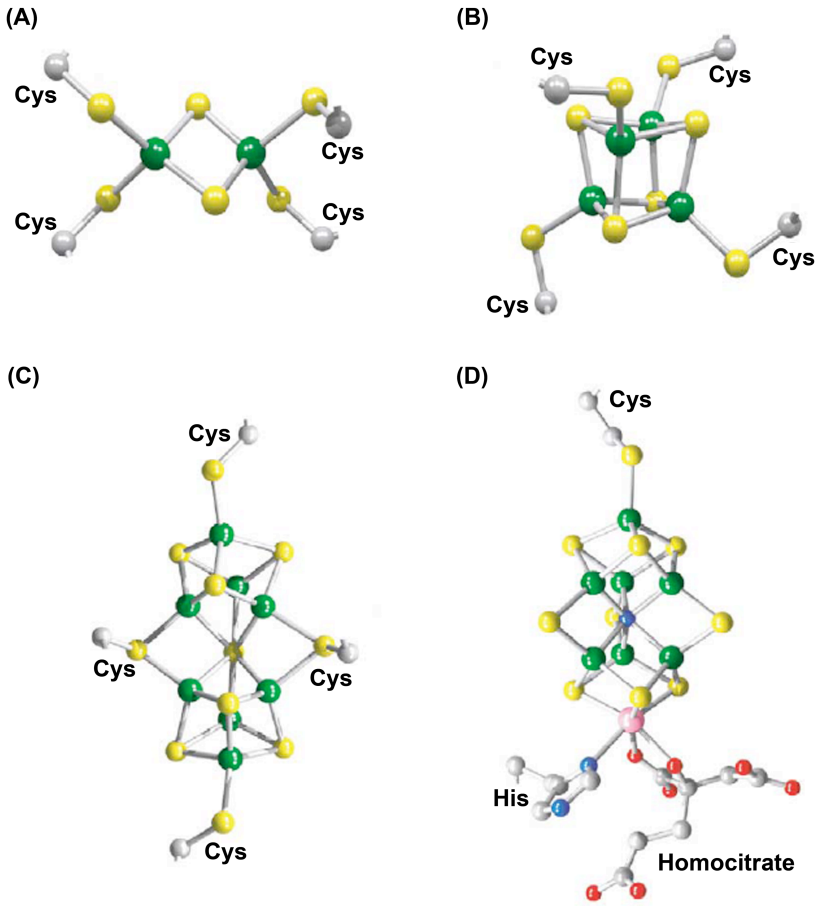

FIGURE 1-1: Various Fe–S clusters found in Fe–S proteins. (A) [Fe_2S_2] and (B) [Fe_4S_4] clusters are coordinated to cysteine ligands of protein. (C) [Fe_8S_7] P cluster and (D) [$MoFe_7S_9$] FeMo-cofactor are found in nitrogenase. (Iron is shown in green, sulfur is yellow, and molybdenum is magenta) [Frazzon, J., and Dean, D. R. (2003) Formation of iron-sulfur clusters in bacteria: an emerging field in bioinorganic chemistry. *Curr. Opin. Chem. Biol. 7*, 166-173].

Three prokaryotic systems have been discovered that function in the biosynthesis of Fe-S cofactors (*6, 7*). The first system was discovered in 1989 by Dennis Dean's group during studies of the nitrogen-fixing bacteria *Azotobacter vinelandii*, and is known

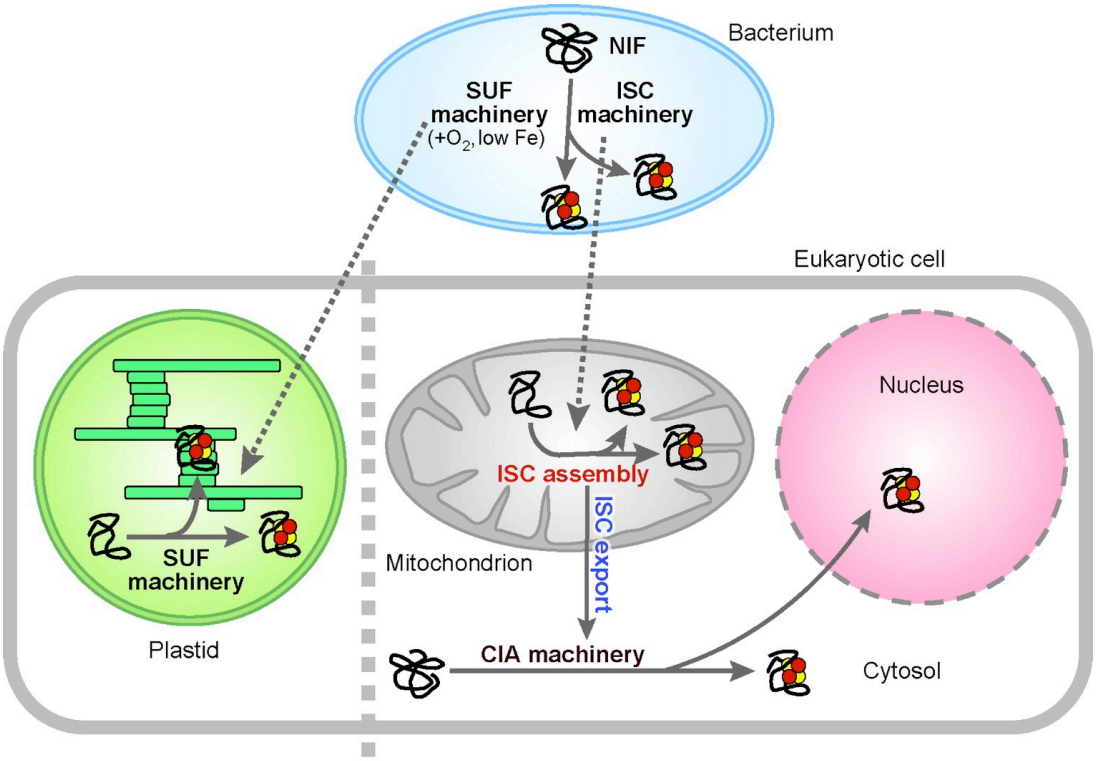

FIGURE 1-2: Eukaryotic machineries for the Fe–S cluster biogenesis and their putative evolutionary origin . [Lill, R. (2009) Function and biogenesis of iron-sulphur proteins. *Nature 460*, 831-838].

as the nitrogen-fixation (NIF) machinery (*8*). The NIF pathway is often a specialized assembly system that is responsible for assembling the Fe–S clusters for nitrogenase, which converts N_2 to NH_3. A second Fe-S cluster assembly system was discovered in 1998 by the Dean group and is now known as the iron-sulfur cluster (ISC) pathway (*9*). The ISC machinery is found in a large variety of bacteria and has a general house-keeping function to generate and insert Fe–S clusters into a majority of the Fe–S proteins found in bacterial cells. A third Fe-S assembly system was discovered by the Tokumoto

group in 2002 and is called the sulfur-mobilization (SUF) machinery (*10*). The SUF system is often found in organisms that also contain the ISC pathway and is thought to be activated under iron-limiting or oxidative stress conditions (*11*). In eukaryotes, the primary Fe-S cluster assembly system shares similarity with the bacterial ISC system and is located in the mitochondria (Figure 1-2).

The ISC-like machinery is required for the maturation of most, if not all, Fe–S proteins in non-photosynthetic eukaryotes. The ISC pathway contains more than a dozen proteins and can be divided into two stages (*12-14*) (Table 1-1). Early steps involve the generation of a transient Fe–S cluster on the scaffold protein Isu2, whereas later steps facilitate the transfer of intact Fe–S clusters from Isu2 to target apo-proteins (Figure 1-3). The sulfur for the biosynthesis of Fe–S clusters is generated by the cysteine desulfurase Nfs1, which catalyzes the conversion of cysteine to alanine (*15*) and transfers of the sulfur atom to Isu2. The iron for the biosynthesis of Fe-S clusters may be donated by Fxn (*16*). Electrons required for the reduction of sulfur may be provided by a ferredoxin (Fdx), which receives its electrons ultimately from NADH through a ferredoxin reductase (FdxR) (*17*). The monothiol glutaredoxin Grx5 is also important for Fe-S biosynthesis, but is not well understood. Initial studies suggest Grx5 may be involved in the regulation of the redox state of Nfs1 and/or scaffold proteins where Fe–S clusters initially assemble (*18, 19*).

In the later steps of Fe-S cluster biosynthesis, the intact Fe-S cluster is transferred from Isu2 to apo target proteins. This process is assisted in humans by the co-chaperone Hsc20, the ATP-dependent chaperone Grp75, and the ADP/ATP exchange factor GrpE.

Table 1-1: Known Components of Fe–S Cluster Biogenesis in Human Mitochondria

Name	Essential in yeast	Yeast homologs	Bacterial homologs	Proposed function & protein interactions
Nfs1	Yes	Nfs1	IscS, NifS, SufS	Cysteine desulfurase, sulfur donor, Interacts with Isd11, Isu2, Fxn, Nfu
Isd11	Yes	Isd11	–	Forms complex with Nfs1, maintains Nfs1 activity, interacts with Nfs1, Fxn
Isu2	Yes (double deletion)	Isu1/2	IscU, NifU (N-terminal domain)	Scaffold for cluster assembly Interacts with Nfs1, Fxn, GRP75, Hsc20, Isa1/2, Nfu
Fxn	No (PET)[a]	Yfh1	CyaY	Iron donor, iron storage, iron sensor, allosteric activator, interacts with Isu2, Nfs1, Isd11
Fdx	Yes	Yah1	Fdx (middle-domain of NifU?)	Ferredoxin, reduction of S^0 to S^{2-} Interacts with FdxR, Nfs1, GRP75
FdxR	Yes	Arh1	–	Ferredoxin reductase, electron transfer to Fdx from NADH, interacts with Fdx
GRP75	No, cold sensitivity	Ssq1	HscA	Hsp70 Chaperone, transfer cluster from Isu2 to apoprotein, interacts with Hsc20, Isu2, Isa1/2
Hsc20	Yes	Jac1	HscB	Cochaperone of GRP75, facilitate Isu2 to bind GRP75, interacts with Isu2, GRP75
GrpE	Yes	Mge1	GrpE (not required in bacteria)	ADP/ATP exchange factor on GRP75, interacts with GRP75
Grx5	No	Grx5	?	Monothiol glutaredoxin
Isa1/2	No (PET)[a]	Isa1/2	IscA, SufA, $IscA^{Nif}$	Iron donor, alternate scaffold for aconitase-like Fe-S proteins , interacts with GRP75, Isu2, Nfs1
Iba57	ND	Iba57	–	Forms complex with Isa1/2, maturation of radical-SAM proteins
Nfu	No	Nfu1	C-terminal of NifU	Unknown?

[a]PET: no growth on glycerol-containing media

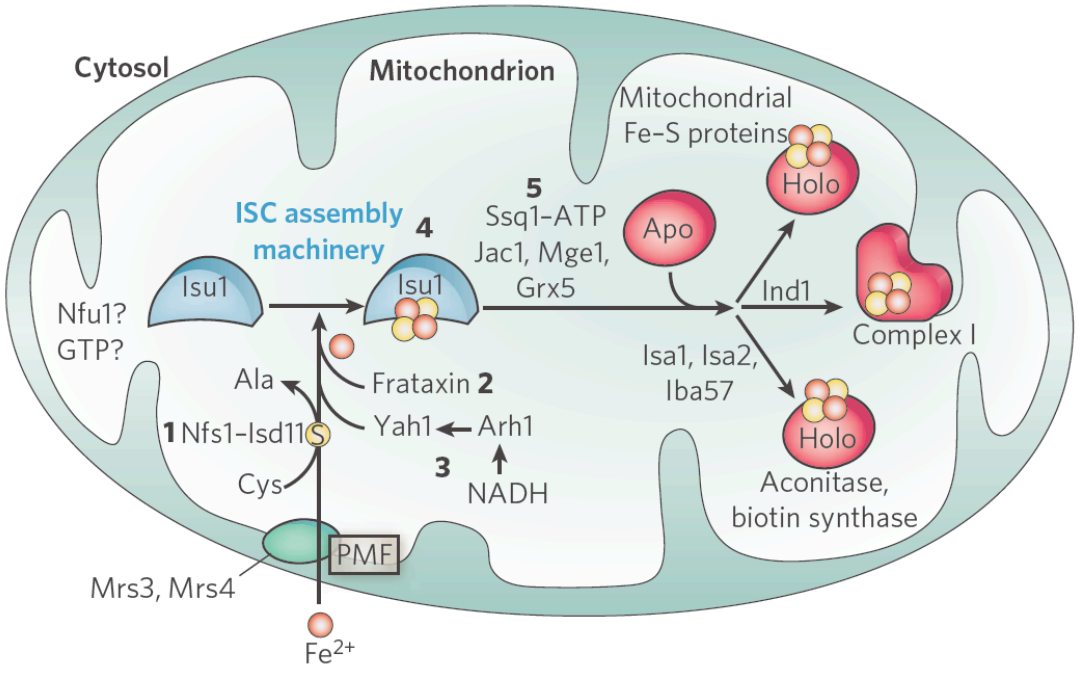

FIGURE 1-3: Proposed model for Fe–S cluster assembly in mitochondria [Lill, R. (2009) Function and biogenesis of iron-sulphur proteins. *Nature 460*, 831-838].

The role of Fe-S assembly proteins Isa1/2 and Nfu are less clear. Isa1/2 is required for the activation of aconitase-type Fe–S proteins and has been suggested to function as an alternate scaffold protein (*20*) or as an iron donor (*21*). Nfu1 has also been proposed to be an alternate scaffold (*22*) and in sulfur transfer (*23*). Human ABCB7 is an ATP-binding cassette (ABC) transporter of the mitochondrial inner membrane and exports an unknown compound that is important for cytosolic and nuclear Fe–S cluster maturation and iron homeostasis (*24, 25*). Fe–S clusters are not only essential for the activities of proteins such as aconitase, succinate dehydrogenase, and iron-regulatory protein 1, but

are also important for the synthesis of other cofactors including heme (*26*), biotin (*27*), thiamin (*28*), and vitamin B_{12} (*29*).

Several human diseases have recently been connected to defects in Fe–S cluster biosynthesis. In general, defects for most of the proteins in the Fe–S cluster biosynthesis pathway result in iron depletion in the cytosol and an increase in both iron accumulation and oxidative stress in the mitochondria. The resulting mitochondrial dysfunction can trigger cell apoptosis (*30*) and can also lead to nuclear genome instability, which is a hallmark of human diseases such as cancer (*31, 32*). More specifically, mutations in Isu2 lead to cardiomyopathy, depletion of Fxn results in Friedreich's ataxia, and defects in Grx5 and ABCB7 result in sideroblastic anemia (*14, 33*).

For Isu2, a splice mutation G7044C in the fourth intron of Isu2 was found in Swedish patients and thought to be responsible for hereditary myopathy with lactic acidosis (*34, 35*). Isu2 protein levels are significantly reduced in patient muscle cells. The depletion of Isu2 causes the dysfunction of Fe–S cluster biosynthesis and mitochondrial iron overload in skeletal muscle. Without sufficient Fe–S cluster biogenesis, the heme synthetic enzyme ferrochelatase is unstable and is significantly degraded in patient muscle (*26*). A new missense mutation G17E on Isu2 has been found recently in two male siblings (*36*). Patients with G17E mutation demonstrate more severe muscle pathology than other Isu2 mutation patients. Clinically, the patients with Isu2 mutation have lifelong severe exercise intolerance that begins in childhood.

Frataxin defects are associated with the autosomal recessive disease Friedreich's ataxia (FRDA), which is the most common neurodegenerative ataxia (*37*). FRDA has

been estimated to affect 1 in 50,000 Caucasians and a deduced carrier frequency of 1 in 120 in European populations. FRDA patients typically present symptoms during adolescence such as progressive limb and gait ataxia and often die prematurely from cardiomyopathy. There is currently no cure. About 96% of FRDA patients have an unstable GAA triplet repeat expansion (66–1700 repeats) in the first intron of the χ25 gene, whereas about 4% of the patients have point mutations in the χ25 gene. The triplet repeat size ranges between 7 and 40 for normal individuals and 66 to >1700 for FRDA patients (*38, 39*). Importantly, larger GAA repeats correlate with lower Fxn expression levels and an earlier age of disease onset (*40*). The *χ*25 gene was identified in the FRDA locus on chromosome 9q13 and encodes the 210 amino acid protein Fxn (*37*). Specific missense mutations in Fxn will be discussed below.

THE CYSTEINE DESULFURASE COMPLEX NFS1/ISD11

Cysteine desulfurases have a critical role in biological sulfur mobilization, including Fe–S cluster assembly, thiamine and biotin synthesis, tRNA modifications, and molybdopterin biosynthesis (*4, 41, 42*). The bacterial cysteine desulfurase IscS is a homodimer (45 kDa per subunit), which contains one pyridoxal 5'-phosphate (PLP) cofactor per subunit. IscS catalyzes the conversion of L-cysteine to L-alanine and generates inorganic sulfur (*15, 43*). During catalysis, a cysteine on a flexible loop attacks a substrate–PLP adduct to generate a persulfide species (Figure 1-4). The resulting sulfane sulfur can then be transferred in a rate-limiting step to sulfur acceptor proteins

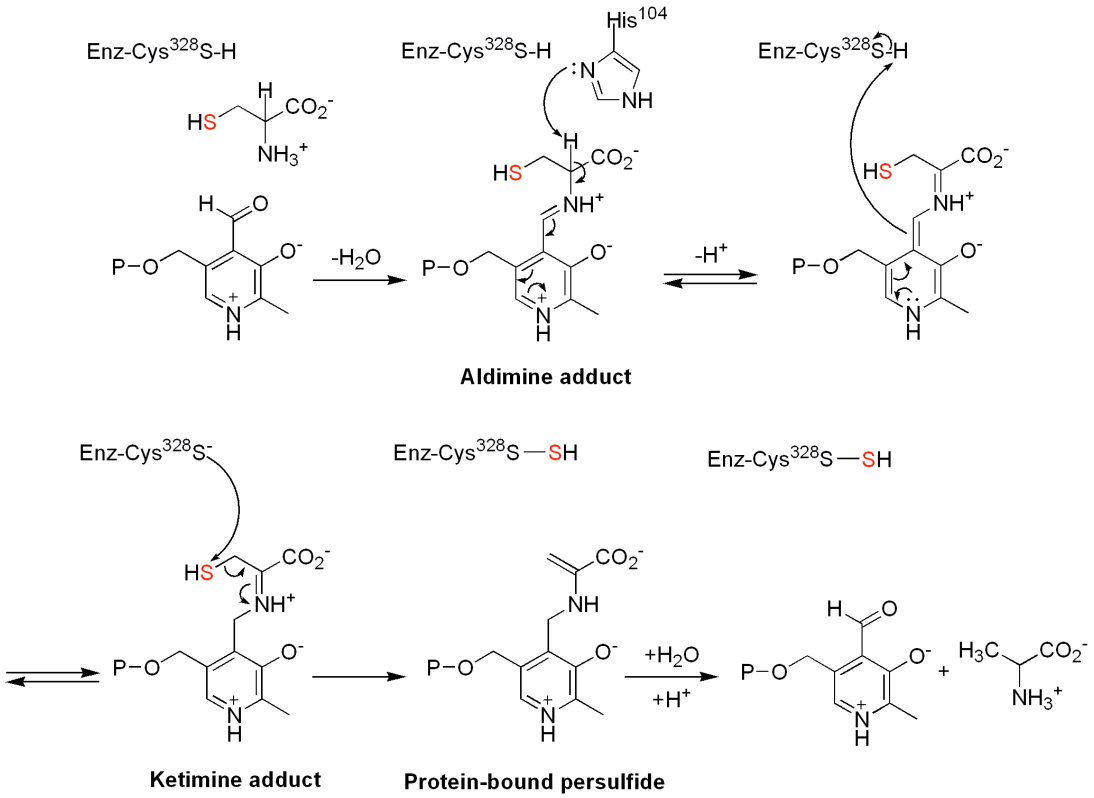

FIGURE 1-4: Proposed mechanism of cysteine desulfurase by catalyzing cysteine substrate to alanine.

such as ThiI, TusA, MoaD/MoeB, or the scaffold protein Isu2 for Fe–S cluster biosynthesis (*44*). Alternately, this persulfide can be reductive cleaved *in vitro* by reducing agents such as DTT to form sulfide ion (*45*).

The cysteine desulfurase IscS from *E. coli* has been extensively studied using both structural and functional approaches. In the 2.1 Å IscS crystal structure, the PLP cofactor lies at the base of an active site pocket located near the surface of the protein

(*46*). The PLP cofactor forms an internal aldimine Schiff base with K206 and interacts with a number of polar and non-polar residues. H104 sits directly above the pyridine ring of PLP and functions as an acid–base catalyst (Figure 1-5A). Remarkably, an estimated distance of greater than 17 Å between the crucial C328 residue and PLP cofactor implies

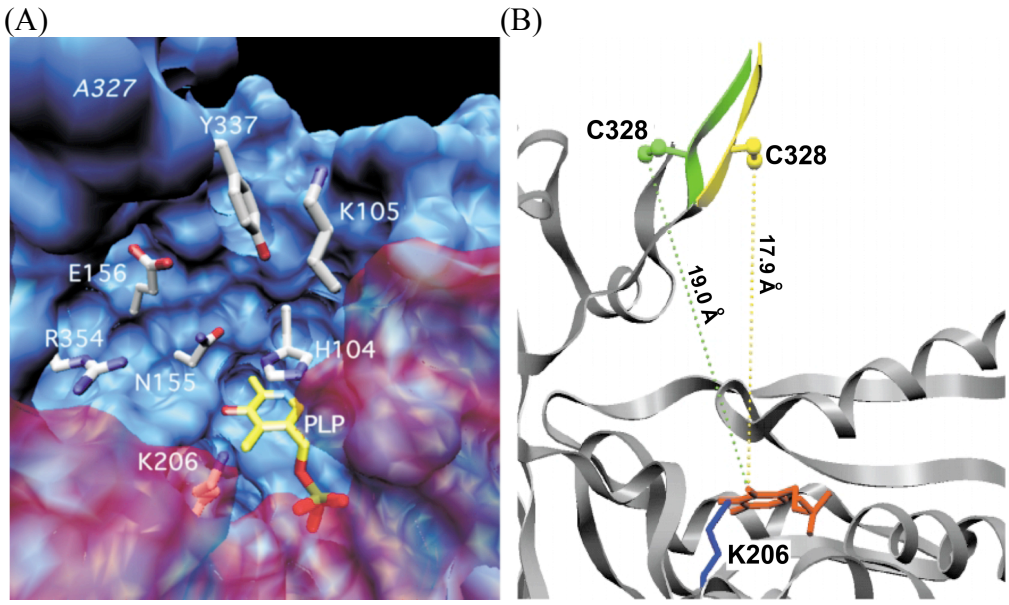

FIGURE 1-5: (A) The active site pocket of cysteine desulfurase IscS (PDB: 1P3W). (B) The distance between catalytic C328 residue and PLP cofactor [Cupp-Vickery, J., Urbina, H. D., and Vickery, L. (2003) Crystal structure of IscS, a cysteine desulfurase from Escherichia coli. *J. Mol. Biol. 330*, 1049-1059].

a large conformational movement is required for the nucleophilic attack by C328 on the substrate cysteine bound to the PLP cofactor (Figure 1-5B).

The human cysteine desulfurase Nfs1 exists in two distinct isoforms: a 47 kDa protein (Δ1-55 a.a.) that is located in the mitochondria, and a 44 kDa (Δ1-60 a.a.) form that is found in the cytosol and nucleus (*47*). There currently is no structural information for eukaryotic cysteine desulfurases. However, the crystal structure of *E. coli* IscS might provide a reasonable model for human Nfs1, as these proteins share 60% sequence identity (*46*). Isolated human Nfs1 (Δ1-55 a.a.) is a 94 kDa homodimeric protein that is reported to be inactive and have a tendency to aggregate and precipitate (*48*).

In 2006, the 11 kDa protein Isd11 was found to have an essential role in Fe–S cluster biosynthesis in mitochondria (*49*). A C-terminal His-tag was attached to Isd11 allowing pull-down assays of crude cell extracts and the identification of its protein partner, Nfs1 (*50*). Homologues of the Isd11 gene have been detected in plant, fungi, and animal genomes, but not in prokaryotes. This suggests that Isd11 is a unique eukaryotic protein that arose after the process of endosymbiosis that generated eukaryotic mitochondria (*51*). Importantly, Isd11 was found to stabilize Nfs1 by forming a tight (~100 nM) complex, and this complex was shown to be catalytically active (*48*). Separate overexpression of Nfs1 and Isd11 in *E. coli* cells resulted in an inactive cysteine desulfurase prone to aggregation and inclusion body formation, respectively. In contrast, coexpression of Nfs1 and Isd11 in *E. coli* cells produced a soluble, well-behaved Nfs1/Isd11 complex in reasonable (~3 mg per liter of cell) yield (*48, 52*). This suggests Nfs1 and Isd11 have to be in complex to maintain their normal function. From the *E. coli* IscS crystal structure (Figure 1-5A), PLP is located near the dimer interface. Perhaps, Isd11 stabilizes the folding of Nfs1 to properly bind the PLP cofactor. Isd11

contains an unusually large number of positively charged amino acids (6 Lys and 14 Arg residues per 91 amino acids) and an estimated *p*I of about 10.7 (http://www.scripps.edu/~cdputnam/protcalc.html). Although the structure of Isd11 is not known, we hypothesize that the positively charged Isd11 stabilizes the negatively charged Nfs1 dimer interface through electrostatic complementation.

THE ISU SCAFFOLD PROTEIN

IscU is small ~14 kDa protein that functions as the catalyst for Fe-S cluster biosynthesis by combining iron, sulfur, and electrons into Fe-S clusters and then transferring these clusters to apo targets. To achieve this biological function, IscU must not only conserve its active site for cluster assembly but also maintain its protein-protein interactions with partner proteins frataxin (*16*), cysteine desulfurase (*44*), and chaperones (*53, 54*). As a consequence of these functional requirements, IscU is one of the more highly conserved proteins in evolution based on sequence identity (*55*). For example, *E. coli* IscU and *S. cerevisiae* Isu1 share 72% and 55% sequence identity with human Isu2 (Figure 1.6).

The human Isu gene encodes two forms of the protein by alternative splicing. The Isu1 (15 kDa) form is located in the cytosol, whereas the Isu2 (14 kDa) form is imported into mitochondria (*56*). Human Isu2 acts as a scaffold protein to assemble $[Fe_2S_2]$ clusters and possibly, $[Fe_4S_4]$ clusters. Isu2 contains three conserved cysteine residues (C35, C61, and C104) that could function as Fe–S cluster ligands (Figure 1-6). The fourth ligand is unclear and has been suggested to be H103 (*57, 58*), the

nonconserved C96 (*59*), and cysteine residues from another Isu2 molecule in a dimeric arrangement (*60*).

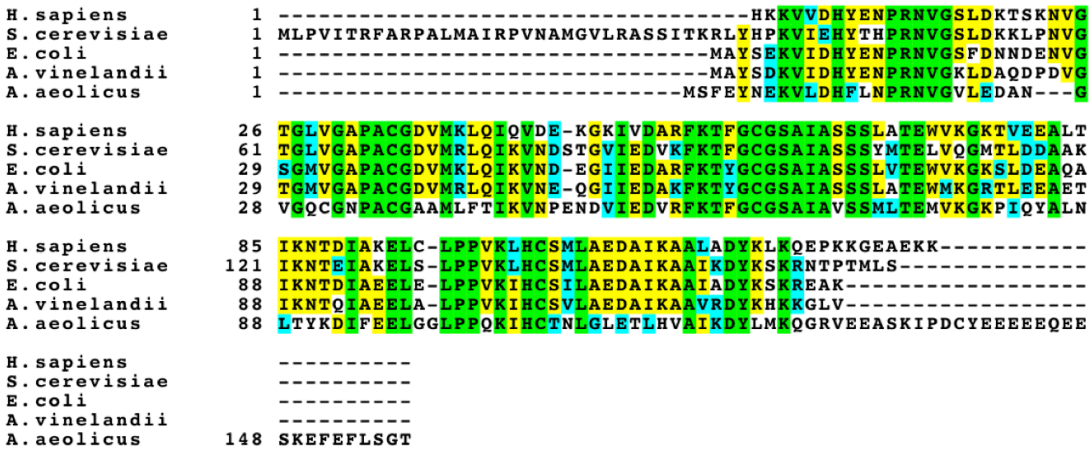

FIGURE 1-6: Sequence alignment of human Isu2 with other indicated species.

In 2003, Bertini *et al.* reported the structural characterization of IscU from *T. maritima* by NMR. IscU displays a dynamic equilibrium between two or more distinct conformations, possibly existing in a molten globular state (*61*). In 2004, the similar studies have been suggested that IscU exists in multiple discrete conformers (*62*). In 2008, Shimomura *et al.* determined the crystal structure of the asymmetric trimeric structure of IscU at 2.3 Å resolution from the hyperthermophilic bacterium *Aquifex*

aeolicus (*58*). A [Fe_2S_2] cluster was bound to residues C36, C63, H106 and C107 in one of the three subunits of the trimer. The N-terminal regions of the different subunits exhibited significantly different conformations and were positioned at the protein-protein interfaces, apparently to stabilize the trimeric unit (Figure 1-7). The two subunits that do not have a [Fe_2S_2] cluster have disulfide bond linkage between C107 (equivalent to human C104) and C36 (equivalent to human C35) and between C107 and C63 (equivalent to human C61). The C-terminal regions of these two subunits near C107 undergo a substantial conformational change that result in a helix to coil conversion.

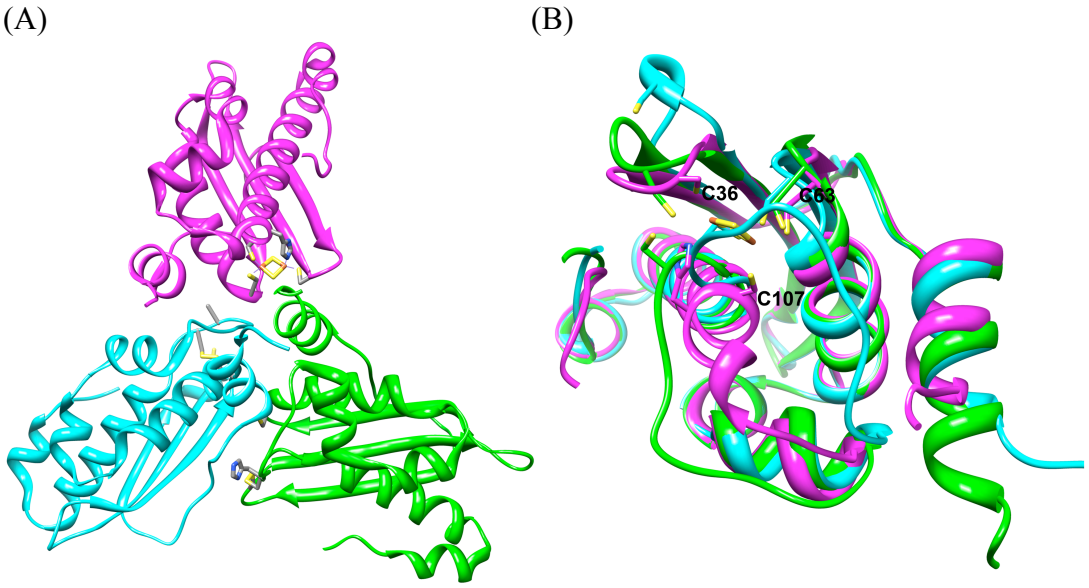

FIGURE 1-7: Crystal structure of *A. aeolicus* IscU trimer (PDB: 2Z7E) (B) Alignment of three IscU subunits. C107 was labeled for subunit colored magenta.

These residues include a LPPVK motif, which is known to become unfolded and interact with the chaperone HscA (equivalent of human Hsc20) (*63*).

THE ROLE OF FRATAXIN AND FRDA MUTANTS

Frataxin (Fxn) has been intensively studied, yet its biological role remains undefined and controversial. In prokaryotes, Fxn is not part of the ISC operon and appears to be dispensable for Fe-S cluster biosynthesis. In eukaryotes, Fxn is a mitochondrial protein and its depletion leads to mitochondrial iron accumulation, oxidative stress, and defects in Fe–S cluster and heme biosynthesis (*64*).

Once Fxn is incorporated into the mitochondria it undergoes a two-step maturation process. The full-length Fxn (1-210 a.a.), which contains a mitochondrial targeting sequence, is cleaved by the mitochondrial processing peptidase (MPP) and results in a protein that contains amino acids 56-210 (Fxn^{56-210}). The Fxn^{56-210} is further cleaved by MPP to a protein with amino acids 81-210 (Fxn^{81-210}), referred to as mature Fxn. When the normal maturation process of Fxn is impaired, Fxn^{56-210} and Fxn^{78-210} (78-210 a.a.) are generated (*65*). Most researchers agree that the mature form of Fxn (Fxn^{81-210}) is physiologically relevant, but the biological roles of the Fxn^{56-210} and m_{78}-Fxn forms are still hotly debated.

Recently, the Isaya group reported the Fxn^{56-210} form can oligomerize into a greater than 1 MDa particle that can stimulate Fe–S cluster formation on Isu2 in the presence of Nfs1 and Isd11, and that both the Fxn^{81-210} and Fxn^{56-210} forms are relevant to FRDA pathophysiology (*66*). Interestingly, EM and EXAFS studies suggest the Fxn^{56-}

^{210} oligomer has an overall structure similar to the iron-storage protein ferritin (*67*), and that the cavity inside the oligomer can store more than 2000 iron in the form of ferrihydrite (*68-70*). The *in vitro* assembly of the oligomer by bacterial and yeast Fxn can be initiated by the addition of ferrous iron in the presence of oxygen (*71, 72*). In contrast, human Fxn$^{56-210}$ does not oligomerize under similar *in vitro* conditions. The oligomeric form for human Fxn can be generated by some unknown factor present during recombinant overexpression (*73*). Once the N-terminus is cleaved and the mature form of Fxn (Fxn$^{81-210}$) is generated the oligomeric form is no longer observed leading to storage is not a critical function of Fxn (*74*). More evidence is required to establish the

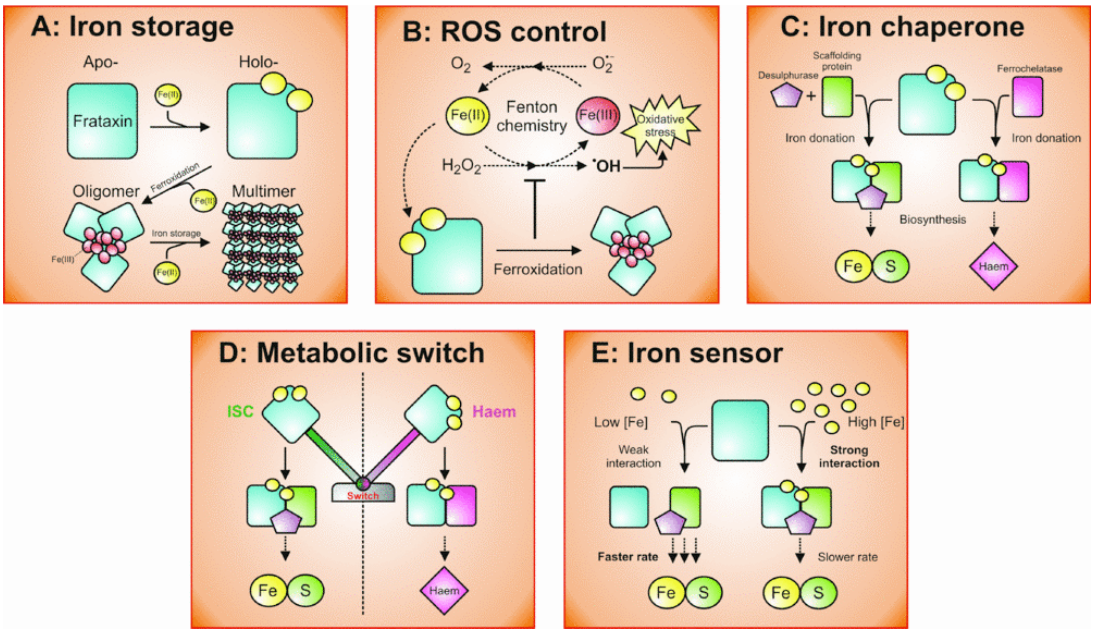

FIGURE 1-8: Proposed functions for frataxin in mitochondria iron metabolism [Lane, D. J. R., and Richardson, D. R. (2010) Frataxin, a molecule of mystery: trading stability for function in its iron-binding site. *Biochem. J. 426*, e1-3].

the suggestion that the non-conserved N-terminal region (56–80 a.a.) is important for Fxn oligomer assembly (*73*). Aloria *et al.* generated an oligomerization-deficient strain in yeast that did not show any growth defects or phenotype, which suggests that iron iron storage role of Fxn oligomer (Figure 1-8A).

Several functions have been proposed for Fxn other than iron storage (Figure 1-8) (*75*). The susceptibility of Fxn-deficient mitochondria to oxidative stress has lead to the proposal that Fxn plays a direct role in oxidative stress control (Figure 1-8B). Oligomeric Fxn is proposed to facilitate an iron-mediated ferroxidase reaction that may remove ferrous iron before it can generate toxic reactive oxygen species through Fenton chemistry (*76*). Fxn is also proposed to function as an iron chaperone (Figure 1-8C) and binds iron through its unique acidic patch (13 carboxylate residues) on its α1 helix

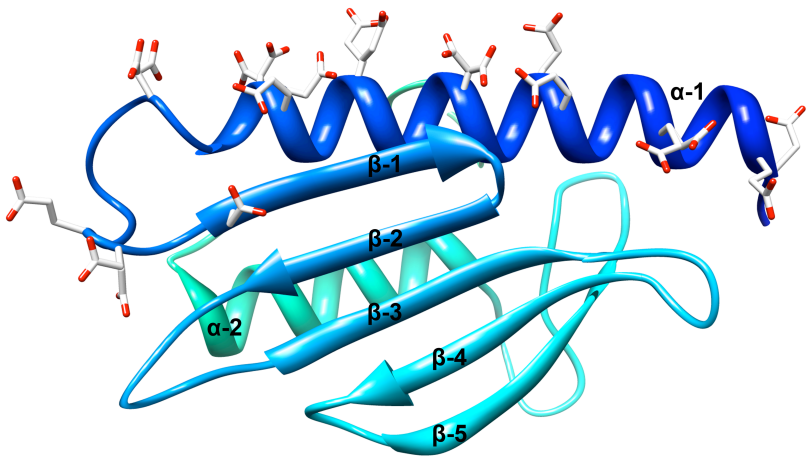

FIGURE 1-9: Ribbon representation of human frataxin structure. Aspartate and glutamate residues on helix 1 (α1) were shown in stick.

(Figure1-9), and then deliver iron for biosynthetic pathways for Fe-S clusters and heme cofactors (*77, 78*). A related proposal suggests Fxn functions as a metabolic switch (Figure 1-8D) to control iron flux between Fe-S and heme pathways (*79*). Finally, an iron sensor role (Figure 1-8E) was recently proposed based on studies of the *E. coli* Fxn homologue CyaY. Results from the Pastore group reveal that CyaY inhibits the rate of Fe-S cluster biosynthesis under high iron conditions, suggesting a negative regulator role (*80*). All of these functions are closely connected to Fe–S cluster and heme biosynthesis or, more specifically, to iron. Indeed, knockout of the Fxn gene alters the regulation of cellular iron homeostasis. Recently, Rouault's group suggested Fxn expression can be regulated by iron (*81*) or transcription factors SRF and TFAP2 (*82*). Fibroblast and lymphoblast cells treated with iron chelator, desferal, have decreased Fxn mRNA and protein expression levels (*81*). Over-expression of either SRF or TFAP2 significantly increased Fxn mRNA and protein levels in HEK293 cells (*82*). Toward to the end, the exact function of Fxn is still a puzzle, but most researchers believe Fxn is directly related to Fe–S cluster biosynthesis and acts as an iron donor.

Fxn has been shown to be associated with the neurodegenerative disease Friedreich ataxia (FRDA) (*37*). A small fraction of FRDA patients have an expanded GAA repeat on one allele and a point mutation on the other allele (*83*). In these cases, the Fxn protein levels do not necessarily correspond to the age of onset (*39, 84*). About 15 point mutations have been found in FRDA patients (*39*) (Figure 1-10A), mostly in exons 3-5a. A comparison of FRDA mutants with the Fxn conserved residues suggests

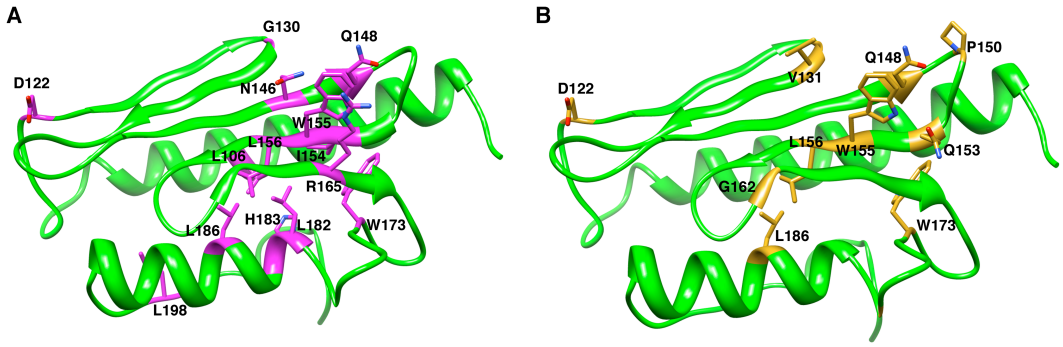

FIGURE 1-10: (A) The distribution of FRDA point mutations (magenta) on human Fxn structure. (B) The distribution of conserved residues (goldenrod) on human Fxn structure.

residues D122, Q148, W155, L156, W173, and L186 are important for Fxn protein function. Mapping these mutations onto the Fxn structure revealed that most are located in the conserved β-sheet region (Figure 1-10B). Recent chemical denaturation studies indicate Fxn mutations decrease the protein stability in the order of wild-type > W155R > I154F > D122Y > G130V (*85-87*). W155 is the only absolute conserved residue in Fxn among all the organisms. Mutation of I154 and W155 residues to alanine inhibit cell growth in yeast cell (*88*). The mutation of W155 to alanine strongly decreases the interaction with yeast Isu1 (homologous to human Isu2) based on pull-down experiments (*88*). Gomes's group also suggest W155 may be a functional hotspot in frataxin for oxidative stress protection based on chemical modification experiments (*86*). Together these results lead to the conclusion that the conserved β-sheet residues, particularly W155, are important for protein stability and function. Unfortunately, little is known about how these residues affect protein function. Therefore, structural studies coupled to

the development of functional assays are required to understand the effects of Fxn FRDA mutants on Fe–S cluster biosynthesis.

ISCU-ISCS INTERACTIONS AND SULFUR TRANSFER

In 2010, a crystal structure of the IscS–IscU complex from *E. coli* was determined to 3.0 Å resolution (Figure 1-11A) (*44*). This was the first structural snapshot that revealed molecular details for the protein complex containing the cysteine desulfurase and scaffold protein for Fe-S cluster biosynthesis. During IscS cysteine desulfurase (homologous to human Nfs1) catalysis, C328 on a mobile loop attacks the substrate-PLP adduct to cleave the C-S bond of the L-cysteine substrate and generate a persulfide species on C328. In the crystal structure of the IscS-IscU complex, the persulfide cysteine loop is not visible in the electron density maps due to conformational disorder. The distance between the expected position of the C328 of IscS and the conserved cysteines on IscU has been estimated to be between 12 and 18 Å (Figure 1-11B). Previously, the Vickery group estimated the distance between C328 and the PLP cofactor to be greater than 17 Å (*46*). Together these results suggest C328 on IscS is able to sample a distance of ~30 Å and transfer the sulfur from the cysteine-PLP adduct to a cysteine residue on IscU (homologous to human Isu2). It is unclear if this sulfur transfer event from IscS C328 is to a specific cysteine residue on IscU.

The sulfur transfer mechanism from IscS to IscU remains elusive. In 2002, Kato *et al.* found that C63 of *E. coli* IscU stimulates the cysteine desulfurase activity of IscS

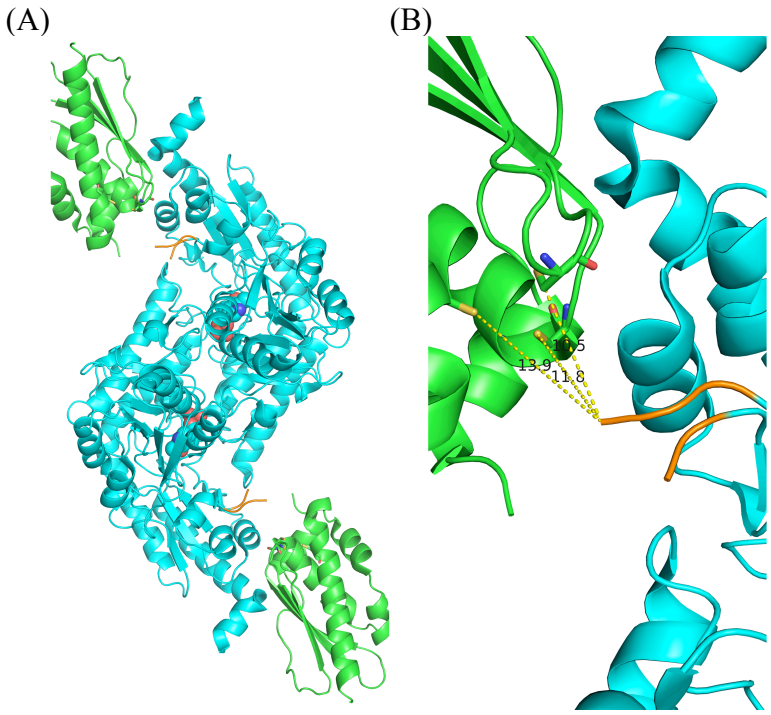

FIGURE 1-11: Crystal structure of *E. coli* IscS-IscU complex (PDB: 3LVL). (A) IscS-IscU forms a heterodimer complex. (B) C328 on the loop of IscS structure was missing. The estimate distances from loop to cysteine residues on IscU were labeled.

(*89*). In addition, C63 of IscU forms a disulfide bridge with C328 of IscS in a covalent IscU-IscS complex (*89*). In 2005, Smith *et al.* showed that a heterodisulfide is formed in the *A. vinelandii* system between IscS and C37 of IscU, and that IscS can transfer sulfur to each of the three cysteine residues (*90*). Smith *et al.* questioned the studies on the heterodisulfide complex using *E. coli* IscU and IscS because the IscU contained a C-terminal His-tag and the experiments were not performed under anaerobic conditions. The equivalent types of sulfur transfer experiments have not been performed on a eukaryotic system.

PROPOSED MECHANISMS FOR FE-S CLUSTER ASSEMBLY

Two possible Fe–S cluster assembly mechanisms that differ in the order of Fe and S incorporation have been proposed for the SUF system (*91-93*). These two proposals are referred to as the "iron-first" and "sulfur-first" mechanisms (Figure 1-12). In the iron-first mechanism, two Fe^{2+} atoms are ligated by two conserved cysteine residues in each subunit of the scaffold protein SufA (homologous to human Isu2) dimer, followed by sulfane sulfur (S^0) transfer from a cysteine desulfurase (Figure 1-12A). The two sulfane sulfurs were reduced a total of four electrons for incorporation into the Fe-S cluster. Two of the electrons come from the ferrous iron atoms, and the other two electrons are derived from either an external electron source (ferredoxin or DTT) or a redox active dithiol group from one of the conserved cysteines (Figure 1-12A) to generate the sulfide-bridged diferric species. In the sulfur-first mechanism, a persulfidic sulfur was transferred from a cysteine desulfurase to one of the cysteines on each subunit of the SufA dimer, followed by the incorporation of two Fe^{2+} that ligated both cysteine and persulfide species (Figure 1-12B). The sulfide-bridged Fe^{2+} species were then reduced by two ferrous iron and two external electrons to generate the $[Fe_2S_2]$ cluster. Evidence against the Fe-first mechanism is the observation that the scaffold protein SufA only weakly binds ferrous iron to residues other than the conserved cysteines (*91*). There is currently no evidence for ferrous iron binding to *E. coli* IscU and *A. vinelandii* IscU (*94, 95*). In contrast, *Thermotoga maritima* IscU binds both ferrous and ferric iron with a binding constant in the μM range (*96*). In the sulfur-first model, it

(A)

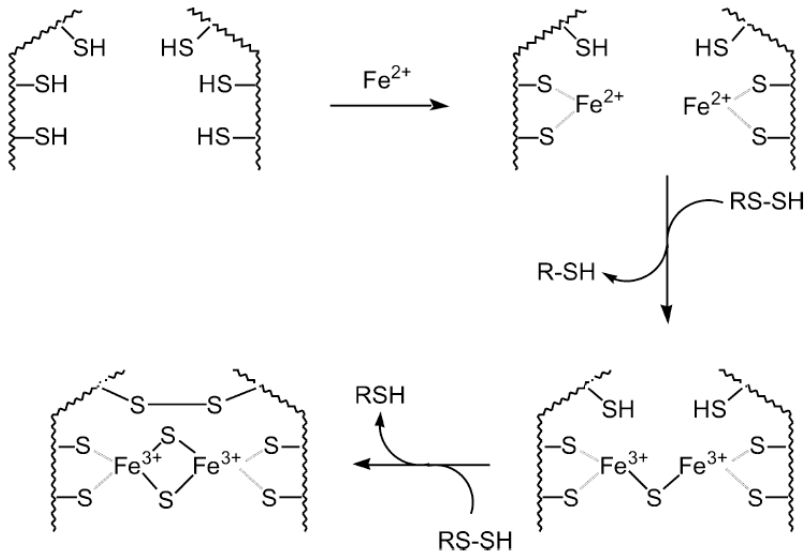

(B)

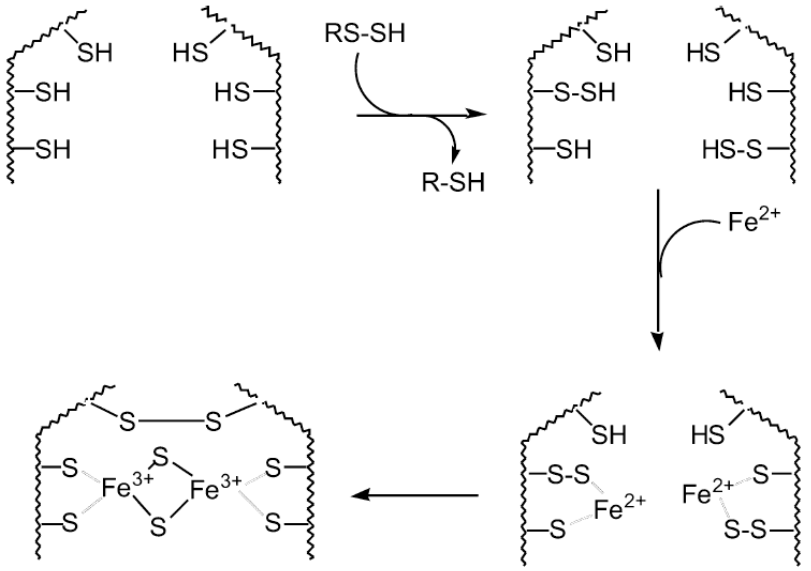

FIGURE 1-12: Proposed Fe–S cluster assembly mechanism. (A) "Fe" first model (B) "S" first model [Fontecave, M., Choudens, S. O. d., Py, B., and Barras, F. (2005) Mechanisms of iron-sulfur cluster assembly: the SUF machinery. *J. Biol. Inorg. Chem. 10*, 713-721].

was shown that persulfide- or polysulfide-bound IscU can be obtained by incubating with IscS and cysteine (*94, 97*). However, the persulfide or polysulfide-bound IscU is not viable to forming Fe–S cluster upon incubation with iron (*94*). The mechanism of Fe-S cluster assembly has yet to be resolved and requires further investigation.

CHAPTER II

HUMAN FRATAXIN IS AN ALLOSTERIC SWITCH THAT ACTIVATES THE FE-S CLUSTER BIOSYNTHETIC COMPLEX*

INTRODUCTION

Iron-sulfur (Fe-S) clusters are essential cofactors that are required for biochemical reactions and processes in all life forms. *In vitro*, iron and sulfide can be used to chemically synthesize Fe-S clusters or activate apo Fe-S proteins (*4, 98*). *In vivo*, Fe-S clusters are synthesized by biosynthetic pathways that are required to circumvent the toxicity and indiscriminant reactivity of "free" iron and sulfide. Fe-S clusters are synthesized in prokaryotes using the nitrogen fixation (NIF), iron-sulfur cluster assembly (ISC), and mobilization of sulfur (SUF) pathways (*7*). In eukaryotes, the biosynthesis of Fe-S clusters occurs in the matrix space of the mitochondria and includes at least a dozen proteins (*13, 33*). Defects in the human Fe-S cluster biosynthesis pathway are associated with cardiomyopathy, neurodegenerative ataxia, and contribute to genomic instability, the development of cancer, and aging (*13, 31, 32*).

Many of the required proteins for Fe-S cluster biosynthesis have been identified and their general biochemical function elucidated. Human Isu2 (homolog of the bacterial

*This chapter is reprinted with permission from "Human Frataxin is an Allosteric Switch That Activates the Fe-S Cluster Biosynthetic Complex" by Tsai, C.-L., Barondeau, D.P., 2010. *Biochemistry, 49*, 9132-9139, Copyright [2010] by American Chemical Society.

IscU) is a 14 kDa monomer (*59*) that provides a scaffold for building [Fe_2S_2] and, possibly, [Fe_4S_4] clusters. Clusters are synthesized on Isu2 through interactions with proteins that mediate sulfur, iron, and electron transfer. Sulfur atoms are provided by the 94 kDa homodimeric cysteine desulfurase Nfs1, which catalyzes the PLP-dependent breakdown of cysteine to alanine (*15, 43*). During Nfs1 catalysis, a cysteine on a flexible loop attacks a substrate-PLP adduct to generate a persulfide species. The resulting sulfane sulfur can then be transferred in a rate-limiting step to the scaffold protein for Fe-S biosynthesis, or, *in vitro*, can be reductively cleaved by redox agents to form sulfide ion (*15, 45*). Iron atoms have been proposed to be donated by both frataxin (Fxn) (*16, 99, 100*) and IscA (*21*). Electrons may be provided by a ferredoxin (*17, 101*). Finally, chaperone proteins interact with Isu and assist in delivering intact Fe-S clusters to their apo targets (*53*). ATP and GTP are also required during some stage of Fe-S cluster biogenesis (*102*).

The role of Fxn in this Fe-S cluster assembly process remains elusive. *In vivo* studies support a role for the 14 kDa monomeric Fxn in Fe-S cluster assembly (*103, 104*), possibly as an iron chaperone. An iron detoxification and storage role has also been proposed (*71, 105*) and refuted (*74, 106*). Recently, Pastore and coworkers provided evidence that the *Escherichia coli* Fxn homolog functions as a negative regulator for Fe-S cluster assembly (*80*). Such a function for eukaryotic Fxn is difficult to reconcile with genetic and biochemical data, which suggest Fxn facilitates rather than inhibits Fe-S cluster biosynthesis (*16, 103, 104, 107, 108*). Further kinetic experiments

that address the effect of human frataxin on Fe-S cluster biosynthesis are required to resolve this issue.

A network of protein-protein interactions appears to be critical for Fe-S cluster biosynthesis (*13, 109*). Fxn, Isu, and Nfs1 physically interact in pull-down experiments using yeast (*108*) and human (*110*) mitochondrial extracts. Iron-dependent Fxn-Isu interactions are further supported by genetic studies in yeast (*111*) and biophysical experiments on recombinant human proteins (*16*). Isu-Nfs1 interactions are defined by a crystal structure of the homologous *E. coli* IscU-IscS complex (*44*). In eukaryotes, an additional protein, Isd11, is also known to complex with Nfs1 and is vital for Nfs1 function (*49, 50, 112*). Deletion of genes encoding Nfs1, Isd11, Isu1, or Fxn in *Saccharomyces cerevisiae* produces similar phenotypes that include defects in Fe-S cluster proteins (*50, 113*). These data hint at a multiprotein complex that functions as a Fe-S cluster assembly machine. Here *in vitro* evidence is presented that the foundation for the human Fe-S cluster assembly machine is made up of a Nfs1, Isd11, Isu2, and Fxn protein complex. In addition, kinetic data is provided that supports a role for human Fxn as an allosteric switch that activates this complex for Fe-S cluster biosynthesis.

EXPERIMENTAL PROCEDURES

Protein Expression and Purification. Plasmids containing human Nfs1 (Δ1-55) and Isd11 (pZM4) were generously provided by S. Leimkühler (*48*). The Nfs1 and Isd11 plasmids were transformed into *E. coli* strain BL21(DE3) for coexpression. Cells were grown at 37 ^{o}C until they reached an OD_{600} of 0.6; the temperature was decreased to 16 ^{o}C, and protein expression was induced with 0.1 mM isopropyl β-D-1-thiogalactopyranoside (IPTG). Cells were harvested 16 h later by centrifugation in 3,500 *g* at 4 ^{o}C for 20 min and transferred to a temperature-controlled (10−15 ^{o}C) anaerobic glovebox (mBraun). Cells were resuspended in 100 mL of Buffer A [50 mM Tris (pH 8.0)] with 500 mM NaCl, 5 mM imidazole, and 100 μM pyridoxal 5'-phosphate (PLP) and ruptured by sonication (Branson sonifier 450, 30 sec ×9, 3 min off). The cell lysate was transferred into centrifuge bottles with O-ring gaskets and centrifuged in 18,000 *g* at 4 ^{o}C for 20 min. The soluble protein was loaded onto a Ni-NTA column (16/13, GBiosciences) and eluted with a linear gradient from 5 to 250 mM imidazole. Yellow fractions were concentrated by Amicon in the glovebox, combined with 100 μM PLP, 5 mM dithiothreitol (DTT), and 2 mM EDTA, and loaded onto a Sephacryl S300 column (26/60, GE) equilibrated in buffer A with 250 mM NaCl. Fractions containing Nfs1 (47 kDa) and Isd11 (11 kDa) were > 95% pure as determined by 14% SDS-PAGE. Protein concentrations were estimated by the Bradford assay (*114*) or using an extinction coefficient of 42670 $M^{-1}cm^{-1}$ at 280 nm (*115*). The yield of Nfs1 and Isd11 was 3 mg/L of cells. Nfs1/Isd11 protein complex (SD) was then aliquoted and frozen in liquid nitrogen and stored at – 80 ^{o}C freezer until use.

The human Isu2 (Δ1-35) and Fxn (Δ1-55) genes were codon-optimized for *E. coli*, synthezied by IDT, and subcloned into pET11a vectors. The resulting plasmids were transformed into *E. coli* BL21(DE3) cells, which were grown at 37 ^{o}C. Protein expression was induced at an OD_{600} of 0.6 with 0.5 mM IPTG. Cells were harvested 5 h later and sonicated (45 sec × 6, 3 min off on ice) in 100 mL of buffer B [50 mM Tris (pH 7.5)]. The cell lysate was centrifuged in 18,000 *g* at 4 ^{o}C for 20 min.

For Isu2 purification, the soluble protein was applied to an anion exchange column (26/22, POROS 50HQ, Applied Biosystems), and the flow-through was collected (Isu2 does not bind, pI ≈ 8.9) and loaded onto a cation exchange column (16/14, POROS 50HS, Applied Biosystems). Isu2 was eluted with a linear gradient from 0 to 400 mM NaCl in buffer B. Isu2 fractions (14 kDa, ran around 17 kDa on 14% SDS−PAGE) were concentrated by Centricon or Amicon and further purified with a Sephacryl S300 column (26/60) equilibrated in buffer C (50 mM HEPES, pH 7.5, 150 mM NaCl). An extinction coefficient of 8250 $M^{-1}cm^{-1}$ at 280 nm (*115*) was used to estimate the protein concentration. This procedure yielded 4 mg of > 95% pure Isu2/L of cells. Isu2 protein was then aliquoted and frozen in liquid nitrogen and stored at – 80 ^{o}C freezer until use.

For Fxn purification, cells were resuspended in 100 mL of buffer B and ruptured by sonication (45 sec × 6, 3 min off) on ice. The cell lysate was centrifuged in 18,000 *g* at 4 ^{o}C for 20 min. The soluble fraction was loaded onto an anion exchange column (26/22, POROS 50HQ) and eluted with a linear gradient from 0 to 800 mM NaCl in buffer B. The monomeric Fxn fractions (monitored by 14% SDS-PAGE) were collected

and further purified on a S300 gel filtration column equilibrated in buffer C. The fractions containing full-length (residues 56-210, 17 kDa) and truncated (residues 82-210, 14 kDa) Fxn were collected and further purified by anion exchange column (26/22) using a linear gradient from 120 to 250 mM NaCl in buffer B. Full-length and truncated Fxn were collected separately and confirmed by N-terminal sequencing. Truncated Fxn was used for all experiments (unless stated otherwise). An extinction coefficient of 26030 $M^{-1}cm^{-1}$ at 280 nm (*115*) was used to estimate the protein concentration. This procedure yielded 6 mg of > 95% pure truncated Fxn/L of cells.

Cysteine Desulfurase Activity Measurements. Sulfide production for SD was measured using slight modification to a methylene blue assay described by Leimkühler and co-workers (*48, 116*). Assay mixtures in a total volume of 0.8 mL contained 1 μM SD, 10 μM PLP, 2 mM DTT, 50 mM Tris (pH 8.0), and 250 mM NaCl. The reactions were initiated by addition of L-cysteine (0.1−1.0 mM) and the mixtures incubated at 37 ^{o}C. Sulfide production was linear for the first 30 min, and an incubation time of 10 min was chosen to generate sufficient product for straightforward detection. Assays were quenched by addition of 100 μM of 20 mM *N*,*N*-dimethyl-*p*-phenylenediamine in 7.2 N HCl and 100 μL of 30 mM $FeCl_3$ in 1.2 N HCl. After being incubated for 20 min to allow for methylene blue synthesis, the samples were centrifuged at 12,000 *g* for 5 min at room temperature, and the absorbance at 670 nm was converted to a sulfide concentration using a standard curve (0−70 μM Na_2S).

Similarly, cysteine desulfurase activities were measured for SD after 30 min anaerobic incubation with 3 equiv. of Isu2 or Fxn. In a separate experiment, 3 equiv. of

Isu2 and Fxn were incubated with SD for 30 min prior to initiation of the reaction with L-cysteine (2.5−200 μM). Michaellis−Menten kinetics for the cysteine desulfurase reaction were also examined for the protein components in the presence of 10 equiv of $Fe(NH_4)_2(SO_4)_2$. All the reactions with $Fe(NH_4)_2(SO_4)_2$ were sealed in round-bottom flask to maintain their anaerobic condition. Reaction rates as a function of cysteine concentration were fit to the Michaelis–Menten equation using KaleidaGraph (Synergy Software).

The cysteine desulfurase activity was also determined at a "physiological" (0.1 mM) cysteine concentration with 1 μM SD alone, and with 3 equiv of Isu2 and/or Fxn. For the Fe titration, the proteins were diluted by a factor of 2 and 0–5 μM $Fe(NH_4)_2(SO_4)_2$ was added. To assess if other metal ions also stimulated cysteine desulfurase activity, the assay of SD with 3 equiv of both Isu2 and Fxn was repeated in the presence of 10 equiv of $MnCl_2$, $FeCl_3$, $CoSO_4$, $NiCl_2$, $CuSO_4$, $Zn(OAc)_2$, $Ca(OAc)_2$, or $MgCl_2$.

Fe–S Cluster Formation Assay. Assay mixtures in 0.25 mL contained 8 μM SD, 24 μM Isu2, 100 μM $Fe(NH_4)_2(SO_4)_2$, 3 mM DTT, and 0–16 μM Fxn in 50 mM Tris (pH 7.4) with 250 mM NaCl. The assay mixture was incubated in an anaerobic glovebox for 30 min before the reaction was initiated with 0.1 mM L-cysteine. Fe–S cluster formation was monitored at 456 nm for 90 min. Units are defined as the amount of Isu2 required to produce 1 μmol of Fe–S cluster per minute at 25 ^{o}C. An extinction coefficient of 5.8 $mM^{-1}cm^{-1}$ was used for $[Fe_2S_2]$ cluster absorption (*117*). The rate of Fe–S cluster

formation was fit to first-order kinetics by using Agilent UV-Visible ChemStation Software.

Protein Complex Determination. Assays included 40 μM SD, 120 μM Isu2, 120 μM Fxn, 10 mM DTT, 10 mM EDTA, 0.8 mM $Fe(NH_4)_2(SO_4)_2$, 100 mM HEPES (pH 7.5), and 50 mM NaCl. Samples were incubated for 30 min in an anaerobic glovebox and evaluated for protein complex formation using blue native gels (*118*) that contained 6.5% separating and 5% stacking layers. The gel running buffer was chilled. Titration experiments with Fxn and Isu2 were performed using the same procedure except the titrant concentration was varied from 5 to 120 μM. The amount of protein on the native gel was estimated by densitometry; gels were scanned with a Typhoon Trio Imager and analyzed with ImageQuant Software (Protein Chemistry Lab, Department of Biochemistry and Biophysics, TAMU). The slower migration band was cut out of the native gel and dehydrated with 66% acetonitrile in 25 mM ammonium bicarbonate (ABC) (pH 8). The protein was extracted by incubation with 0.1% SDS and 10 mM ABC (pH 8) for 30 min at room temperature and mixed with an equal volume of 66% acetonitrile and 25 mM ABC (pH 8). The solution was centrifuged in 12,000*g* for 5 min. The supernatant was concentrated with a speed-vac to about 12 μL, and the protein was analyzed by 14% SDS-PAGE.

Protein Complex Isolation. SD was incubated with 3 equiv of Isu2 and Fxn, 2 equiv of PLP, 5 mM Tris(2-carboxyethyl)phosphine (TECP) or DTT, and 50 mM Tris (pH 7.4) with 50 mM NaCl buffer for 30 min in an anaerobic glovebox. The Nfs1, Isd11, and Isu2 complex (SDU) and the Nfs1, Isd11, Isu2, and Fxn complex (SDUF) were

loaded onto a Sephadex S200 gel filtration column (16/30, GE) and compared to molecular weight standards (Bio-Rad) included bovine thyroglobulin (670 kDa), bovine γ–globulin (158 kDa), chicken ovalbumin (44 kDa), horse myoglobin (17 kDa), and vitamin B_{12} (1.4 kDa). SDU and SDUF were also further purified on a cation exchange column and eluted with a linear gradient from 150 to 1000 mM NaCl in buffer B. Protein complexes were confirmed by 14% SDS-PAGE.

RESULTS

Isu2 and Frataxin Stimulate Nfs1 and Isd11 Cysteine Desulfurase Activity. Human recombinant Fxn and Isu2 were assayed for their ability to alter the kinetics of the cysteine desulfurase for Fe–S cluster assembly biosynthesis. In this assay, substrate cysteine was converted to alanine and the resulting persulfide intermediate was reduced with DTT and detected as sulfide. In the absence of additional proteins, purified human recombinant SD exhibited Michaelis–Menten kinetics (Figure 2-1) for sulfide production with a Michaelis constant (K_M) of 0.34 mM for cysteine and a k_{cat} of 1.9 min^{-1} (Table 2-1). The resulting catalytic efficiency (k_{cat}/K_M) of 93 $M^{-1}s^{-1}$ for recombinant human SD was nearly identical to a previously reported value (*48*) of 96 $M^{-1}s^{-1}$. The kinetics parameter k_{cat} and K_M were not significantly changed upon addition of Fxn to SD. In contrast, the k_{cat} was lowered by a factor of 2 and the K_M nearly doubled upon addition of Isu2 to SD (Table 2-1).

Both the k_{cat} and the K_M were dramatically altered by the addition of Fxn to SD in

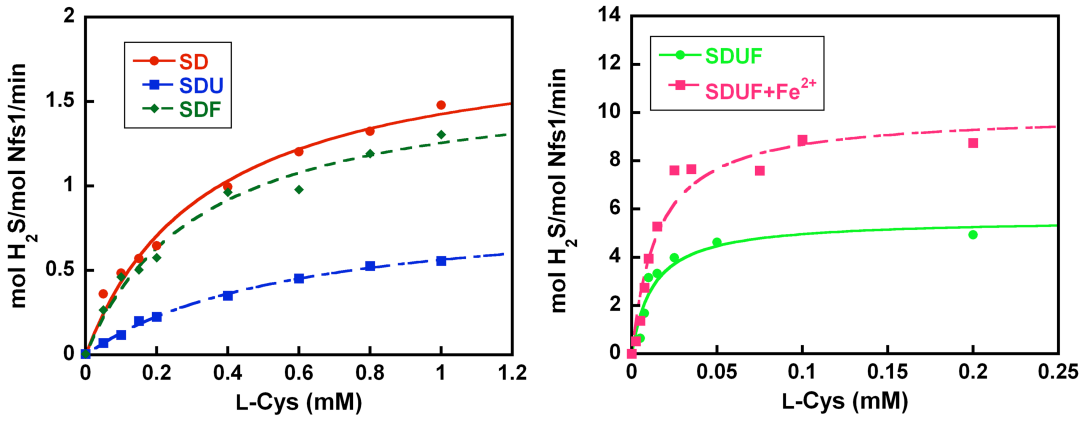

FIGURE 2-1: Human cysteine desulfurase Nfs1 activity with (A) Isu2 or Fxn. (B) Isu2 and Fxn in the absence or presence of ferrous iron

Table 2-1: Rate Constants for Human Nfs1 activity with Isu2 and Fxn

Complexes	k_{cat} (min^{-1})	K_M^{cys} (mM)	k_{cat}/K_M ($M^{-1}s^{-1}$)
Nfs1/Isd11 (SD)	1.9 ± 0.1	0.34 ± 0.06	93 ± 17
SD + Fxn	1.7 ± 0.1	0.33 ± 0.06	86 ± 16
SD + Isu2	0.89 ± 0.04	0.59 ± 0.05	25 ± 10
SD + Isu2 + Fxn	5.2 ± 0.4	0.011 ± 0.003	7900 ± 2200
SD + Isu2 + Fxn + Fe^{2+}	10.7 ± 1.0	0.017 ± 0.005	10500 ± 1500

the presence of Isu2, which resulted in an increase in the catalytic efficiency from 25 to 7900 $M^{-1}s^{-1}$ (Table 2-1). This increase in catalytic efficiency was due to a nearly 6-fold faster k_{cat} for sulfide production and a change in K_M for cysteine from 0.59 to 0.011 mM. Because the physiological concentration of cysteine in eukaryotic cells is thought to be

0.1 mM (*119-121*), the cysteine desulfurase activities were determined at this concentration to mimic cellular conditions. The sulfide production activity for SD was similar when either Isu2 or Fxn was individually added but dramatically increased when both were present (Figure 2-2A). Together, these data indicate that Fxn greatly stimulates the cysteine desulfurase in an Isu2-dependent manner, facilitating catalysis at physiological cysteine concentrations.

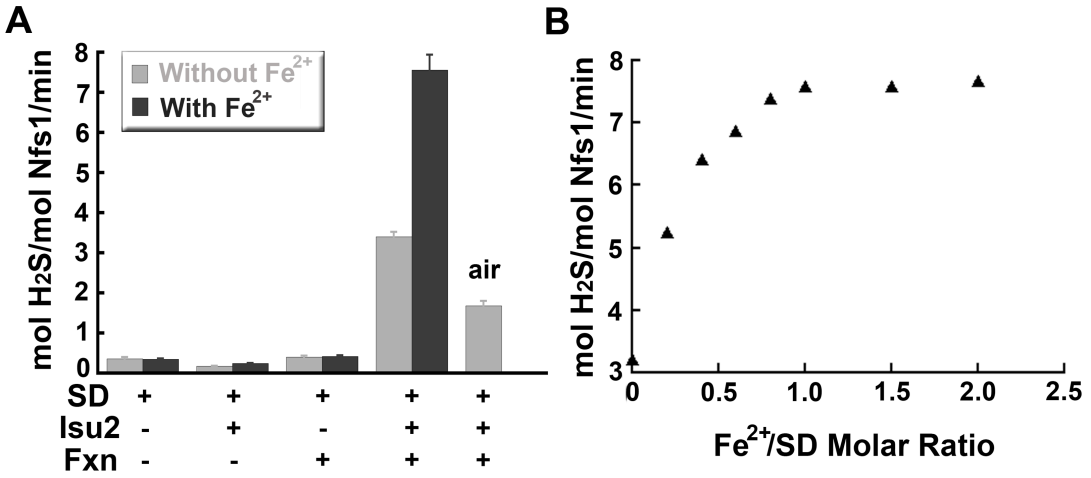

FIGURE 2-2: Frataxin and ferrous iron stimulate cysteine desulfurase activity. (A) Rates of SD sulfide production were determined in the presence of 3 equivalents of Isu2, 3 equivalents of Fxn, and either 0 or 10 equivalents of ferrous iron. Equivalents are calculated based on the concentration of SD. For the oxidized sample, SD was incubated with Isu2 and Fxn for 30 minutes in air and then the reaction was initiated with cysteine and DTT. Error bars are for three independent measurements. (B) Rates of sulfide production were determined for SD in the presence of 3 equivalents of Isu2 and Fxn, and increasing amounts of ferrous iron.

Given the iron dependent of Fxn–Isu interactions (*16, 108, 122*), the ferrous iron dependence of the kinetics of sulfide production was explored. Iron had little effect on the cysteine desulfurase activities of SD, SD with Isu2, and SD with Fxn (Figure 2-2A). In contrast, iron stimulated the activity of SD when both Isu2 and Fxn were present; kinetics analysis revealed that this increase in activity was due to a doubling of the k_{cat} rate rather than a significant change in the K_M (Table 2-1). A reaction mixture containing SD, Isu2, and Fxn was titrated with iron, and the maximal activity was achieved after the addition of 1 equiv of iron (Figure 2-2B). A similar SD, Isu2, and Fxn reaction was not

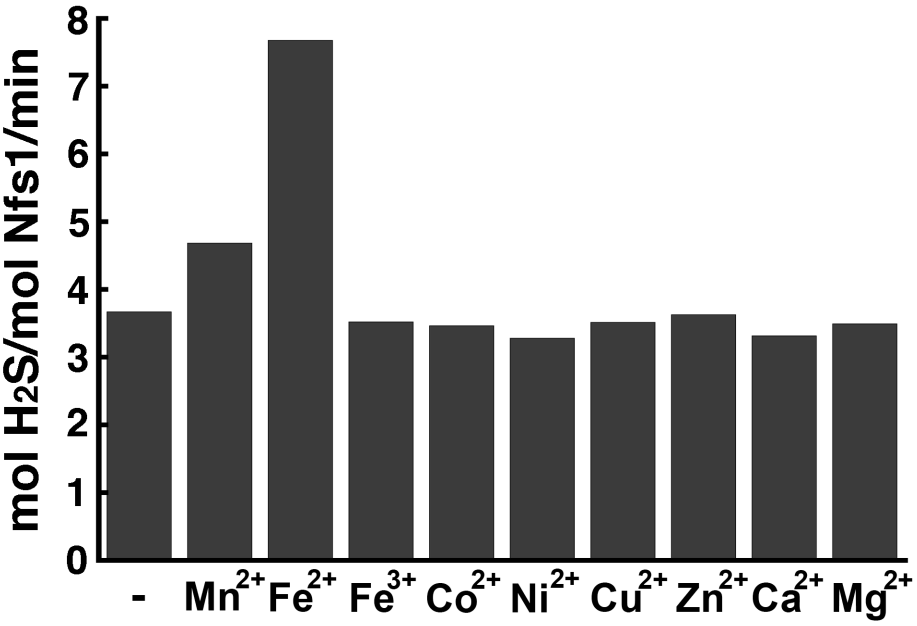

FIGURE 2-3: Stimulation of cysteine desulfurase activity by metal ions. Rates of sulfide production were determined for SD in the presence of 3 equivalents of Isu2 and Fxn, and 10 equivalents of metal ions.

significantly stimulated by ferric iron and other first row transition metals, with the possible exception of Mn^{2+} (Figure 2-3). Together, these data indicate that both Isu2 and Fxn are necessary for the activation of the SD cysteine desulfurase, which can be further stimulated by 1 equiv of ferrous iron.

Human Frataxin Accelerates Fe–S Cluster Assembly. Fe–S cluster biosynthesis rates were determined by following the increase in absorbance at 456 nm, commonly used to monitor [Fe_2S_2] cluster formation (*117*), in the presence of 0.1 mM cysteine and 0.1 mM Fe^{2+}. An assay containing SD with Isu2 exhibited a specific activity of 0.0027 unit/mg, whereas addition of Fxn increased the rate by a factor of 25 (Figure 2-4A).

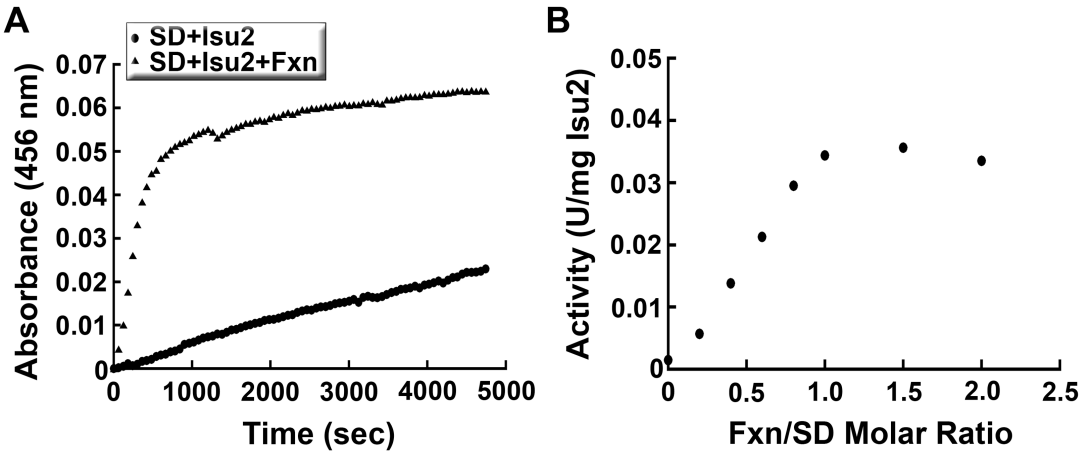

FIGURE 2-4: Frataxin accelerates the rate of Fe-S biosynthesis. (A) Fe-S cluster formation was monitored by an increase in absorbance at 456 nm as a function of time. Assays included SD with 3 equivalents of Isu2, and SD with 3 equivalents of both Isu2 and Fxn. (B) The rate of Fe-S biosynthesis was determined as a function of added Fxn.

Titration of Fxn into a reaction mixture containing SD and Isu2 revealed that the specific activity increased linearly with added Fxn and was maximal after the addition of 1 equiv of Fxn and SD (Figure 2-4B). These results revealed that Fxn stimulates formation of Fe–S clusters on Isu2 and indicated that Fxn functions as an activator for human Fe–S cluster biosynthesis.

Human Nfs1, Isd11, Isu2, and Fxn Form a Multiprotein Complex. Because Isu2 and Fxn together dramatically changed the kinetic parameters of the cysteine desulfurase (Table 2-1), we hypothesized that Nfs1, Isd11, Isu2 and Fxn may form a multiprotein complex. To test this hypothesis, SD, Isu2, and Fxn were incubated with 5–10 mM DTT in an anaerobic glove box for 30 min and then tested for protein–protein interactions using native gel electrophoresis (Figure 2-5A). Addition of all four proteins resulted in the appearance of a slower migrating band compared to Fxn on the native gel that was consistent with formation of a protein complex. The slower migrating band was dependent upon the presence of each of the protein components (Figure 2-5A). This protein complex formed in the presence of 10 mM EDTA and the addition of ferrous iron had no obvious affect on band intensity. Cutting this band out of the native gel and analyzing with SDS–PAGE revealed the presence of all four added proteins (Figure 2-5B). This slower migrating band on the native gel was therefore associated with a non-covalent Nfs1, Isd11, Isu2, and Fxn protein complex (SDUF) that was stable in the presence of metal chelators.

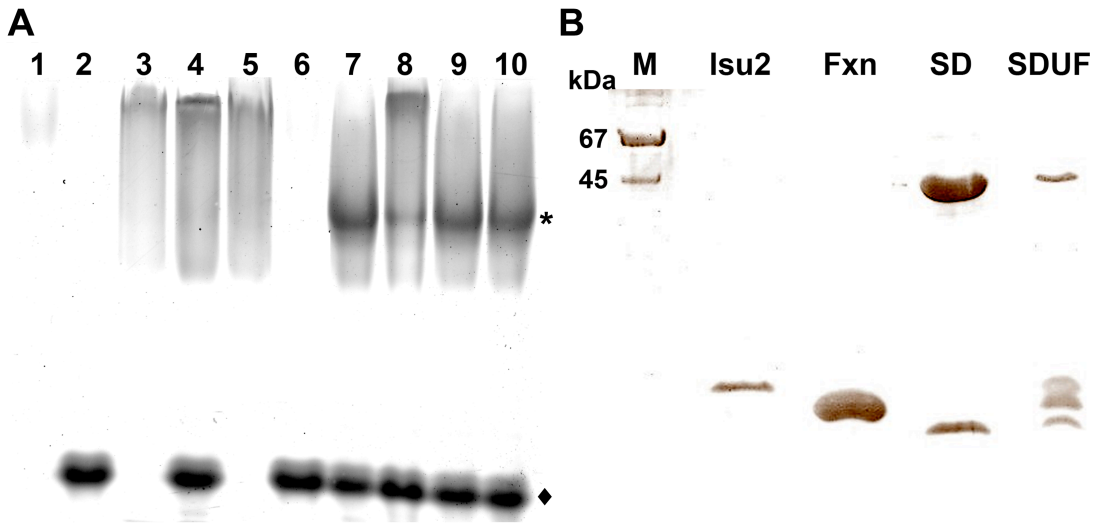

FIGURE 2-5: Nfs1/Isd11, Isu2, and Fxn form a multiprotein complex. (A) Native gel showing protein requirements for complex formation. Lane1: Isu2 (Isu2 has an estimated pI of 8.9 and is difficult to observe under the native gel conditions); 2: Fxn; 3: SD; 4: SD + Fxn; 5: SD + Isu2; 6: Isu2 + Fxn; 7: SD + Isu2 + Fxn; 8: SD + Isu2 + Fxn - DTT; 9: SD + Isu2 + Fxn + EDTA; 10: SD + Isu2 + Fxn + Fe^{2+}. An asterisk (*) and diamond (♦) mark the positions of the slower migrating band and Fxn, respectively. (B) SDS-PAGE gel showing the protein components of the slower migrating band. The band from (A) was extracted and analyzed by SDS-PAGE.

Next, protein titration experiments were performed to probe the requirements for complex formation and provide an indication of the subunit stoichiometry. First, 0–3 equiv of Fxn was added to a mixture of SD and 3 equiv of Isu2, followed by native gel electrophoresis to monitor SDUF formation (Figure 2-6A). The slower migrating band was not observed in the absence of Fxn, increased in intensity with added Fxn, and was maximal after the addition of 1 equiv of Fxn (Figure 2-6B). Similarly, Isu2 was titrated into a mixture of SD and 3 equiv of Fxn (Figure 2-7A). The slower migrating band was not formed in the absence of Isu2, increased with added Isu2, and was maximal after the

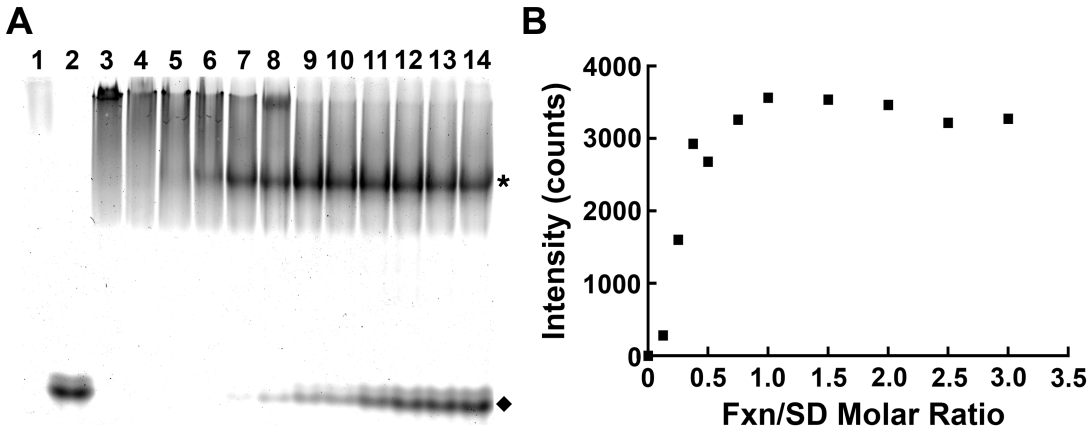

FIGURE 2-6: Fxn induces formation of the SDUF complex. (A) Native gel showing SDUF complex formation with added Fxn. Lane 1: Isu2; 2: Fxn; 3: SD; 4-14: SD + Isu2 with 0-3 equivalents of Fxn. An asterisk (*) and diamond (♦) mark the positions of the SDUF and Fxn, respectively. (B) One equivalent of Fxn is required to form the SDUF complex. Densitometry was used to quantitate the SDUF band from (A).

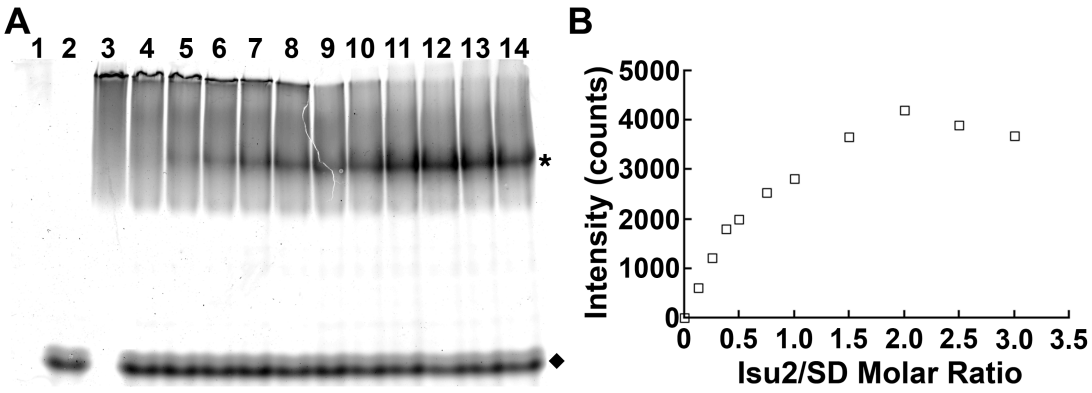

FIGURE 2-7: Isu2 induces formation of the SDUF complex. (A) Native gel showing SDUF complex formation with added Isu2. Lane 1: Isu2; 2: Fxn; 3: SD; 4-14: SD + Fxn with 0-3 equivalents of Isu2. An asterisk (*) and diamond (♦) mark the positions of the SDUF and excess Fxn, respectively. (B) Densitometry was used to quantitate the SDUF band from (A).

addition of 2 equiv of Isu2 (Figure 2-7B). These experiments further supported SD, Isu2, and Fxn as components of the protein complex associated with the slower migrating band and placed an upper limit on the stoichiometry at one Fxn and two Isu2 subunits for each SD.

Oxidizing Conditions Inhibit Complex Formation. The redox requirements for complex formation and Fxn-dependent activation were determined. First, a native gel assay was used to determine that in the absence of a reducing agent (DTT or TCEP), the intensity of the slower migrating band was diminished (Figure 2-5A, lane 8). Second, a SD sample was incubated with Isu2 and Fxn in air for 30 min, DTT and cysteine were added, and the cysteine desulfurase activity was measured. This air-oxidized sample exhibited diminished cysteine desulfurase activity compared to the equivalent anaerobic sample with all four components (Figure 2-2A). Together, the data indicated a correlation between SDUF formation and activation of the Fe–S cluster assembly machinery that was influenced by redox conditions.

Nfs1, Isd11, Isu2, and Fxn Form ~ 150–180 kDa Complexes. Analytical gel filtration chromatography was used to estimate the oligomeric state and molecular weight of the human proteins and complexes. SD, Isu2, and Fxn exhibited retention times consistent with estimated molecular weights of 150, 17, and 17 kDa, respectively (Figure 2-8A). Gel filtration chromatographic analysis of SD incubated with both Isu2 and Fxn revealed an apparent 180 kDa species (Figure 2-8A). SDS–PAGE analysis revealed the presence of Nfs1, Isd11, Isu2 and Fxn (Figure 2-8B), which was consistent

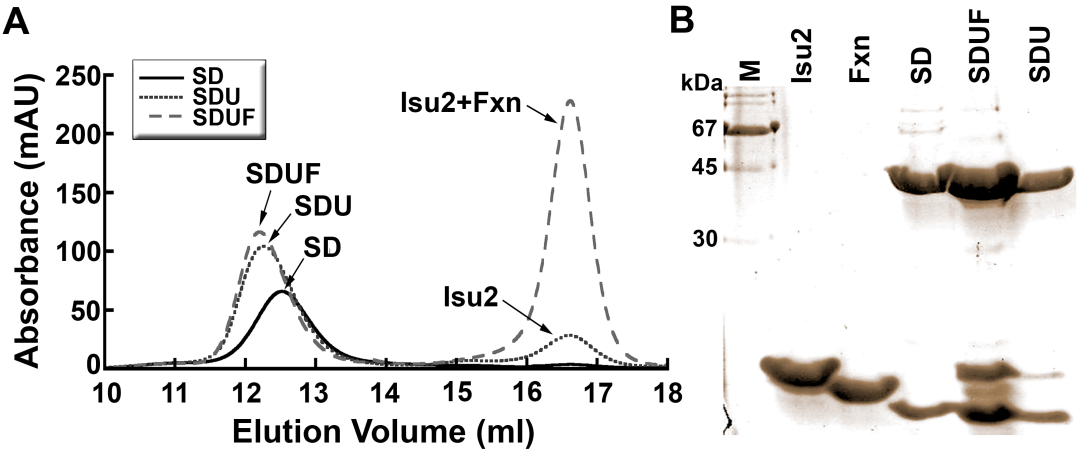

FIGURE 2-8: Molecular mass estimates and protein components for SD, SDU, and SDUF complexes. (A) Three equivalents of Isu2 were added to SD to generate the SDU complex. Three equivalents of both Isu2 and Fxn were added to SD to form the SDUF complex. Samples were analyzed with anaerobic gel filtration chromatography. (B) SDS-PAGE analysis of Fe-S cluster assembly complexes confirms protein components.

with SDUF. Interestingly, gel filtration analysis of a SD sample incubated with Isu2 resulted in a slightly different retention time and an estimated molecular weight of 170 kDa (Figure 2-8A). SDS–PAGE analysis of the 170 kDa fractions revealed the presence of Nfs1, Isd11, and Isu2, consistent with SDU. In contrast, a similar experiment with SD incubated with Fxn provided no evidence of SDF (Nfs1, Isd11, and Fxn protein complex). The formation of SDU and not SDF was consistent with the perturbation of the SD kinetic parameters upon addition of Isu2 or Fxn (Table 2-1). No higher-molecular weight species or aggregate, such as oligomeric Fxn, was observed in these experiments. These gel filtration results were consistent with human Nfs1, Isd11, and

Isu2 assembling into SDU, and Nfs1, Isd11, Isu2, and Fxn assembling into SDUF in which Fxn binding depends on the presence of Isu2.

DISCUSSION

Human Fe–S cluster assembly proteins were isolated and conditions discovered for forming previously uncharacterized SDU and SDUF comprised of Nfs1, Isd11, and Isu2 and Nfs1, Isd11, Isu2, and Fxn, respectively. Previously, a protein complex was proposed for Fe–S cluster biosynthesis in yeast that included oligomeric rather than monomeric Fxn (*123*). Gel filtration results presented here (Figure 2-8A) revealed no evidence of oligomeric Fxn and confirmed human Fxn is in the monomeric form. Together, these data suggest that SDU and SDUF have molecular weights of approximately 170–180 kDa, represent distinct functional states for Fe–S cluster biosynthesis (see below), and are the mechanistically relevant species for future study.

SDU is essentially inactive at physiological cysteine concentrations. The concentration of cysteine in mouse liver or brain homogenates is reported to be 0.1 mM (*119*). The concentration of cysteine in rate liver mitochondria was originally undetectable (*124, 125*), but recent studies revealed a concentration of 0.07 mM (*121*). Kinetics analysis of human SDU (SD and Isu2) using 0.1 mM cysteine revealed very low sulfide production and Fe–S cluster biosynthetic activities (Figure 2-2A and 2-4A). The modest activities are explained by the low "physiological" substrate concentration (0.1 mM) compared to the high K_M (0.59 mM) for human SDU. We proposed SDU is in the "off" state for Fe–S cluster assembly.

Binding of Fxn to SDU generates an ~180 kDa SDUF species with a possible $\alpha_2\beta_2\gamma_2\delta_2$ stoichiometry. A recent crystal structure revealed that a bacterial IscS (Nfs1 homologue) binds to IscU (Isu2 homologue) with an elongated $\alpha_2\beta_2$ stoichiometry (*44*). Titration results indicated that each Nfs1 binds a maximum of one Fxn (Figure 2-6B). If we assume each Nfs1 also binds one Isd11, the resulting $\alpha_2\beta_2\gamma_2$ for SDU and $\alpha_2\beta_2\gamma_2\delta_2$ for SDUF have calculated molecular weights of 144 and 172 kDa, respectively, which are close to the estimated masses (170 and 180 kDa, respectively) determined by gel filtration chromatography (Figure 2-8A). The similar retention times for SDU and SDUF are consistent with the elongated architecture for the bacterial IscS–IscU structure, and a model suggesting a more globular IscS–IscU–Fxn species (*44*). Together, these results suggest $\alpha_2\beta_2\gamma_2$ SDU and $\alpha_2\beta_2\gamma_2\delta_2$ SDUF stoichiometries but do not rule out alternate stoichiometries with additional Isd11 and Isu2 molecules.

Fxn binding and stimulation of cysteine desulfurase activity are reminiscent of sulfur acceptor proteins in bacterial systems. Fxn binding to SDU increased the sulfide production activity 20-fold (Figure 2-2A). Stimulation of cysteine desulfurases by binding partners is well-known. In *E. coli*, IscS activity is stimulated 6-fold by IscU binding (*89*) and SufS activity is increased 50-fold by SufE interactions (*126*). SufE is a sulfur transfer protein (*92*) that is structural similar to IscU (*127*). In *bacillus subtilis*, the scaffold apo-protein SufU stimulated SufS activity 40-fold, whereas the cluster-bound SufU stimulated SufS at a much lower level (*128*). Cysteine desulfurases are also stimulated by molecular chaperones involved in Fe–S cluster assembly (*129*) and proteins involved in tRNA (*130*) and molybdopterin (*42*) biosynthesis.

Fxn binding activates SDU, possibly through a conformational change. Fxn binding increased the k_{cat} nearly 6-fold and decreased the K_M for cysteine by more than 50-fold (Table 2-1). Because there is no evidence that Fxn directly participates in cysteine desulfurase catalysis, we suggest Fxn acts indirectly as an allosteric activator and induces a conformational change that positions Nfs1 persulfide loop and a conserved cysteine on Isu2 for direct sulfur transfer and Fe–S cluster biosynthesis. In this model (Figure 2-9), Fxn binding to SDU switches the Nfs1 flexible loop from a nonfunctional to a catalytic conformation, which enhances substrate binding and lowers the K_M for cysteine. We hypothesize that Fxn binding to SDU also induces a conformational change in Isu2 that facilitates the transfer of sulfur from Nfs1 and thereby increases the cysteine turnover number (k_{cat}). The persulfide cleavage or sulfur transfer step is the rate-limiting step in other cysteine desulfurases (*45*). Regardless of the molecular details, the binding of Fxn to SDU dramatically increases the catalytic efficiency of the complex and essentially turns the assembly system "on" for Fe-S cluster biosynthesis at physiological cysteine concentrations.

Iron enhances the ability of Fxn to activate the cysteine desulfurase. The addition of ferrous iron to SDUF doubles the k_{cat} but had minimal effects on the K_M for cysteine (Table 2-1). The maximum stimulation was observed after the addition of 1 equiv of iron (Figure 2-2B). Previously, 1 equiv of iron was shown to be required for Fxn and Isu interactions (*16, 80*). Iron does not appear to be required for the formation of SDUF (Figure 2-5A, lane 9 and 10), but a role for iron in complex stabilization has not been evaluated. The addition of ferric iron or most of the first row transition metals did not

significantly increase the cysteine desulfurase activity (Figure 2-3). The one exception is Mn^{2+}, which slightly activated (128% of the control) the cysteine desulfurase activity and is a good mimic of ferrous iron. This result is consistent with Fe^{2+}, and possibly Mn^{2+}, functioning in conjunction with Fxn to accelerate the sulfur transfer step in catalysis, possibly by inducing a conformational change in Isu2.

The addition of Fxn to SDU accelerated the rate of Fe-S cluster biosynthesis 25-fold at physiological cysteine concentrations. In this experiment (Figure 2-4A), the absorbance maximized after a calculated 12 μM [Fe_2S_2] cluster was formed, which is approximately the concentration (8 μM) of SDUF. This calculation is based on the assumption that the absorbance at 456 nm is due to [Fe_2S_2] clusters with an extinction coefficient of 5.8 $mM^{-1}cm^{-1}$ (*117*); this [Fe_2S_2] cluster assignment should be viewed as tentative until it is supported by additional spectroscopic studies. Strikingly, addition of Fxn to SDU results in mirrored increases in the rate of Fe–S cluster biosynthesis (Figure 2-4B) and the amount of SDUF formation (Figure 2-6B), with both exhibiting a maximum effect after the addition of 1 equiv of Fxn. These data strongly support a model in which Fxn is an activating component of the core Fe–S cluster assembly machine (Figure 2-9).

An allosteric activator role for Fxn in Fe–S cluster biosynthesis is consistent with most previous studies. This newly discovered function for Fxn is consistent with *in vivo* experiments that show Fxn depletion results in the loss of activity for Fe–S cluster enzymes (*103, 104*). Enzyme assay results (Figure 2-4) indicate that SDU is still able to

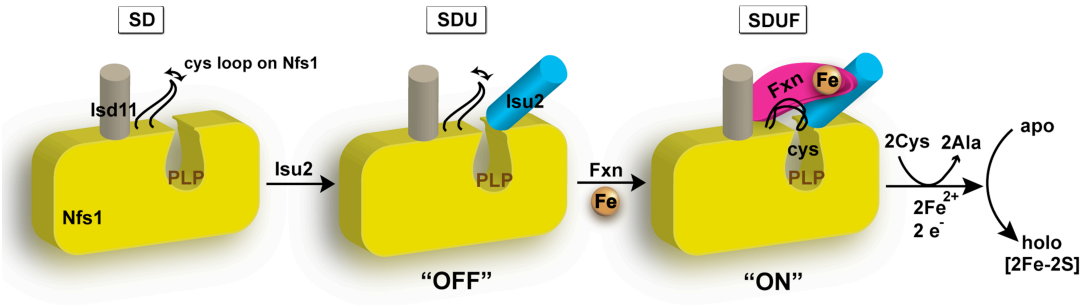

FIGURE 2-9: Working model for Fxn activation of the Fe-S cluster assembly complex. The Nfs1 flexible loop is stabilized in a non-functional conformation for the SD and SDU complexes. Fxn binding favors the catalytic loop conformation, enhances substrate binding, and accelerates persulfide bond formation. Fxn and Fe binding also induce a conformational change in Isu2 that accelerates sulfur transfer from Nfs1 to Isu2 for Fe-S cluster biosynthesis.

synthesize Fe–S clusters in the absence of Fxn, albeit at a much lower rate. This explains the residual level of Fe-S enzyme activity in Fxn-depleted yeast mitochondria (*107*). A role for Fxn as an allosteric activator for Fe-S cluster biosynthesis is also consistent with the neurodegenerative and cardiovascular impairment in Friedreich's ataxia (FRDA). FRDA patients with low frataxin levels would be expected to contain only residual or "unactivated" levels of Fe-S cluster biosynthesis, have depleted Fe-S clusters in their respiratory chain, and exhibit mitochondrial dysfunction. Because heart and brain tissue are especially rich in mitochondria, these tissues are particularly susceptible to Fxn deficiencies and Fe-S cluster defects. This allosteric activator role for human Fxn is in contrast to studies of the *E. coli* homologue that suggest Fxn functions as an inhibitor for Fe-S cluster biosynthesis (*80*). An allosteric activator function for Fxn does not

necessarily rule out other functions, such as mediating iron delivery for Fe-S cluster synthesis.

Fxn levels *in vivo* may be used to regulate the Fe-S cluster assembly activity in response to environment stimuli. The results presented here clearly indicate Fxn is an activating component for SDUF Fe-S cluster assembly complex. What is unclear is if Fxn protein levels are controlled by environmental cues as a mechanism for regulating Fe-S cluster biosynthesis. Fxn protein levels are known to vary by a factor of > 3 in normal individuals (*131*). Two possible environmental stimuli are iron and oxidative stress. Iron regulates Fxn expression (*81*) and stimulates Fe-S cluster biosynthesis in a Fxn-dependent manner (Figure 2-2B). Oxidative stress results in chemical modification of Fxn (*86*), whereas oxidizing conditions weaken SDUF formation (Figure 2-5A, lane 8) and Fxn-based activation (Figure 2-2A). Additional experiments are required to determine if these or other environmental stimuli are part of a regulatory mechanism that uses Fxn to modulate Fe-S cluster biosynthesis.

Here we establish that a four-protein component complex that includes Nfs1, Isd11, Isu2, and Fxn is capable of synthesizing Fe-S clusters. Future studies are required to clarify if this SDUF interacts transiently with additional biosynthetic components, such as the electron donor (ferredoxin) and iron donor machinery, or if an even larger assembly complex is formed. Additional studies are also required to determine if the molecular chaperones, which facilitate transfer of Fe-S cluster to apo target proteins, interact with SDUF, a subcomplex such as SDU, or dissociated holo-Isu2. In addition, few details are currently available for the mechanisms of human [Fe_2S_2] and [Fe_4S_4]

cluster assembly, target recognition, and cluster transfer. The results presented here provide strong evidence that SDU and SDUF represent the off and on states for Fe-S cluster biosynthesis, respectively, lead to testable hypotheses for cellular regulation of Fe-S cluster assembly, and provide a foundation for addressing these mechanistic questions.

CHAPTER III

FRATAXIN-DEPENDENT SULFUR TRANSFER MECHANISM FOR THE HUMAN FE-S CLUSTER BIOSYNTHETIC COMPLEX

INTRODUCTION

Sulfur is a critical element for all life forms and is found in a variety of protein cofactors including molybdopterins, lipoic acid, thiamin, biotin, and iron-sulfur clusters. Even though these cofactors are functionally well understood, mechanistic details are just emerging for how sulfur is incorporated into these biomolecules (*41, 132*). A common early step for these pathways is the cysteine desulfurase dependent degradation of cysteine to alanine and generation of a protein-bound persulfide species. The activated persulfidic sulfur is reductively cleaved by distinct acceptor proteins for the biosynthesis of sulfur-containing cofactors and modification of tRNA (*41*). Redox agents such as cysteine and DTT (*in vitro*) can also release the persulfidic sulfur in a rate-limiting step that produces hydrogen sulfide (*15, 45*).

In prokaryotic Fe-S cluster biosynthesis, a cysteine desulfurase IscS forms a complex with a scaffold protein IscU to facilitate sulfur transfer and Fe-S cluster assembly (*94, 97*). IscS catalyzes the PLP-dependant cleavage of the C-S bond of its cysteine substrate to form alanine and a persulfide species on residue C328 (*46*). Remarkably, a recent IscS-IscU crystal structure revealed that C328 is located on a highly flexible loop that appears to sample a distance of ~30 Å by interacting with both the IscS substrate-PLP adduct and conserved cysteines on IscU (*44*). The IscU cysteines

C37 and C63 are located on loops at the IscS-IscU interface, whereas C106 is somewhat buried on the C-terminal helix of IscU (Figure 1-11). Although the functional significance for sulfur transfer is unclear, disulfide crosslinks between IscS C328 and IscU residues C37 (*90*) and C63 (*89*) confirm that these IscU residues can interact with the flexible loop of IscS. Mass spectrometry data for the *A. vinelandii* system indicates that all three IscU variants can function as sulfur (or polysulfide) acceptors (*90*). Kinetic data for the *E. coli* ISC system revealed that native, C37S, and C106S, but not C63S, IscU are able to stimulate IscS activity (*89*), suggesting C63 attacks the C328 persulfide on IscS.

In eukaryotes, recent evidence suggests Fe-S biosynthesis occurs through an assembly complex that exists in at least two forms: a mostly inactive complex of Nfs1, Isd11, Isu2 (SDU) and an activated complex of Nfs1, Isd11, Isu2, and frataxin (SDUF) subunits (*52*). In humans, the 94 kDa homodimeric cysteine desulfurase Nfs1 (homolog of IscS) provides sulfur for Fe-S cluster biosynthesis (*15, 43*) on the 14 kDa scaffold protein Isu2 (homolog of IscU). Isd11 is an 11 kDa eukaryotic-specific protein that interacts and stabilizes Nfs1 (*49, 50, 112*). Frataxin (Fxn) has been intensively studied since it was discovered that its depletion is associated with the neurodegenerative disease Friedreich's ataxia (*37*). The mature form of Fxn (residues 81-210) has been proposed to function as an allosteric activator (*52*) and as an iron donor for Fe-S cluster assembly (*16, 99, 100*). Little is known about the eukaryotic hand-off mechanism from Nfs1 to Isu2 and the role of Fxn in this process. Here we present enzyme kinetic data

that indicate human Fxn induces a conformational change in Isu2 that positions C104 to attack the persulfide species on Nfs1 for sulfur transfer and Fe-S cluster biosynthesis.

EXPERIMENTAL PROCEDURES

Protein Expression and Purification. Human Nfs1/Isd11, wt-Fxn, and wt-Isu2 were expressed and purified as described on page 30–31 (*52*). Eight human Isu2 cysteine variants [C35A(S), C61A(S), C104A(S), C96S, and C35A/C61A] were created by QuikChange site-directed mutagenesis (Stratagene) using a pET11a-hIsu2 plasmid template, and the mutation sites were confirmed by DNA sequencing (Gene Technologies Lab at TAMU). The resulting Isu2 variant pET11a plasmids were transformed into BL21(DE3) cells and grown at 16 ^{o}C until reaching an OD_{600} of 0.5. Protein expression was then induced with 0.5 mM IPTG and the cells were harvested 16 hrs later. The variants were purified using the same protocol as wild-type Isu2 (page 31). Undergraduate Andrew Winn and graduate student Jennifer Bridwell-Rabb assisted on the construction, purification, and determination of activity for the C35S, C61S, C104S, and C35A/C61A variants.

Isu2 Variant Binding to and Stimulation of Fe-S Assembly Complex. The rate of sulfide production for the Nfs1, Isd11, Isu2, and Fxn (SDUF) complex was measured using a previously described methylene blue assay (*52*). For the titration of Isu2 variants, the reaction mixture included 0.5 μM SD, 2.5 μM Fxn, 2 mM DTT, 10 μM PLP, 50 mM Tris pH 8.0, 250 mM NaCl. Different amounts of Isu2 variants (0-5 μM Isu2, C35A, C35S, or C96S; 0-30 μM C61A or C61S; 0-10 μM C140A or C104S; 0-125 μM

C35A/C61A) were added in the absence or presence of 5 μM $Fe(NH_4)_2(SO_4)_2$, the samples were incubated in the anaerobic glove box for 30 min, and then the reactions were initiated with 100 μM L-cysteine. The number of equivalents for the Isu2 variants (calculated based on the SD concentration) that maximized the cysteine desulfurase activities were then determined to be 3 (native Isu2 and C96S), 5 (C35A), 15 (C35S), 40 (C61A), 60 (C61S), 10 (C104A and C104S), and 100 (C35A/C61A). These amounts of the Isu2 variants were then used to determine the activity under standard assay and Michaelis-Menten conditions.

Determination of Kinetic Parameters for Isu2 Variants. Reaction mixtures included 0.5 μM SD, 2.5 μM Fxn, 2 mM DTT, 10 μM PLP, 5 μM $Fe(NH_4)_2(SO_4)_2$, 50 mM Tris (pH 8.0), 250 mM NaCl, and the saturating amount of Isu2 variant (determined above). The samples were incubated in the glove box for 30 min prior to initiation with cysteine. The cysteine concentration ranges used were 5-200 μM for native, C35A, and C61A variants, 25-1000 μM for C35S, C61S, C104S, and C35A/C61A, and 25–1500 μM for C104A. Reaction rates as a function of cysteine concentration were fit to the Michaelis-Menten equation using KaleidaGraph (Synergy Software).

Cysteine Desulfurase Activities with Isu2 Variants at a Physiological Cysteine Concentration (0.1 mM). The cysteine desulfurase activities were determined at 0.1 mM cysteine concentration with 0.5 μM SD, 2 mM DTT, 10 μM PLP, 50 mM Tris pH 8.0, 250 mM NaCl, and saturated amounts of Isu2 variants in the absence or presence of 5 μM $Fe(NH_4)_2(SO_4)_2$. Three independent measurements were conducted and averaged. Similar experiments were also performed with 3 equivalents (2.5 μM) Fxn.

RESULTS

Conserved Cysteines on Isu2 Contribute to Binding the SDUF Complex. Eight mutants of Isu2 were constructed to examine the sulfur transfer mechanism for the human Fe-S cluster assembly complex. The three conserved cysteines (C35, C61, and C104) were each mutated to alanine and serine, whereas the nonconserved cysteine (C96) was mutated to serine. In addition, the double mutant C35A and C61A variant was constructed. These mutants were individually added into an assay mixture that included Nfs1, Isd11, and Fxn, the cysteine desulfurase reaction was initiated with 100 μM cysteine, and the sulfide produced was converted into methylene blue and quantitated.

The addition of increasing amounts of the Isu2 variants increased the sulfide production rate that then plateaued at different total activities. This saturation behavior was interpreted as binding phenomenon in which the addition of Isu2 generates the catalytically active SDUF complex, and that the Isu2 variants have distinct binding affinities and ability to activate the complex. Native Isu2 and C96S (not shown) required 3 equivalents to saturate the cysteine desulfurase activity (Figure 3-1A). The addition of the C104A and C104S variants had little effect on the cysteine desulfurase activity (Figure 3-1A). The C104S variant slightly increased and the C104A variant slightly decreased activity. These changes in activity appeared to be complete after the addition of 10 equivalents of Isu2. The C35A variant saturated after 5 equivalents (Figure 3-1A), whereas the C35S variant required 15 equivalents (Figure 3-1B). The C61A and C61S

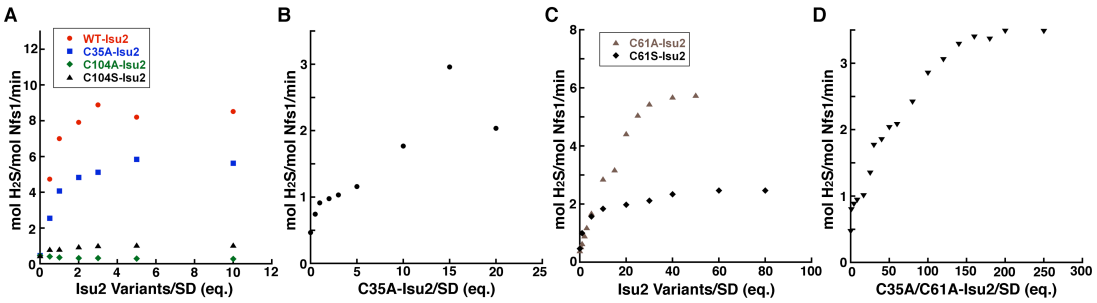

FIGURE 3-1: Cysteine desulfurase activity measurement with the titration of Isu2 variants in the presence of Fxn and ferrous iron. The molar ratio is compared to SD. The assay contains SD, Fxn, DTT, ferrous iron, PLP, cysteine (100 μM), and Isu2 variants. (A) WT-, C35A-, C35S-, C014A-, and C104S-Isu2 (B) C35S-Isu2 (C) C61A- and C61S-Isu2 (D) C35A/C61A-Isu2 double mutant.

Isu2 saturated at 40 and 60 equivalents, respectively (Figure 3-1C). Finally, the double mutant C35A/C61A required 200 equivalents to saturate the cysteine desulfurase activity (Figure 3-1D). Together this data indicates that mutation of any of the three conserved cysteines for Isu2 resulted in weaker binding, and that C61 has the largest role in complex formation.

Scheme for the Sulfide Rate Enhancement by Isu2 and Fxn. Previously, the rate of sulfide production from Nfs1 was shown to be stimulated by the presence of Isu2 and Fxn (*52*). We propose the simplified figure 3-2 to explain the rate enhancement. In the absence of Fxn, we hypothesize that internal sulfur transfer from Nfs1 to Isu2 either does not occur or occurs at a minimal rate compared to sulfide release from the Nfs1 persulfide loop by DTT (reaction [1]). In the presence of Fxn, we hypothesize that internal transfer from Nfs1 to Isu2 (reaction [2]) is favored and that the sulfide is release

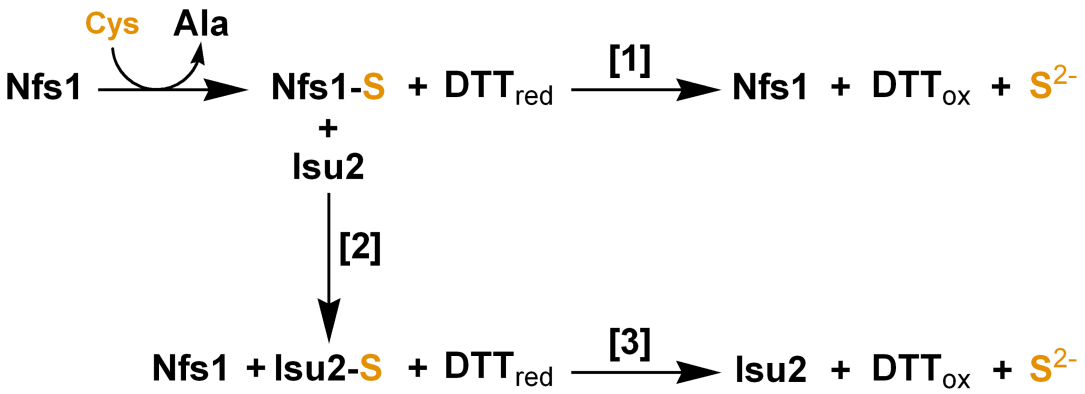

FIGURE 3-2: Reaction scheme for sulfur transfer from Nfs1 to Isu2 in the absence and presence of Fxn.

from a persulfide on Isu2 at a faster rate than from Nfs1 (reaction [3] > [1]). This scheme explains the overall rate enhancement for sulfide production by Fxn and predicts that if the sulfur acceptor on Isu2 were removed the rate enhancement by Fxn would be lost.

Sulfur Transfer from Nfs1 to Isu2 Residue C104. Here the cysteine desulfurase activities for the 8 different Isu2 variants were determined in the presence of Fxn. Saturating amounts of Isu2 (Figure 3-1) and 5 equivalents of Fxn/SD were used in these assays to remove complications from weaker binding of Isu2 variants to the SDUF complex. The C35A and C35S Isu2 mutants exhibited similar Fxn-dependent stimulation of Nfs1 activity (80% of native Isu2) using a physiological cysteine concentration of 100 μM (Figure 3-3). Examination of the Michaelis-Menten kinetics revealed catalytic efficiencies (k_{cat}/K_M) of 10,500 $M^{-1}s^{-1}$ for the C35A variant and 10,800 $M^{-1}s^{-1}$ for the

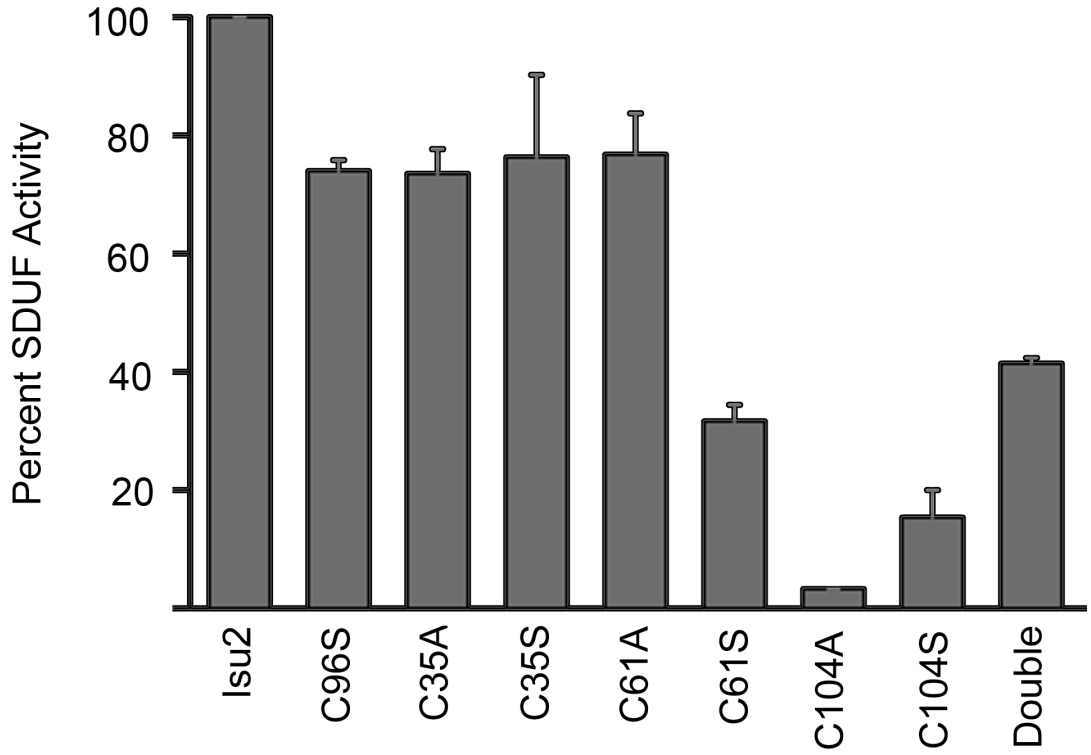

FIGURE 3-3: Percent of SDUF activity with Isu2 variants in the presence of Fxn. A mixture contains SD, Fxn, DTT, ferrous iron, cysteine (100 μM), and saturated amount of Isu2 variants (except only 3 equiv of C96S-Isu2 was used). Double means C35A/C61A-Isu2 mutations.

C35S variant, which are essentially identical to the 10,100 $M^{-1}s^{-1}$ of native Isu2 (Table 3-1). The C61A and C61S Isu2 mutants exhibited 80 and 40%, respectively, of the control activity under standard assay conditions (Figure 3-3). The catalytic efficiency of the C61A was 9,600 $M^{-1}s^{-1}$, whereas the C61S variant exhibited a k_{cat}/K_M of 6,500 $M^{-1}s^{-1}$ (Table 3-1). In contrast, the C104A and C104S Isu2 variants stimulated activity at about 5 and 15%, respectively, of native Isu2 (Figure 3-3). Both of the C104 variants exhibited

Table 3-1: Rate Constants for Human Nfs1 Activity with Isu2 Cysteine Variants

Complex	Eq. Isu2/SD	k_{cat} (min^{-1})	K_M $^{L\text{-}cys}$ (mM)	k_{cat}/K_M (M^{-1} s^{-1})
SD with WT-Isu2, Fxn,	3	8.5 ± 0.3	0.014 ± 0.002	10100 ± 1700
SD with C35A-Isu2, Fxn	5	7.2 ± 0.2	0.011 ± 0.002	10500 ± 2300
SD with C35S-Isu2, Fxn,	15	3.9 ± 0.1	0.006 ± 0.001	10800 ± 2100
SD with C61A-Isu2, Fxn,	40	8.6 ± 0.5	0.015 ± 0.004	9600 ± 3200
SD with C61S-Isu2, Fxn,	60	3.1 ± 0.1	0.008 ± 0.002	6500 ± 2000
SD with C104A-Isu2, Fxn	10	0.83 ± 0.14	0.51 ± 0.21	27 ± 15
SD with C104S-Isu2, Fxn	10	1.2 ± 0.02	0.014 ± 0.002	1400 ± 200
SD with C35A/C61A-Isu2, Fxn	200	3.5 ± 0.1	0.007 ± 0.001	8100 ± 1400

8-10 fold lower k_{cat} than native Isu2 (Table 3-1). Interestingly, the K_M for the C104A variant was 0.51 mM, which is significantly higher than the 0.014 mM K_M for both native Isu2 and C104S, and similar to samples that did not contain Fxn (0.59 mM) (*52*).

The slower kinetics of the C104 variants suggests that this residue may be involved in reaction [2] or [3]. To explore if one of the other cysteines was the initial acceptor and, after internal Isu2 sulfur transfer, a persulfide on C104 was generated and then released by DTT, the double mutant (C35A/C61A) was constructed and its kinetics were examined. The double mutant exhibited about 50% of the activity of native Isu2 in a standard assay and a catalytic efficiency of 8,100 $M^{-1}s^{-1}$ (Figure 3-3 and Table 3-1). As a control, the fourth non-conserved cysteine (C96) in human Isu2 was mutated to a serine and this variant was shown to have similar activity as native Isu2 and the C35A

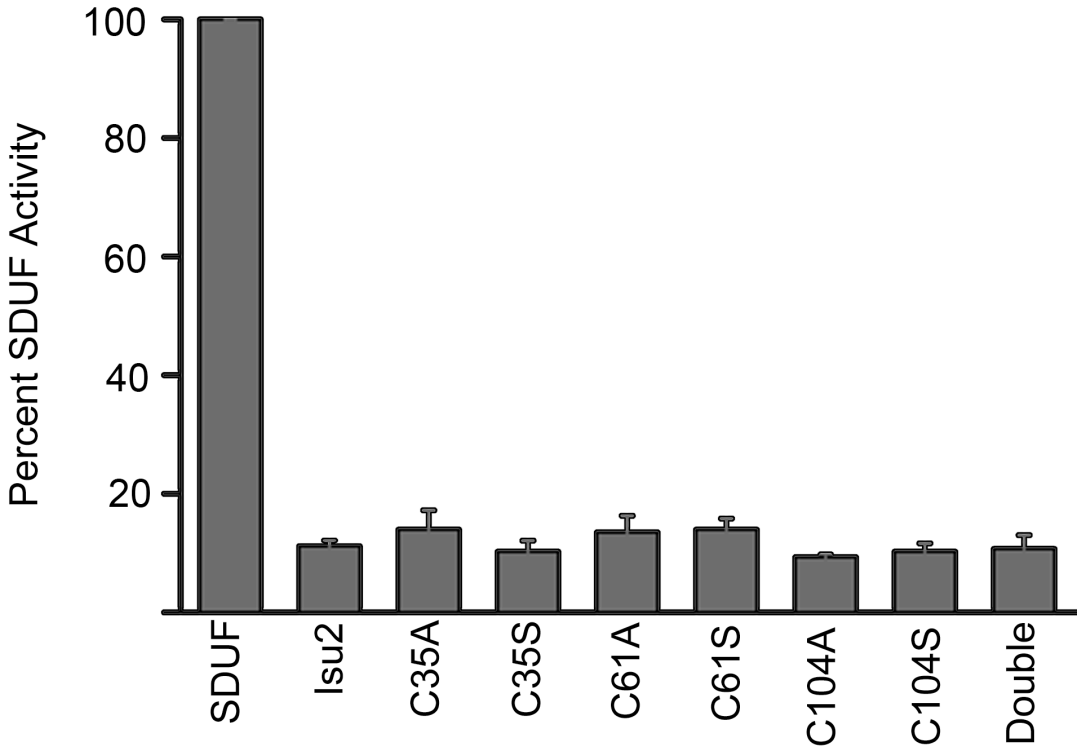

FIGURE 3-4: Percent SDUF activity of Isu2 variants in the absence of Fxn. The assay mixture contains SD, DTT, ferrous iron, cysteine (100 μM) and saturated amount of Isu2 cys variants. Double means C35A/C61A-Isu2 mutant. The control experiment is the assay mixture with 5 equiv of Fxn.

and C61A variants (Figure 3-3). Together, the kinetics results were consistent with the C104 residue on Isu2 serving as the primary sulfur acceptor from Nfs1 for Fe-S cluster assembly.

Fxn Facilitates Sulfur Transfer From Nfs1 to Isu2. Here the cysteine desulfurase activities for the 8 different Isu2 variants were determined in the absence of Fxn. Saturating amounts of the Isu2 variants that were determined in the presence of Fxn (above) were added to overcome differences in binding affinities. The mutants all

exhibited 10-15% of the sulfide production activity of the SDUF complex (Figure 3-4). Importantly, the Isu2 dependent differences in sulfide production activity were no longer apparent in the absence of Fxn.

DISCUSSION

Despite the importance of Fe-S clusters, few details are known about their assembly mechanisms. Sulfur is mobilized by a cysteine desulfurase from a cysteine substrate in the form of a reactive persulfide intermediate that can be transferred to a scaffold protein for Fe-S cluster biosynthesis. In prokaryotes, sulfur transfer from IscS to IscU has been suggested as the first step in Fe–S cluster biosynthesis (*94*). However, there is controversy over whether a particular cysteine, and, if so, which cysteine accepts the sulfur atom donated by the cysteine desulfurase for Fe-S cluster biosynthesis (*90*). To elucidate this issue, three conserved cysteine residues (C35, C61, and C104) on human Isu2 were investigated. First, titration of Isu2 variants was conducted to determine the relative binding affinities for the Isu2 variants to the SDUF complex. The titrations indicated that residue C61 variants on Isu2 require 40–60 equivalents to maximize the Nfs1 activity, which implies C61 is critical for interactions in the Fe-S assembly complex (Figure 3-1). Recently, a crystal structure of the *E. coli* IscS-IscU complex (*44*) revealed that IscS binds to IscU near C63 (equivalent to human C61) on IscU (Figure 3-5A). In that study, mutation of Isu2 residue K103 residue, which H-bonds with IscS residue E311, disrupted protein-protein interactions that were monitored

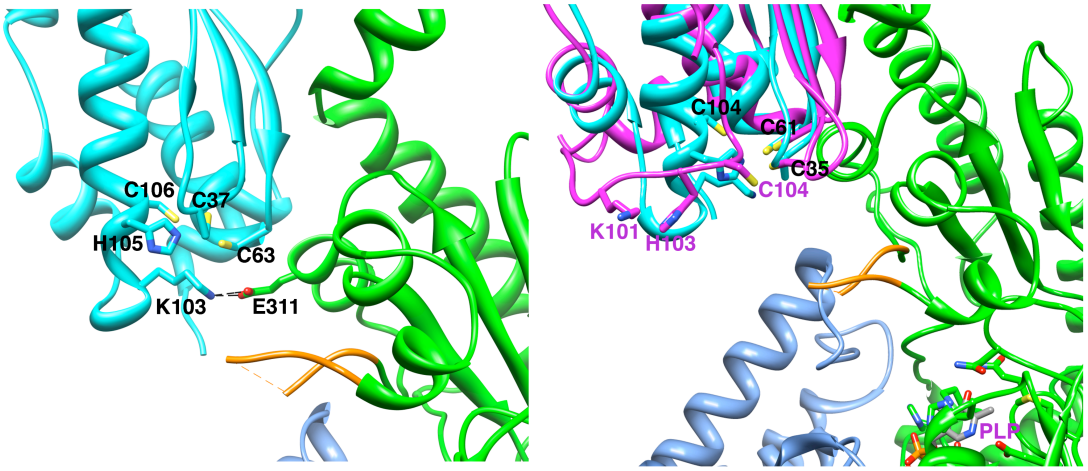

FIGURE 3-5: (A) *E. coli* IscS-IscU complex structure (PDB: 3LVL). IscU (cyan); IscS (green and cornflower blue); catalytic cysteine loop on IscS (orange). (B) Structure alignment of *A. aeolicus* IscU subunit A (PDB: 2Z7E) to *E. coli* IscU. *A. aeolicus* IscU (magenta); residues are numbered based on human Isu2 sequence.

with a pull-down assay (*44*). Hence, the mutation of human C61, which is expected to be adjacent to this K103-E311 interaction, may result in a conformational change and weaken the binding of Isu2 to Nfs1 (Figure 3-1). At saturating amounts of the C61-Isu2 mutants, the cysteine desulfurase activity is similar to native Isu2, suggesting the mutation results in weaker binding but is not catalytically compromised (Figure 3-3 and Table 3-1). The mutations of C35 and C104 residues on Isu2 exhibited similar binding characteristics, essentially 1–2-fold weaker than native Isu2 (Figure 3-1), but dramatically different functional properties. The C35-Isu2 mutants maintain similar catalytic activities as native Isu2, whereas C104-Isu2 mutants abolish Nfs1 activity (Figure 3-3 and Table 3-1). No stimulation on Nfs1 with C104-Isu2 mutants suggests

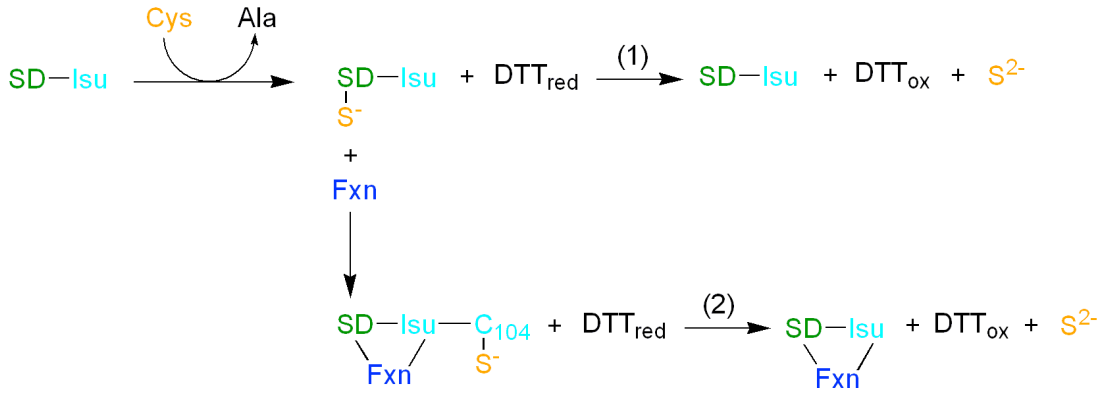

FIGURE 3-6: Proposed sulfur transfer mechanism from Nfs1 to Isu2 in the presence of Fxn. SD represents Nfs1/Isd11.

C104 residue is important for sulfur transfer. Therefore, Isu2 double mutant (C35A/C61A) was made to confirm if C104 residue alone can stimulate the Nfs1 activity.

The Isu2 double mutant (C35A/C61A) shows a catalytic efficiency of 8,100 $M^{-1}s^{-1}$, which is fairly close to that of native Isu2 (Table 3-1). The fact that the C35A/C61A double mutant, and not the C104 mutants, is stimulated by Fxn suggests C104 is the sulfur acceptor residue on Isu2. In the absence of Fxn, native Isu2 and its variants exhibit the same level of sulfide production (Figure 3-4), which implies that either the sulfur is not transferred from Nfs1 to Isu2 or the rate for sulfur transfer is inefficient. In both cases, sulfide production seen in the assay was detected because persulfide product on Nfs1 was cleaved directly by DTT. Therefore, the sulfur transfer mechanism was proposed to explain our results (Figure 3-6). In reaction (1), the SDU (Nfs1/Isd11/Isu2)

complex represents an inactive form in which the sulfur transfer reaction from Nfs1 to Isu2 doesn't occur (or occurs infrequently/inefficiently) and the Nfs1-based persulfide is cleaved by DTT. The resulting rate of sulfide production would therefore be independent of Isu2 or mutations on Isu2. This is supported by the observation that the Nfs1 activity is the same for the different Isu2 variants (Figure 3-4). In reaction (2), the SDUF (Nfs1/Isd11/Isu2/Fxn) complex represents an active form in which sulfane sulfur was transferred from Nfs1 to Isu2, specifically to residue C104, in the presence of Fxn. The persulfide-bound Isu2 was then cleaved by DTT. The rate of sulfide production is dependent on Fxn binding and on a specific cysteine residue on Isu2. The reaction (2) was supported by the results that the C104 mutant exhibited low sulfide production and the C35A/C61A double mutant showed high sulfide production (Figure 3-3 and Table 3-1). These two proposed reactions are consistent with our previous results that Fxn forms a complex with SDU and activates Nfs1 activity (*52*).

Previously, the Johnson and Dean groups proposed that there was not a specific cysteine on IscU that accepted the sulfur from IscS in a prokaryotic system based on mass spectrometry data that indicated persulfide or polysulfide species on each of the three cysteine-to-alanine substitutions for IscU (*90*). Another explanation for this data is that a residue such as C37 residue (equivalent of human C35), which exhibits the shortest distance (~12 Å) of the three cysteines to the IscS catalytic cysteine loop (Figure 1-11 and 3-5A), could be the initial sulfur acceptor and be followed by secondary internal persulfide transfer to C63 and C106 (*44*). Nobuyoshi's group proposed a different mechanism in which C63 on IscU forms a disulfide-bridge with C328 on IscS

and responsible for accepting the sulfur during catalysis (*89*). These results could be explained by lacking of required protein partner, Fxn, for sulfur transfer to specific cysteine residue on IscU or lacking of maintaining the anaerobic environment for sulfur transfer experiments. Cysteine is known as a reducing agent as well (*45*). Incubation of IscS and IscU alone with cysteine could result in transpersulfuration from IscS to an external cysteine in solution and then incorporation from persulfide-bound cysteine species to IscU in a nonspecific mechanism.

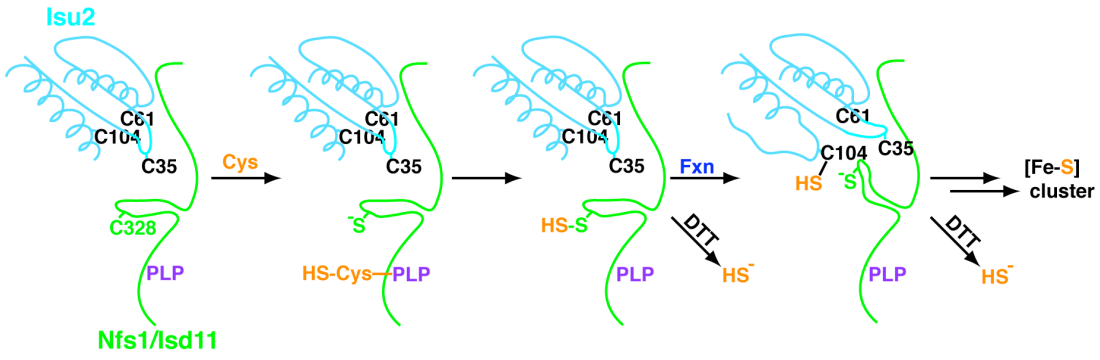

FIGURE 3-7: A working model for sulfur transfer from Nfs1 to Isu2 in the presence of Fxn.

The crystal structure of the trimeric *A. aeolicus* IscU shows IscU conformations in both Fe–S cluster bound (subunit B) and apo (subunits A and C) forms (*58*). A primary difference between the holo and apo conformations are a helix to coil changes in the C-terminal region (residues 103–109), which contains K103 (equivalent of human

K101), H106 (equivalent of human H103), and conserved C107 (equivalent of human C104) residues. Structure alignment of *A. aeolicus* apo-IscU subunit A and *E. coli* apo-IscU shows that C104 (human Isu2 residue number) can undergo a helix-to-coil switch (Figure 3-4B). In the crystal structure of the IscU-IscS complex, residue C104 of Isu2 is buried on the C-terminal helix and about 18 Å away from catalytic cysteine loop on IscS. After helix-to-coil switch, C104 is exposed and close to catalytic cysteine loop on IscS. Two distinct conformations of IscU in solution were also suggested by the Vickery group (*54*). One is largely disordered (apo-form) and the other is largely ordered (metal- or cluster-bound form). These two states interconvert on the millisecond time scale. The most perturbed regions were identified as the two N-terminal strands and the C-terminal helix upon addition of cochaperone HscB. Taken together, we proposed a working model to explain how sulfur is transferred from Nfs1 to Isu2 in the presence of Fxn (Figure 3-7). First, the cysteine substrate is bound to PLP in the active site of Nfs1. Second, the substrate is convered to alanine and generates a persulfide intermediate on residue C328 of Nfs1. Third, Fxn binds SDU, induces the helix-to-coil switch on Isu2, and repositions C328 catalytic loop of Nfs1. The C-terminal coil conformation of Isu2 exposes C104 to persulfide-bound C328 on Nfs1 for sulfur transfer. The persulfide-bound C104 on Isu2 is either cleaved by DTT or used for Fe–S cluster assembly. Taken together, the results suggest C104 residue on Isu2 is the initial and primary sulfur acceptor from Nfs1 in the presence of Fxn, which requires the helix-to-coil conformational change on Isu2.

CHAPTER IV

HUMAN FRATAXIN I154F AND W155R CLINICAL VARIANTS LOSE ABILITY TO ACTIVATE THE FE-S BIOSYNTHETIC COMPLEX

INTRODUCTION

Friedreich's ataxia (FRDA) is an autosomal recessive neurodegenerative disease caused by reduced amounts of the protein frataxin (Fxn) (*37*). The loss of Fxn results in a complicated phenotype that includes increased iron in the mitochondria, deficiencies in Fe-S cluster enzymes, and enhanced sensitivity to oxidative stress (*64*). FRDA patients typically present symptoms during adolescence such as progressive limb and gait ataxia and often die prematurely from cardiomyopathy. There is currently no cure. The majority (>95%) of FRDA patients are homozygous for an unstable GAA trinucleotide expansion in the first intron of the FXN gene (*39*). The repeat size ranges between 7 and 40 for normal individuals and 66 to >1700 for FRDA patients (*38, 39*). Importantly, larger GAA repeats correlate with lower Fxn expression levels and an earlier age of disease onset (*40*). A small fraction of FRDA patients have an expanded GAA repeat on one allele and a point mutation on the other allele (*83*). In these cases, the Fxn protein levels do not necessarily correspond to the age of onset (*39, 84*).

Most researchers agree that Fxn has a critical role in iron-sulfur (Fe-S) cluster assembly (*103, 104*). In eukaryotes, the biosynthesis of Fe-S clusters occurs in the matrix space of the mitochondria and includes at least a dozen proteins (*33*). Human Isu2 is a 14 kDa monomer (*59*) that provides a scaffold for building $[Fe_2S_2]$ and, possibly,

[Fe_4S_4] clusters. Human Nfs1 is a 94 kDa homodimer that catalyzes the PLP-dependent breakdown of cysteine to alanine and transfers the resulting sulfur species to the scaffold protein Isu2 (*13, 43*). Isd11 is an 11 kDa protein that is known to form a complex with Nfs1 and has an undefined but vital role for Nfs1 function (*49, 50, 112*). Chaperones then interact with the scaffold protein and assist in delivering intact Fe-S clusters to their apo targets (*53*). Both *in vivo* and *in vitro* data support physical interactions between eukaryotic Nfs1, Isd11, Isu, and Fxn (*16, 50, 108, 110-112*). Recently, biochemical evidence was provided for Nfs1, Isd11, and Isu2 (SDU) and Nfs1, Isd11, Isu2, and Fxn (SDUF) Fe-S cluster assembly complexes (*52*).

Multiple roles have been proposed for Fxn in Fe-S cluster biosynthesis. Fxn is encoded in the nucleus, imported into the mitochondria, and proteolytically processed to generate at least four different products (*65, 133-138*). A 14 kDa monomeric form includes residues 81-210 (referred to as Fxn in this dissertation) and is commonly thought to function as an iron chaperone in Fe-S cluster biosynthesis (*139*). A larger form of Fxn that includes residues 56-210 ($Fxn^{56\text{-}210}$) can oligomerize and has been proposed to function in iron detoxification and storage (*71, 105*), and as an iron donor for Fe-S cluster biosynthesis (*66, 123*). A negative regulator role in Fe-S cluster biosynthesis has also been proposed for Fxn based on functional studies of the *Escherichia coli* homolog CyaY (*80*). In contrast, a positive allosteric activator role for human Fxn was proposed based on the Fxn-dependent ~400 fold increase in catalytic efficiency (k_{cat}/K_M) for the cysteine desulfurase component of the Fe-S assembly complex (*52*).

Understanding how Fxn missense mutations such as I154F and W155R compare to native Fxn may provide additional insight into its role in Fe-S cluster biosynthesis. FRDA patients with missense Fxn mutations I154F and W155R have similar expression levels (18% of native Fxn), yet the age of disease onset (4 for W155R patient; 16 for I154F patient) are dramatically different (*84*). The I154F and W155R variants are reported to have decreased thermodynamic stability (*85*), and diminished binding to Isd11 (*110*) and Isu1 (*88*). Incorporation of I154F into a mouse model system results in a FRDA like phenotype that included the loss of iron-sulfur cluster enzyme activity (*140*). Surprisingly, functional analysis of the *E. coli* W61R (equivalent of human W155R) indicates enhanced activity compared to native Fxn (*80*). It is difficult to reconcile the decreased iron-sulfur cluster activity for human FRDA clinical variants in a mouse model system and also increased iron-sulfur cluster activity for FRDA-related mutants of a bacterial homolog. To address this issue, we extended previous *in vitro* cysteine desulfurase and Fe-S cluster assembly assays (*52*) and show that the human I154F and W155R and related Fxn mutants lose the ability to bind and activate the Fe-S assembly complex in a manner that corresponds to the clinical phenotype. Structure-function analysis of W155R, W155A, and native Fxn coupled to results from an associated sulfur trafficking manuscript (Chapter III) lead to a model for Fxn-induced sulfur transfer from Nfs1 to Isu2 for human Fe-S cluster biosynthesis.

EXPERIMENTAL PROCEDURES

Protein Expression and Purification. The expression and purification procedures for Nfs1/Isd11 complex, Isu2, and wt-Fxn were described as page 30–31. Fxn mutants (I154F, W155R, W155A, and W155F) were made by site-directed mutagenesis from pET11a-f-Fxn plasmid (page 31) using standard protocol and the mutation sites were confirmed by DNA sequencing. Plasmid pET11a containing I154F, W155R, W155A, and W155F-Fxn, individually, was then transformed into BL21(DE3) cells. Fxn mutants were expressed at 16 ^{o}C with 0.5 mM IPTG for 16 hrs and purified using the same protocol as wt-Fxn (page 31).

Cysteine Desulfurase Activity Assay with 3 Equiv. of Fxn Variants. Reaction mixtures containing SD (0.5 μM), Isu2 (1.5 μM), PLP (10 μM), DTT (2 mM), $Fe(NH_4)_2(SO_4)_2$ (5 μM), Fxn variants (1.5 μM), 50 mM Tris pH 8.0, and 250 mM NaCl were incubated in the anaerobic glovebox (10~14 ^{o}C) for 30 min before addition of L-cysteine substrate (100 μM). The reaction was incubated at 37 ^{o}C anaerobically for 10 min and then quenched by addition of 100 μL DPD (20 mM) in 7.2 M HCl and 100 μL $FeCl_3$ (30 mM) in 1.2 M HCl. The methylene blue product was formed after 20 min incubation at 37 ^{o}C. The absorption at 670 nm corresponding to methylene blue formation was measured for quantization of H_2S production by comparing with Na_2S standard curve.

Cysteine Desulfurase Activity Assay with the Titration of Fxn Variants. Similarly, cysteine desulfurase activity assay was conducted with the titration of Fxn variants in the presence of 10 equiv of $Fe(NH_4)_2(SO_4)_2$. The same reaction mixtures described above

were titrated with Fxn variants to obtain the maximum cysteine desulfurase activity. The cysteine desulfurase activity was saturated after addition of 3 equiv of wt-Fxn, 8 equiv of I154F, 40 equiv of W155R, 40 equiv of W155A, and 30 equiv of W155F, separately. The similar experiments were performed in the absence of $Fe(NH_4)_2(SO_4)_2$. The resulting saturation of cysteine desulfurase activity was 5 equiv for wt-Fxn, 25 equiv for I154F-Fxn, 45 equiv for W155R-Fxn, 50 equiv for W155A-Fxn, and XX equiv for W155F-Fxn.

Binding Constant Determination for Fxn Variants to SDU Complex. The 5 ~ 8 different concentrations within saturated amount of Fxn variants were mixed with reaction mixture (0.5 μM SD, 1.5 μM Isu2, 10 μM PLP, 2 mM DTT, 5 μM $Fe(NH_4)_2(SO_4)_2$, 50 mM Tris pH 8.0, and 250 mM NaCl), separately, for 30 min anaerobically. The cysteine desulfurase activity was measured after initiation with 0.01 ~ 1 mM L-cysteine substrate. The k_{cat} and K_M for each Fxn variant concentration was calculated by fitting into Michaelis-Menten equation. k_{cat} versus Fxn variant concentration was plotted and fitted with type II allosteric activation equation 4.1 (*141*).

$$k_{cat} = \frac{k_{SDU} + k_{SDUF}^{\infty}\left(\frac{[Fxn]}{Kd}\right)}{1 + \frac{[Fxn]}{Kd}} \qquad (4.1)$$

*K*d is the dissociation constant; k_{SDU} is the k_{cat} in the absence of Fxn; and k_{SDUF}^{∞} is the k_{cat} in the saturated amount of Fxn.

Fe-S Cluster Formation Assay. Assay mixtures in 0.2 mL contained 8 μM SD, 24 μM Isu2, 24 μM Fxn variants, 5 mM DTT, 200 μM $Fe(NH_4)_2(SO_4)_2$, 100 μM L-cysteine, 50 mM Tris, pH 8.0, and 250 mM NaCl. The Isu2 was incubated with DTT and buffer in anaerobical glovebox for 1 hr before the remaining reaction components were added. 100 μM L-cysteine was injected 1 cm pathlength anaerobic cuvette with gas-tight syringe to start the reaction. The Fe-S cluster formation was monitored at 456 nm at room temperature for 90 min. The rate of Fe-S cluster formation was fitted to first-order kinetics using KaleidaGraph. The rate was converted to specific activity of Isu2 using extinction coefficient 5.8 $mM^{-1}cm^{-1}$ (*117*). Units are defined as the amount of Isu2 required to produce 1 μmol of $[Fe_2S_2]$ cluster per minute at 25 ^oC.

Crystallization, Data Collection, and Refinement of WT, W155R, and W155A-Fxn. Crystallization conditions were setup using hanging-drop vapor diffusion methods by mixing 2 μL of protein with 2 μL of reservoir solution and stored at 22 ^oC incubator. WT-Fxn (15 mg/mL) in 50 mM HEPES pH 7.5 and 50 mM NaCl was crystallized in 30% 2-Methyl-2,4-pentanediol, 0.1 M sodium citrate pH 5.6, and 0.2 M ammonium acetate after 1 month. ; W155R-Fxn (25 mg/mL) in 25 mM HEPES pH 7.5 was crystallized in 16% PEG monomethyl ether 2000 and 0.1 M MES pH 6.0 after 2~3 days; and W155A-Fxn (10 mg/mL) was crystallized in 1.8 M ammonium sulfate, 0.2 M potassium sodium tartrate tetrahydrate, and 0.1 M sodium citrate tribasic dihydrate pH 5.0 with seeding solution from higher precipitant (2 M ammonium sulfate). The WT-Fxn single crystal was flash frozen in liquid nitrogen without adding extra cryo-protecting reagents; W155R-Fxn single crystal was transferred into cryo-protecting solution

containing 16% ethylene glycol and reservoir solution and then flash frozen in liquid nitrogen; and W155A-Fxn single crystal was transferred into cryo-protecting solution containing 20 % glycerol and reservoir and then flash frozen in liquid nitrogen. The x-ray diffraction data for WT and W155R-Fxn crystal were collected on the detector ADSC Quantum-315R CCD at the SSRL Beamline 7-1, and W155A-Fxn crystal diffraction data was collected on MAR 300 CCD at APS beamline 23-ID-D. The collected images were integrated and scaled using iMosflm (*30*) and Scala (*64*) programs. The crystal resolution cut off was based on the criteria of $I/(\sigma I) \geq 2$. For WT-Fxn, the resolution cutoff is 1.30Å in space group $P2_12_12_1$ with one molecule per asymmetric unit and crystal contained 46% solvent content. For W155R-Fxn, the resolution cutoff is 1.31Å in space group $P2_12_12_1$ with one molecule per asymmetric unit and crystal contained 46% solvent content. For W155A-Fxn, the resolution cutoff is 1.50 Å in space group C2 with one molecule per asymmetric unit and crystal contained 46% solvent content. The structure of Fxn variants was determined by molecular replacement with human frataxin (PDB code: 1EKG) as the initial search model using Phaser (*39*) program. The output model was refined with rigid body and restrained refinement along with anisotropic temperature factors using Refmac5 (*142*) program and built by Xfit (*54*) programs. The R_{work}/R_{free} for WT, W155R, and W155A-Fxn structures were refined to 15.3/18.7, 15.1/19.7, and 16.9/19.2, respectively.

RESULTS

Fxn Variants I154F and W155R(A)(F) Lose Ability to Activate Fe-S Cluster Biosynthetic Complex. Previously, the binding of native Fxn was shown to activate the Nfs1/Isd11/Isu2 complex for sulfide production for Fe-S cluster assembly, and the addition of ferrous iron further stimulated this activity (*52*). In this assay, cysteine was converted to alanine and the resulting persulfide intermediate was reduced with DTT, and the resulting sulfide was converted to methylene blue and quantitated. Here we compared the ability of native Fxn, the recombinant FRDA I154F and W155R variants, and W155A and W155F variants to activate the Nfs1/Isd11/Isu2 complex using a physiological cysteine concentration of 0.1 mM (*119, 121*). The reason that we chose I154F and W155R FRDA mutants is because they have the similar expression levels in FRDA patients (17.6% and 17.9% of control, respectively), but the patients with W155R point mutation showed a more severe phenotype than I154F (*39, 86*). All of the mutants showed lower activation than native Fxn (WT > I154F > W155F > W155A > W155R) under the same protein concentration (Figure 4-1). I154F-Fxn lost activation ability about 50%, 80% for W155F, 90% for W155A, and 92% for W155R. The Fxn clinical mutant W155R is worse than I154F to activate the cysteine desulfurase activity, which is consistent to the published results that W155R-Fxn exhibited more severe early-onset than I154F-Fxn (*39, 86*). In their studies, similarly expressed I154F and W155R point mutants display distinct disease severities and ages of onset, suggesting differences in Fxn functional impairment.

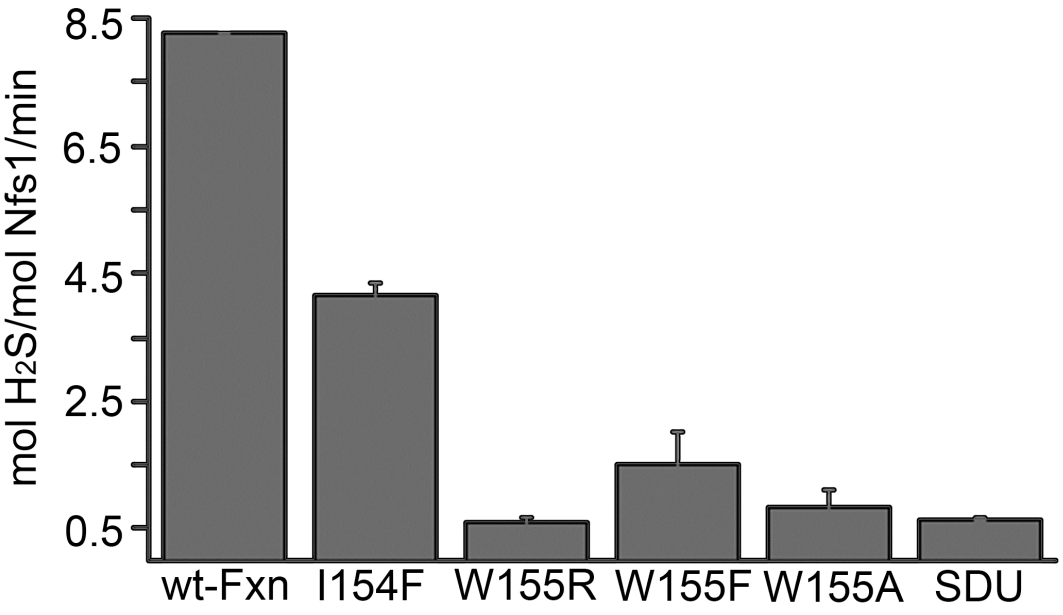

FIGURE 4-1: Fxn variants loss ability to stimulate cysteine desulfurase activity. Rates of SD sulfide production were determined in the presence of 3 equiv of Fxn variants, 3 equiv of Isu2, and 10 equiv of ferrous iron. Error bar are for three independent measurements.

Next, the binding ability and specific activity were explored to understand if this activation impairment is due to weaker binding to SDU complex. Cysteine desulfurase activity was measured with the titration of Fxn variants in the presence of Isu2 and ferrous iron to obtain the needed saturated amount of Fxn variants. The enzyme kinetics experiments were conducted with a titration of Fxn variants within saturated amount. The binding constant *K*d for Fxn variant to SDU complex was calculated by fitting k_{cat} over Fxn concentrations into type II allosteric activation equation 4.1. Type II allosteric activation is described as the value of k_{cat} changes from a finite low value to a higher value, which is consistent to our results that Nfs1 still shows activity in the absence of

Table 4-1: Binding and Rate Constants for Nfs1 Activity with Fxn Variants in the Presence of Isu2 and Ferrous Iron

Complex	K_d (μM)	k_{cat} (min^{-1})	$K_{M}^{L\text{-}cys}$ (mM)	k_{cat}/K_M (M^{-1} s^{-1})
SD with Isu2 and Fxn	0.22 ± 0.05	8.5 ± 0.3	0.014 ± 0.002	10100 ± 1700
SD with Isu2 and I154F Fxn	0.63 ± 0.14	6.6 ± 0.4	0.025 ± 0.004	4400 ± 800
SD with Isu2 and W155R Fxn	6.73 ± 1.28	1.8 ± 0.1	0.013 ± 0.003	2300 ± 500
SD with Isu2 and W155A Fxn	6.12 ± 1.36	3.9 ± 0.2	0.012 ± 0.003	5400 ± 1600
SD with Isu2 and W155F Fxn	1.78 ± 0.31	4.5 ± 0.1	0.018 ± 0.003	4200 ± 800

Fxn (activator) (*141*). The k_{cat} and K_M for saturated amount of Fxn variants were calculated by fitting to Michaellis–Menten equation. The binding ability for Fxn variants to SDU complex with Ferrous iron decreased 3-fold for I154F, 30-fold for W155R and W155A, and 8-fold for W155F (Table 4-1). These data suggest W155R and W155A bind much weaker to SDU complex than WT-, I154F-, and W155F-Fxn. By comparing the k_{cat}, K_M and k_{cat}/K_M parameters, k_{cat} slightly decreased from 8.5 to 6.6 min^{-1} and kcat/km decreased about 2-fold for I154F-Fxn mutant. For W155F and W155A mutants, both k_{cat} and k_{cat}/K_M decreased about 2-fold. The most significant change among these mutants is W155R mutant, both k_{cat} and k_{cat}/K_M greatly decreased about 5-fold. Since the rate-limiting step for cysteine desulfurase is persulfide cleavage/transfer step (*45*), the decreases in k_{cat} would suggest Fxn clinical mutants, especially for W155R mutant, loss the ability to activate the sulfur transfer.

Fxn Variants Decrease Fe–S Cluster Assembly Rate. Fe–S cluster assembly rate was determined by monitoring the increase in absorbance at 456 nm, commonly used for [Fe_2S_2] cluster formation (*117*). An assay containing SD, 3 equiv Isu2, and 3 equiv wt-Fxn showed the specific activity of 0.49 unit/mg Isu2 (Figure 4-2 and Table 4-2). The Fe–S cluster formation rate for I154F, W155F, W155A, and W155R Fxn mutant are 61%, 26%, 15%, and 7% of control wt-Fxn, which shows the same trend as the activation activity for cysteine desulfurase (Figure 4-1). The Fe–S cluster formation for W155R is almost the same as SDU complex itself (5% of control) (Table 4-2), which implies that W155R weakly binds SDU complex and loses the activation ability. The rate of Fe–S cluster formation for W155A-Fxn is 2-fold higher than W155R, but the

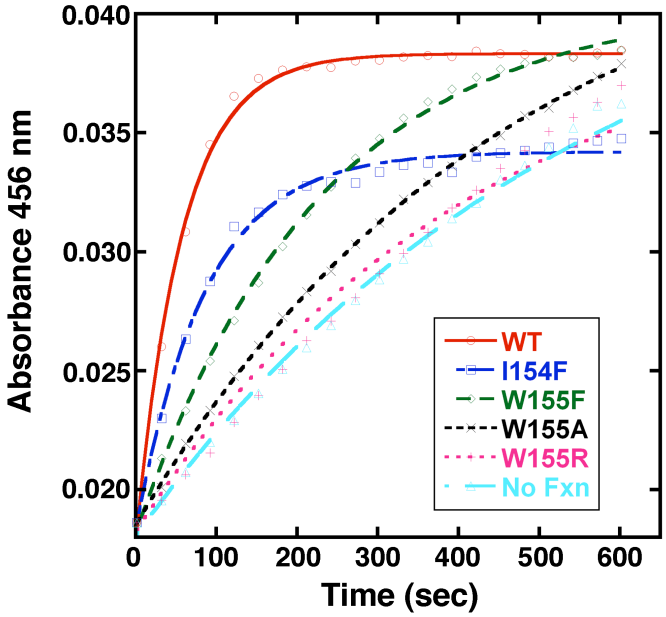

FIGURE 4-2: Fe–S cluster formation kinetics with Fxn variants. Assay contained 8 μM SD, 24 μM Isu2, 100 μM cys, 200 μM Fe^{2+}, 5 mM DTT, and 24 μM Fxn variants.

Table 4-2: Fe–S Cluster Formation Rate with Fxn Variants

complex	U/mg Isu2	Nfs1 activity
SDU	0.025 ± 0.004	0.65 ± 0.02
SDU + Fxn	0.490 ± 0.015	8.25 ± 0.90
SDU + I154F	0.300 ± 0.020	4.14 ± 0.20
SDU + W155F	0.130 ± 0.005	2.09 ± 0.51
SDU + W155A	0.075 ± 0.005	0.83 ± 0.28
SDU + W155R	0.035 ± 0.003	0.60 ± 0.07

binding constant is similar (Figure 4-1), which suggests positive charged arginine residue (W155R) inhibits activation even more. Together, the results suggest Fxn variants loss the ability to assembly Fe–S cluster and W155-Fxn residue is critical for Fe–S cluster formation.

Comparison of Crystal Structures of WT, W155R, and W155A-Fxn. To understand the impact of W155-Fxn mutants on Fe–S cluster biosynthesis, WT, W155R, and W155A-Fxn crystal structures were determined at 1.30, 1.31, and 1.50 Å resolution, respectively, using SSRL and APS synchrotron facilities. Both wt and W155R-Fxn structures are in $P2_12_12_1$ space group, and W155A-Fxn structure is in C2 space group (Table 4-3). Human wt-Fxn crystal structure was previously published at 1.80 Å resolution in year 2000 (*143*). Higher resolution of wt-Fxn crystal structure was provided

Table 4-3: X-ray Data Collection and Refinement Statistics

Fxn Variants	Wild-type	W155R	W155A
Data Collection	SSRL BL7-1	SSRL BL7-1	APS BL23-ID-D
Wavelength (Å)	0.97945	0.97945	1.03315
Space Group	$P2_12_12_1$	$P2_12_12_1$	C2
Unit cell (Å and °)	42.9, 44.8, 69.0 90^o, 90^o, 90^o	38.9, 49.2, 67.1 90^o, 90^o, 90^o	87.5, 32.3, 44.8 90^o, 91.4^o, 90^o
Resolution (Å)	44.86-1.30	39.68-1.31	44.797-1.50
Outer shell (Å)	1.37-1.30	1.38-1.31	1.58-1.50
Observations	258690	476216	147672
Unique Observations	33576	31647	20101
Redundancy	7.7	15.0	7.3
Completeness (%)*	100.0 (100.0)	99.8 (99.7)	99.3 (98.6)
Mean I/(σI)*	14 (2.6)	22.2 (5.6)	12.0 (6.6)
R_{sym} (%)*†	8.2 (62.4)	6.4 (41.3)	13.8 (48.3)
Refinement			
Residues not in model	82-88, 210	82-87, 209-210	82-89
Solvent atoms	201	169	101
Ligand		Mg	SO_4
R_{work}/R_{free} (%)‡	15.3/18.7	15.1/19.7	16.9/19.2
r.m.s.d. bond lengths (Å)	0.032	0.023	0.029
r.m.s.d. bond angles (°)	2.7	1.8	2.6
Ramachandran (%)			
Most favored	93.4	93.4	91.5
Additional allowed	6.6	6.6	8.5
Generous	0	0	0
Disallowed	0	0	0
PDB code	2XXX	2XXX	2XXX

*Values in parentheses are the statistics for the highest resolution shell of data
†$R_{sym} = S \mid I_{hkl} - \langle I \rangle \mid / S \langle I \rangle$, where $\langle I \rangle$ is the average individual measurement of I_{hkl}.
‡$R_{work} = (S \mid F_{obs} - F_{calc} \mid) / S \mid F_{obs} \mid$, where F_{obs} and F_{calc} are the observed and calculated structure factors, respectively. R_{free} is calculated the same as R_{work}, but from the data (5%) that were excluded from the refinement.

at 1.30 Å resolution here. Applying anisotropic thermal factor refinement to wt and W155R- Fxn, the wt-Fxn structure showed several rotamers on "acidic patch" α1 helix and β1 sheet (Figure 4-3), but not in W155R-Fxn structure. These carboxylate residues (Asp or Glu) were previously suggested as putative iron binding site (*144-146*). The different orientations of carboxylate side chain on W155R and W155A structures might impact on binding to iron or Fxn protein partners. The electrostatic surfaces of native and Fxn variant crystal structures without minor rotamers were compared. There are only slightly changes on acidic patch near α1 and β1 regions (Figure 4-4A), and some positive residues (Lys and Arg) re-orientated to different positions (Figure 4-4B). By looking into W155 mutation site, the loop between β3 and β4 is shifted due to the empty pocket on W155 position and loss of H-bonding between N148 and Q151 (Figure 4-5).

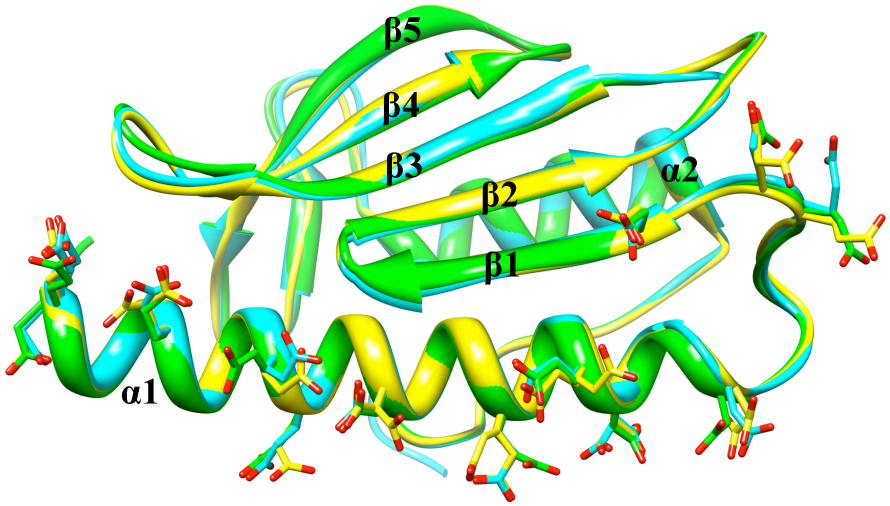

FIGURE 4-3: Comparison of acidic regions on Fxn variant structures. wt (yellow); W155R (green); and W155A-Fxn (cyan).

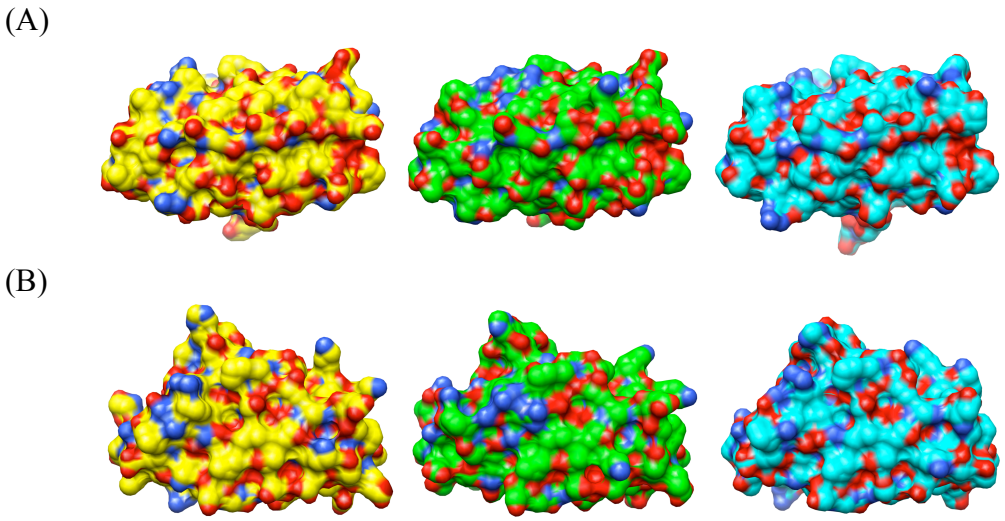

FIGURE 4-4: Comparison of the electrostatic surfaces of wt (yellow), W155R (green), and W155A (cyan). (A) acidic patch (α1 and β1). (B) W155 mutation site on β4.

WT and Fxn variant structures were aligned and the residues near W155 mutation site were compared (Figure 4-6). The loop between β3 and β4 has a significant 3 Å movement on W155R-Fxn structure and only about 1 Å shift on W155A-Fxn structure by comparing wt-Fxn structure. For W155A mutant, there are some residues (T149–N151 and R165) slightly shift comparing to wt-Fxn structure. Surprisingly, the mutation W155R perturbed the surrounding residues (Q148–Q153 and R165) significantly. W155R lost the H-bonding with Q153, which caused the shifting of Q148 toward the W155 mutation site and further lost H-bonding between Q148 and N151. R165 moved toward W155R mutation that created a weak H-bonding with Q148. These

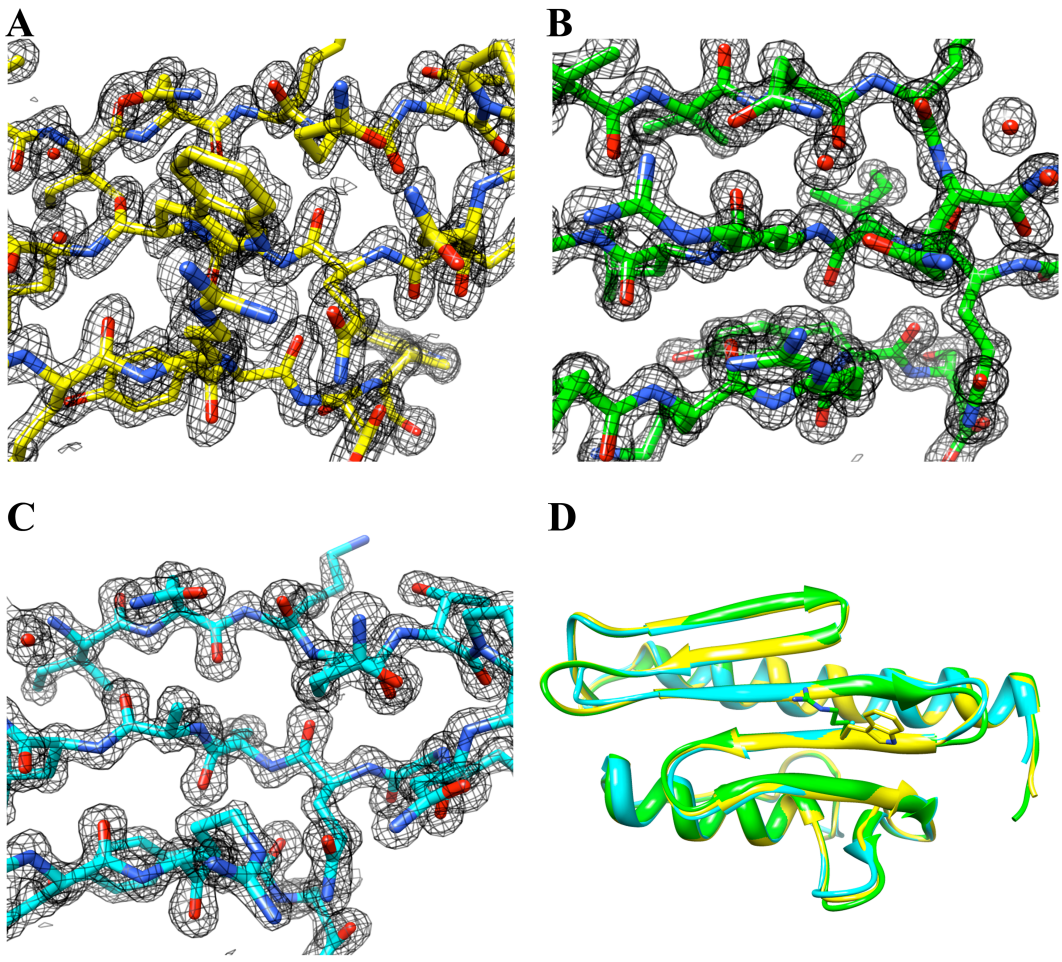

FIGURE 4-5: The $2F_o$-F_c electron density map in the W155 region of Fxn variants. Electron density is contoured at 2σ. (A) wt (B) W155R (C) W155A (D) Structure alignment. Color coding of oxygen red and nitrogen blue.

significant movements might be due to the loss of H-bonding interactions between W155 and Q153 and between Q148 and N151, and cation-π interactions (*79*) between W155 and R165. Unfortunately, I154F-Fxn is difficult to be crystallized and the diffraction for W155F-Fxn was poor so that the structure cannot be determined yet.

However, by comparing the kinetic results and structure alignment of wt-Fxn with W155R and W155A-Fxn, we can predict the structure of W155F would be very similar to wt-Fxn and the loop between β3 and β4 has less movement than W155A-Fxn.

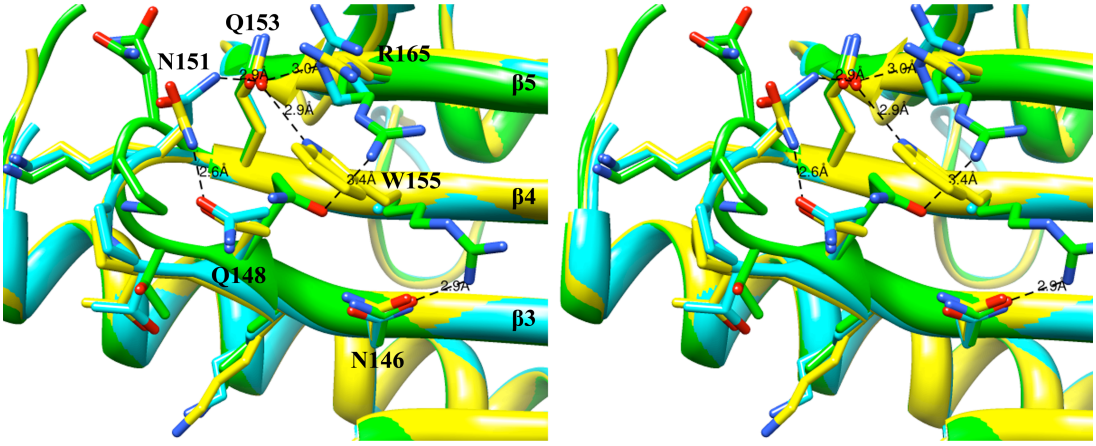

FIGURE 4-6: Stereo-view of structure alignment of conserved β-sheets on wt (yellow), W155R (green), and W155A-Fxn (cyan).

DISCUSSION

Here Fxn variants were characterized by comparing their allosteric activation ability for cysteine desulfurase activity, binding ability to form SDUF complex, Fe–S cluster formation rate, and structural dissimilarity. First, the cysteine desulfurase activity were measured under physiological 100 μM cysteine concentration and compared under the same level of protein concentration (Figure 4-1). The results showed I154F and W155R lost 50% and 92% activation activity, respectively, compared to wt-Fxn. These results can explain why W155R FRDA patient had more severe phenotype than I154F under the same expression level (*86*). The I154F and W155R variants are reported to have decreased thermodynamic stability (*85*), and diminished binding to Isd11 (*110*) and Isu1 (equivalent of human Isu2) (*88*). To test whether the loss of activation ability is due to the impairment of SDUF complex formation. Their binding ability to form SDUF complex were compared by titrating Fxn variants and monitoring H_2S formation (see experimental procedures). I154F bound 3-fold weaker than wt-Fxn and, more significantly, W155R decreased the binding ability about 30-fold than wt-Fxn (Table 4-1). Under the condition with the saturated amount of Fxn variant, I154F activation ability increased to 6.6 min^{-1} for k_{cat} and 4,400 $M^{-1}s^{-1}$ for k_{cat}/K_M compared to k_{cat} 8.5 min^{-1} and 10,100 k_{cat}/K_M for wt-Fxn, but W155R only increased to 1.8 min^{-1} for k_{cat} and 2,300 $M^{-1}s^{-1}$ for k_{cat}/K_M (Table 4-1). It has been reported that the expression level of I154F and W155R-fxn point mutations are only about 18% of wt-Fxn level from FRDA patients (*86*), which result the deficiency of Fe-S cluster biosynthesis. Incorporation of I154F into a mouse cellular model system results in a FRDA like phenotype that

included the loss of iron-sulfur cluster enzyme activity (*140*). Surprisingly, functional analysis of the *E. coli* W61R (equivalent of human W155R) indicates enhanced activity compared to native Fxn (*80*). It is difficult to reconcile the decreased iron-sulfur cluster activity in the mouse model system and enhanced iron-sulfur cluster activity in the bacterial system for FRDA clinical variants. In our Fe–S cluster formation studies, I154 and W155R depress the Fe–S cluster formation rate to 61% and 7% of control, respectively (Figure 4-2). Together, both I154F and W155R lose the allosteric activation ability due to low expression level and weaker binding ability. Specifically for W155R Fxn mutant, the activation activity cannot be rescued even under saturated amount protein concentration. It also suggests that W155R-Fxn loses activation ability might be contributed from structure differences to wt-Fxn.

The first FRDA mutant W155R crystal structure was determined at 1.31 Å resolution and compared with wt-Fxn and W155A-Fxn crystal structures (Table 4-2 and Figure 4-5). The loop between β3 and β4 along with R165 residue were rearranged in W155R structure (Figure 4-6). The studies from Foury's group suggested that the spatial relationship on residues Q129, W131, and R141 in yeast Fxn (equivalent of human Fxn residues Q148, W155, and R165) is important for protein function (*88*). In their studies, W131A mutation strongly decreases the interaction with Isu1, which is consistent to our result that W155A has weaker binding ability to SDU complex (Table 4-1), possibly to Isu2. The binding constant for W155R, W155A, and W155F is 6.7, 6.1, and 1.8 μM, respectively. Compared to the binding constant of wt-Fxn (0.2 μM), the results suggest W155 is important for the binding to SDU complex to activate the cysteine desulfurase

activity and sulfide production. Phenylalanine residue (W155F) can partial rescue the binding and activation suggests the importance of the aromatic ring on residue 155 of Fxn.

To further understand the interaction of Fxn with Isu2, the subunit A of *A. aeolicus* IscU (equivalent of human Isu2) crystal structure (*58*) was aligned with *E. coli* IscS-IscU complex structure (*44*) (Figure 3-4B). The structure alignment of human Isu2 and *A. aeolicus* IscU hints that the C-terminal helix, which contains one of the conserved cysteine residues (C104, human sequence number), could possibly switch between helix and coil conformation. The coil conformation of the C-terminal region of Isu2 may expose H103 and K101 residues in order to put the C104 in the proper position to accept the sulfide from catalytic cysteine loop on Nfs1 (Figure 3-4B). W155 is in the right position to interact with K101 and H103 residues through cation-π or π-π interactions (*79*). Therefore, a working model for Fxn activation was proposed (Figure 4-7). Fxn binds Isu2 and SD, residue W155 on Fxn stabilizes coil conformation via the interaction with K101 and H103 on Isu2. This stabilization allows sulfur transfer from Nfs1 to C104 residue on Isu2. K101 and H103 residues can "hug" W155 residue only if W155 is standing straight, which means Q148 and R165 residues on Fxn play important role to keep W155 standing still. Any perturbation from other surrounding residues would mess up the position of W155 residue. This model can explain why W155R and W155A have the similar weak binding ability. Mutation of W155F showed stronger binding ability than W155A and W155R that also supports the idea of cation-π interaction. But the

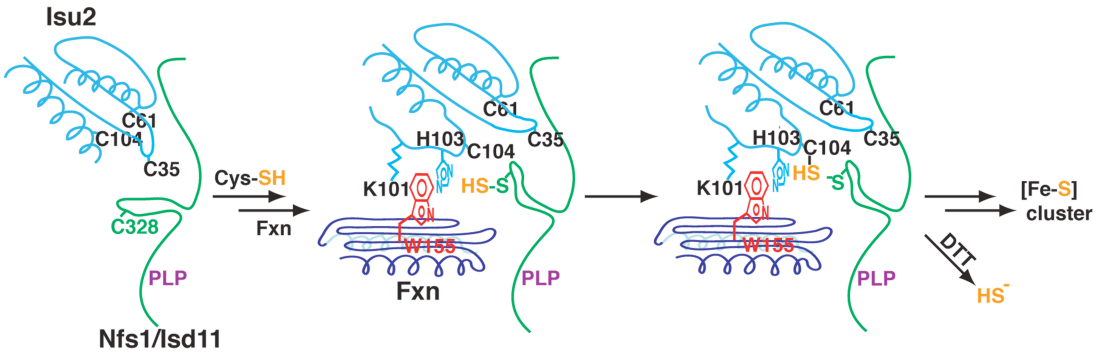

FIGURE 4-7: Proposed model for the activation of SDU complex by Fxn. W155 residue is required to induce the conformational change on C-terminal helix of Isu2 and possibly stabilized by K101 and H103 via cation-π or π-π interactions. The induced coil conformation on Isu2 positions C104 for sulfide transfer from catalytic cysteine328 on Nfs1. The persulfide bound Isu2 can be cleaved by DTT or form Fe–S cluster. Note, catalytic cysteine loop on Nfs1 may also have conformational change upon Fxn binding.

reason that W155F has weaker binding than wt-Fxn is because phenylalanine only has one aromatic ring, which is not enough to reach the proper position to interact with K101 and H103 residues on Isu2. Based on our model, the interactions of other known FRDA clinical mutants such as N146K, Q148R, and R165C with Isu2 can be predicted. N146K and Q148R point mutation would create the positive repulsion interactions to K101 and H103 that would result weak binding of Fxn to Isu2. R165C mutation would lose its duty to keep W155 residue in the proper position, which would also weaken the Fxn–Isu2 interaction. Together, structure comparison of wt, W155A, and W155R-Fxn coupled with *in vitro* functional studies showed W155 is critical for Fxn and Isu2 interaction and the residue rearrangement between β3 and β4 on Fxn further impair the sulfide transfer and Fe-S cluster formation.

CHAPTER V

STRUCTURAL ANALYSIS OF FE-S CLUSTER ASSEMBLY COMPONENTS

INTRODUCTION

A network of protein–protein interactions appears to be critical for Fe–S cluster biosynthesis (*13, 109*). Fxn, Isu, and Nfs1 physically interact in pull-down experiments using yeast (*108*) and human (*110*) mitochondrial extracts. Iron-dependent Fxn-Isu interactions are further supported by genetic studies in yeast (*111*) and biophysical experiments with recombinant human proteins (*16*). Isu–Nfs1 interactions are defined by a crystal structure of the homologous *E. coli* IscU–IscS complex (*44*) (Figure 1-11). In eukaryotes, an additional protein, Isd11, is also known to form a complex with Nfs1 and is vital for Nfs1 functions (*49, 50, 112*). Fxn interacts with Isd11 has also been supported by pull-down experiments using human cell extract (*110*). Depletion of genes encoding Nfs1, Isd11, Isu, or Fxn in *S. cerevisiae* produces similar phenotypes that include defects in Fe–S cluster proteins (*50, 113*). These data hint a multiprotein complex that functions as a Fe–S cluster assembly machine.

Crystal structure of *E. coli* IscS-IscU complex is the only known structure for protein-protein interaction. Little has known about how frataxin interacts with Isu2 , Nfs1, and Isd11. Therefore, the need for obtaining the structural information will help to understand the protein-protein interactions in molecular levels. Here we are using low-resolution structural techniques such as small-angle x-ray scattering and electron microscopy to determine the protein shape of each component and SDUF protein

complex coupled with high-resolution protein crystallography technique to determine Nfs1/Isd11 complex. In addition, protein docking was used to provide the initial idea for understanding how Fxn interacts with Nfs1 and Isu2.

EXPERIMENTAL PROCEDURES

The Shape Determination of Fe-S Cluster Components Using Small-Angle X-Ray Scattering (SAXS). Human Isu2, m_{82}–Fxn (82-210 aa.), m_{56}–Fxn (56-210 a.a.) were dialyzed against 50 mM Tris pH 7.5 and 150 mM NaCl. The resulting buffer was used for buffer subtraction in the SAXS experiments. The samples were shipped to Stanford Synchrotron Radiation Laboratory (SSRL) in California under 4~10 ^{o}C sealed styrofoam box. A series of concentrations (1.25, 2.5, 5, 10 mg/mL for Fxn; 2.5, 5, 7.5, 8.75 mg/mL for Isu2) were used to evaluate the concentration-dependent aggregation or interparticle interference (*2*). 20 μL of each protein sample was injected into flow cell on Beamline 4-2 at SSRL. The sample to detector distance is 2.5 m; beam energy is about 11 keV; and the exposure time is 5 sec for buffer and sample. Total 10 measurements were taken to evaluate radiation damage. The scattering curve, $I(q)$, was obtained from the subtraction of the buffer from the sample. The data was processed by Atsas 2.2 suite (*19*). Each sample with different concentration was scaled, merged and analyzed using Primus program. The radius of gyration R_G and absolute Intensity $I(0)$ were extrapolated by Guinier approximation $\log I(q)$ vs. q using the criteria $qR_G \leq 1.3$ for globular proteins. $I(0)$ was used for estimating the molecular mass of protein by comparing $I(0)$ with the

molecular mass standards A206K-GFP (25 kDa), A206C-GFP (51 kDa), and RFP (104 kDa) using equation 5.1.

$$Mc = I(0)\left(\frac{N_A}{\upsilon\Delta\rho^2}\right) \cong 1.468I(0) \qquad (5.1)$$

M is molecular mass of protein; *c* is the concentration of protein in mg/mL; *I*(0) is the absolute intensity extrapolated to $q = 0$; N_A is Avogadro constant; ν is partial specific volume of protein; and Δρ is X-ray constant. The scattering data was indirect Fourier transform to pair-distribution function *P*(*r*) by using Gnom program to estimate maximum dimension (*r*) of the protein. The output file was used for *ab-initio* SAXS envelope reconstruction using GASBOR program. 10 GASBOR models were generated and averaged to get the final averaged SAXS model. The SAXS models were superimposed with known crystal structures (PDB: 1EKG for Fxn; 1WFZ for Isu2). Experimental SAXS scattering curves also compared with calculated SAXS scattering curve from known crystal structures using CRYSOL program. IscU dimer docking model was generated with ClusPro server using mouse NMR structure (1WFZ). The top ten models were converted to scattering curve using CRYSOL program. The best fit based on χ^2 was used to superimpose into human Isu2 experimental SAXS model.

Determination of Isu2 Oligomeric States Using Analytical Ultracentrifugation (AUC). Human Isu2 protein (30 mg/mL, 0.4 mL) with 10 mM DTT was dialyzed against 0.5 L (x2) of 10 mM sodium phosphate buffer pH 7.4 and 50 mM NaCl in the anaerobic glove box. The Isu2 protein was then diluted to OD_{280} of 0.3, 0.6, and 0.9. The 0.5 mL of

each samples were sent to Dr. Demeler in the Center for Analytical Ultracentrifugation of Macromolecular Assemblies (CAUMA) at the University of Texas Health Science Center at San Antonio in Texas. Sedimentation velocity data were analyzed with the ULTRASCAN software. The samples were centrifuged at 20 ^{o}C in 60,000 rpm using standard Epon two-channel centerpieces. Velocity measurements were taken at 281 nm using the buffer as the same as dialysis buffer and hydrodynamic corrections for buffer density, viscosity, and partial specific volume were applied as implemented in ULTRASCAN . The partial specific volume was determined to be 0.7444 cm3/g for Isu2. All data were analyzed by two-dimensional spectrum analysis, van Holde-Weischet analysis, and finite element analysis (*28, 29, 52*).

Crystallization of SD Complex. 1 uL of SD protein (10 mg/mL in 50 mM Tris pH 8.0, 250 mM NaCl) with 5 mM TCEP was mixed with 1 uL of Hampton Research sparse matrix screening solution using Phoenix crystallization robot in the Dr. Sacchettini's lab. The trays were incubated at 22 ^{o}C. After 2 weeks, yellow crystals were found in PEG/ION 2 # 39 crystallization condition with 20% PEG3350 and 0.04 M citric acid/0.06 M bis-tris propane (CBTP) pH 6.4. The crystallization conditions were optimized using additive screening from Hampton Research. The crystal grew to size 0.5 mm x 0.5 mm x 0.5 mm with the additive #40 (hexammine cobalt chloride) after 2 weeks at 22 ^{o}C in the crystallization condition 4% PEG3350 and 0.04M/0.06M CBTP pH 6.4. Other additives, such as LiCl, NaCl, NaI, CsCl, non-detergent NDSB-201, and NDSB-211, were also found to have beautiful crystals about 0.3 mm size. The crystals were transferred to different cryo-protecting solution, such as 25–35% ethylene glycol,

25–35% glycerol, 100% paratone, 35% MPD, 25% sucrose, 30% DMSO, 35–35% PEG400, 1.5 M NaCl, and 1M Sodium Malonate pH 7, and flash frozen in liquid nitrogen. The crystals were screened on Beamline 7-1 at SSRL. The crystal diffracted at a resolution of 6.9 Å with either 30% ethylene glycol or 30% glycerol cryo-protecting solution. The diffraction data were analyzed using Phenix and CCP4 suites.

Electron Microscopy (EM) for SDUF Complex. The SDUF complex was prepared by incubating SD (100 μM), Isu2 (250 μM), Fxn (250 μM), and DTT (10 mM) in the buffer 100 mM HEPES pH 7.5 and 150 mM NaCl for 30 min in the glove box. The reaction was loaded on S200 analytical gel filtration column and run with the buffer 50 mM HEPES, pH 7.5 and 150 mM NaCl. The fraction contains SDUF complex was diluted to 0.05 mg/mL and sent to Dr. Holzenburg at the Microscopy and Imaging Center at TAMU. 100 μL of protein sample was deposited on the carbon-coated grid, after one minute for blotted dry, then covered with a small drop of the 2% uranyl acetate stain. After a few seconds to allow this drop to be blotted dry, the sample is ready for negative stain microscopy. Since SDUF complex is a small complex about 180 kDa for EM, the negative stain EM is better than cryo-EM due to its high contrast property. Data was divided and averaged to different classes with 3485 particles and then calculated after multi-reference alignment using initial, reference-free classes as references. The final class was averaged and re-projected by applying to 2-fold symmetry to reconstruct 3D EM model using rendering threshold of 8.0. The resolution was calculated about 24 Å.

Protein Docking for Fxn to IscS-IscU Crystal Structure. Human version of Nfs1-Isu2 complex was built based on *E. coli* IscS-IscU structure (PDB: 3LVL) using SWISS-MODEL server. The *E. coli* IscS-IscU complex was modified and energy-minimized based on human Nfs1 and Isu2 sequences. Human Fxn (Ligand) was docked to *E. coli* IscS-IscU crystal structure (Receptor) (PDB: 3LVL) using ClusPro protein docking server (http://cluspro.bu.edu) (*65, 66*). The protein complex was predicted without selecting any constraints. The initial structures from PIPER (*69*), an FFT-based rigid body docking program, were selected using shape complementarity, an approximation of the van der Waals contact energy, desolvation, and electrostatics. The top 1000 energetically favorable structures were then clustered on the basis of a pairwise binding site root mean squared deviation (RMSD) criterion. Clusters were formed by selecting the ligand that has the most neighbors below 10Å. Each member within the cluster was then eliminated from the matrix to avoid overlaps between clusters. This is repeated until at least 30 clusters were formed. The ligand with the most neighbors is the cluster center. The top cluster centers are then minimized in the presence of the receptor, and concatenated into PDB format. The model with lowest free energy and the most neighbors is selected as our docking model.

RESULTS

N-Terminal Region of Human Fxn Shows a Long Disordered Tail. To understand why human Fxn^{56-210} can form oligomer, but mature Fxn^{82-210} cannot. Low-resolution small-angle x-ray scattering (SAXS) experiments were performed at SSRL beamline 4-2. The SAXS data of Fxn^{56-210} and Fxn^{82-210} were compared. The R_G and D_{max} for Fxn^{82-210} and Fxn^{56-210} are 15.4 Å and 49 Å, and 20.0 Å and 67 Å, respectively (Figure 5-1). The SAXS model of Fxn^{56-210} shows a long extra tail by comparing to Fxn^{82-210}. This extra tail is corresponding to extra N-terminal region (residues 56-81). Fxn (Fxn^{56-210}) has extra 27 residues on N-terminal region and the length of this N-terminal tail is about 18 Å, which is possibly a disorder coil. This disordered N-terminal tail can be readily cleaved to become mature Fxn (Fxn^{82-210}), which is consistent with previous *in vivo* observations by Puccio's group (*65*).

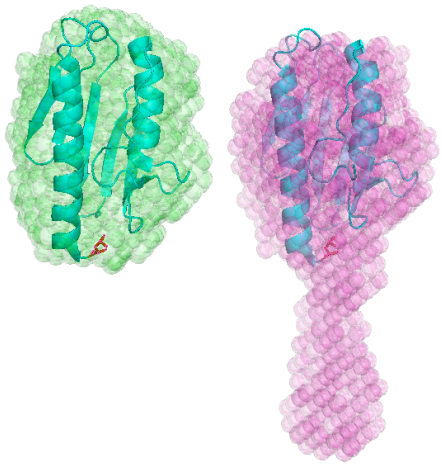

FIGURE 5-1: Docking Fxn crystal structure into *ab initio* SAXS model. Fxn crystal structure (cyan). (*Left)* Fxn^{82-210}. R_G = 15.4 Å, D_{max} = 49 Å; (*right*) Fxn^{56-210}. R_G = 20.0 Å, D_{max} = 67 Å.

Human Isu2 Behaves in Concentration-dependent Monomer–dimer Equilibrium. Oligomeric state of bacterial NifU/IscU/SufU has been shown to function as a dimer (*60, 89, 147, 148*). *A. vinelandii* IscU could bind [Fe_2S_2] cluster in its dimer interface and sequentially assemble [Fe_4S_4] cluster (*117*). In contrast, eukaryotic human Isu2 D37A mutant has been suggested as a monomer that can bind [Fe_2S_2] cluster (*59*). Up to date, all the proposed Fe–S cluster assembly mechanisms have been using IscU dimer as a model (*91, 149*). To reconcile human Isu2 oligomeric state, the small-angle x-ray scattering (SAXS) and analytical ultracentrifugation (AUC) experiments have been conducted. In SAXS experiment, the human Isu2 SAXS model was compared with NMR structures of mouse IscU monomer and dimer. The mouse IscU dimer was generated by docking two mouse IscU monomer structures (PDB: 1WFZ) by submitting to ClusPro protein docking server. The top 10 dimer models were converted to scattering curves and compared to human Isu2 SAXS scattering curve. The best fit gives χ^2 about 5.7 (Figure 5-2A). The calculated R_G and χ^2 for mouse IscU monomer are 16.4 Å and 10.7. The calculated R_G for mouse IscU dimer is 20.9 Å, which is very close to the R_G (20.6 Å) for human Isu2 SAXS data. The SAXS results suggest human Isu2 is close to a dimer form, but not a monomer form. The SAXS data was further analyzed by pair-distribution function to obtain the maximum dimension for human Isu2. The estimated maximum distance is 70 Å (Figure 5-2B). This data was then used to reconstruct the *ab initio* SAXS model. The reconstructed human Isu2 SAXS model was superimposed with best mouse IscU dimer model (Figure 5-3). Therefore, the SAXS model suggests human

FIGURE 5-2: (A) Overlay of human Isu2 scattering curve with calculated mouse IscU dimer scattering curve generated by CRYSOL. (B) Pair-distribution function for human Isu2. The maximum dimension is estimated as 70 Å using GNOM program.

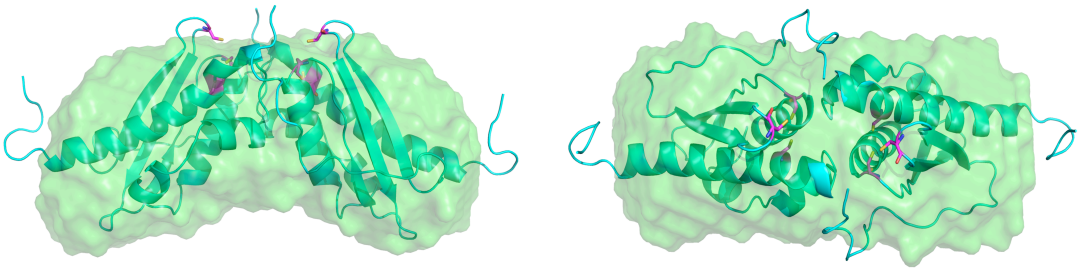

FIGURE 5-3: Superimposition of human Isu2 SAXS model (green) with mouse IscU dimer docking structure (cyan). Conserved cysteine residues (magenta). (A) side view (B) top view.

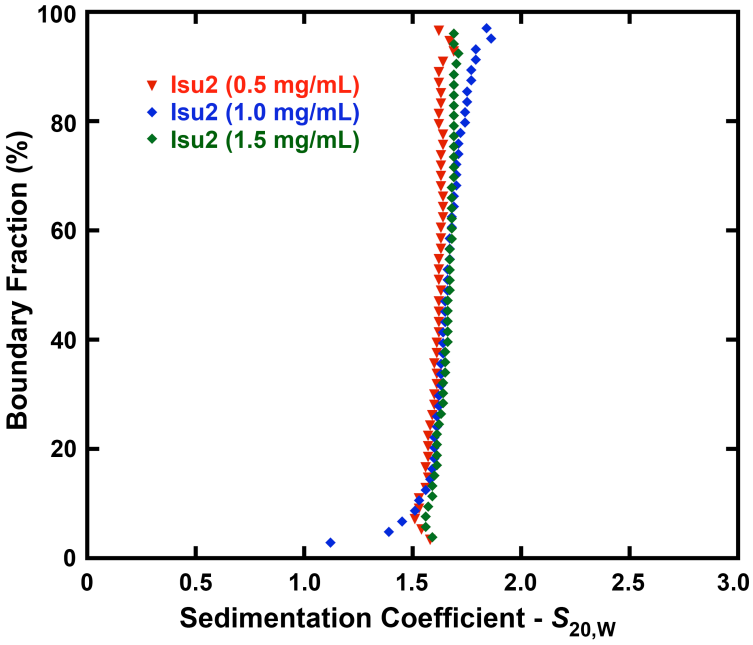

FIGURE 5-4: van Holde–Weischet distribution plot of sedimentation coefficients for human Isu2.

Isu2 is a dimer in the solution at the protein concentration greater than 2.5 mg/mL.

The oligomeric state of Isu2 was also investigated by using AUC. The protein was reduced with DTT in the anaerobic glove box and then dialyzed to remove DTT. The results shown here are the human Isu2 from low (OD_{280} of 0.3, 0.5 mg/mL) to high concentration (OD_{280} of 0.9, 1.5 mg/mL) in van Holde-Weischet distribution plot (Figure 5-4). Plots of boundary fraction versus $S_{20,w}$ (sedimentation coefficient corrected for water at 20 ^{o}C) will be vertical if the sample is homogeneous and will show positive slope if the sample is heterogeneous. The sedimentation coefficient (*S* value) is ~1.60, 1.65, 1.70 for low, medium, and high concentration Isu2. The AUC results indicate

human Isu2 is concentration-dependent monomer-dimer equilibrium when protein concentration increases above 0.5 mg/ml (34 μM). Together, AUC and SAXS results suggest that human Isu2 behaves as monomer-dimer equilibrium in a concentration-dependent manner.

Nfs1 and Isd11 Complex Crystallizes Only under Reduced Condition. Crystallization trials of cysteine desulfurase Nfs1 and Isd11 complex have been setup using sparse-matrix methods. Three crystallization conditions were found to produce yellow crystals from random screening solutions. These three conditions are PEG/ION #5 (12% PEG3350, 0.1 M Na malonate pH 6.0), PEG/ION #27 (12% PEG3350, 0.1 M Na formate pH 7.0), and PEG/ION #39 (20% PEG3350, 0.04/0.06 M CBTP pH 6.4). Only PEG/ION #39 can be reproduced in optimization solution, but in lower precipitant percentage (2–6% PEG3350). In the 2% PEG3350, 0.04/0.06 M CBTP pH 6.4 condition, the hanging-drop was setup and incubated at 22 ^{o}C. Two to four big yellow crystals (size about 0.4~0.5 mm) grew after 5 days (Figure 5-5A). The crystals were optimized and sent to SSRL for data collection. The crystals diffracted poorly, the best resolution was about 6.9 Å (Figure 5-5B). The reasons for poor diffraction might be due to improper cryo-protecting solution, protein degraded or oxidized, or loosely crystal packing. The crystallization condition was optimized with additive screening in order to get better quality of crystals. Different cryo-protecting solutions were also tested to minimize osmotic shock. The resolution of crystal diffraction was not improved. The fact that crystals only grew in the presence of TCEP indicates Nfs1-Isd11 complex tends to be

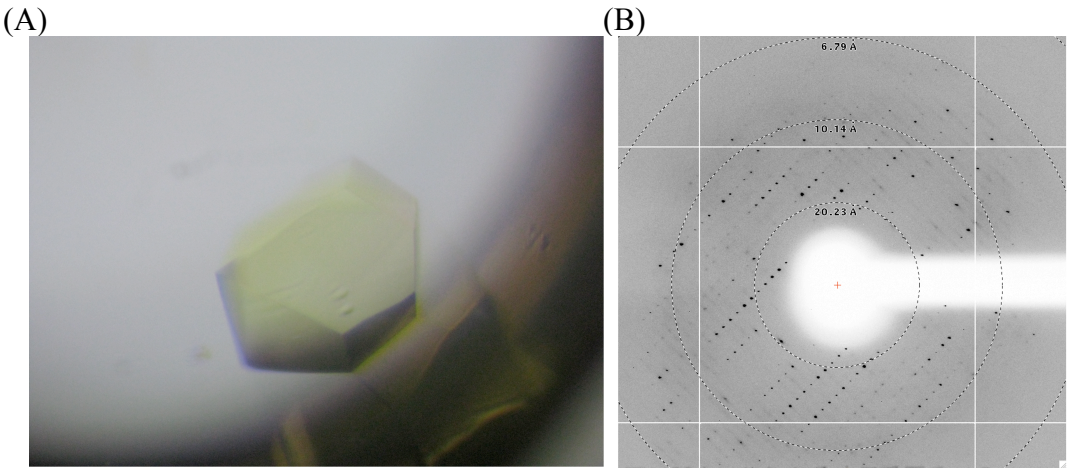

FIGURE 5-5: (A) Nfs1/Isd11 crystal. (B) Diffraction image of Nfs1/Isd11 at 6.9 Å.

oxidized and forms heterogenerous oligomer. Crystallization was then setup at 16 °C anaerobically. Only small crystals grew due to the vibration of the glove box when compressor turned on and off. The crystals were tested at SSRL and the results were depressing. Therefore, new condition or higher purity of protein will be tried to get higher quality of SD crystals. The 6.9 Å diffraction data was collected and analyzed. The results showed one molecule per asymmetric unit with the unit cell dimension 145.02 Å x 145.02 Å x 167.18 Å, 90^o x 90^o x 90^o. The space group was indexed as P422 and the estimated molecule weight was 160 kDa.

Shape Determination of SDUF Complex Using Electron Microscopy. SDUF complex has been isolated using gel filtration chromatography. The low-resolution structure of SDUF complex was obtained using electron microscopy (EM). Over 3000

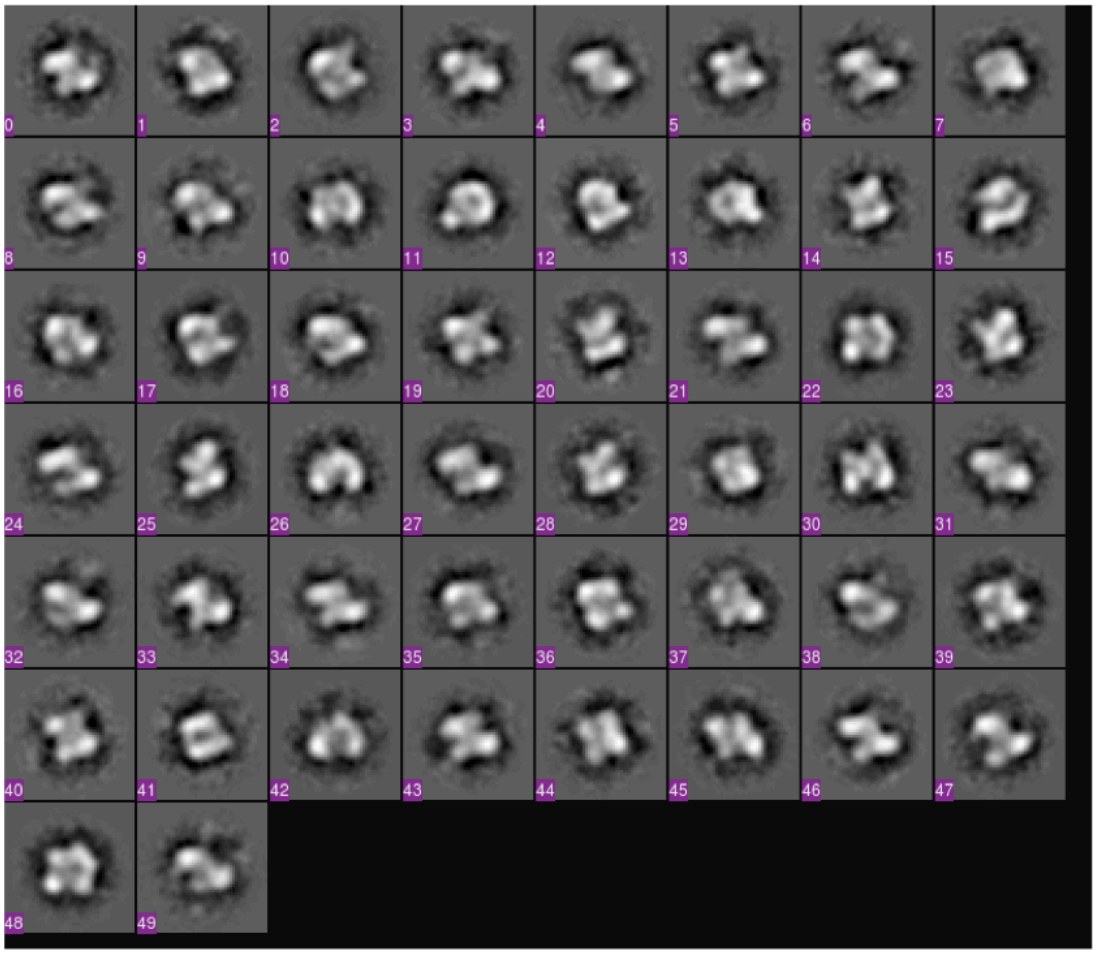

FIGURE 5-6: Averaged and classed single particle of SDUF complex using negative-stain electron microscopy.

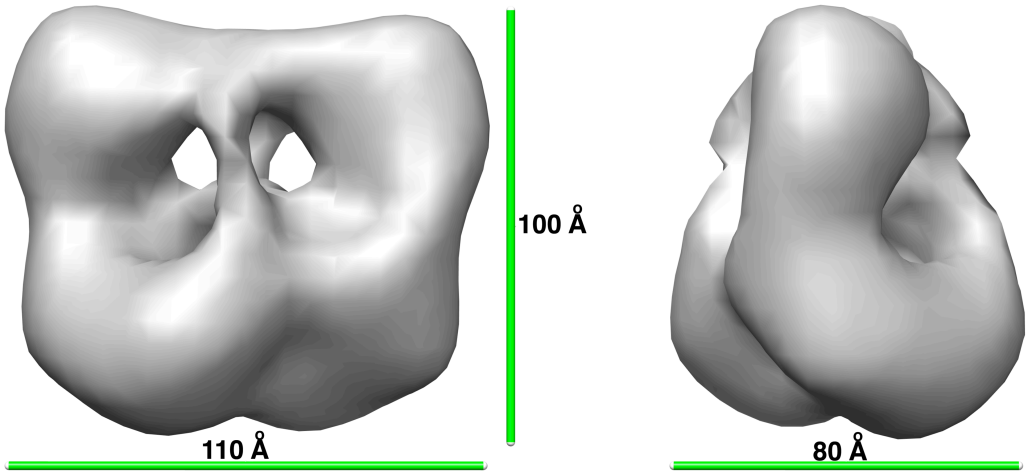

FIGURE 5-7: Reconstruction of EM model on SDUF complex at 24 Å resolution.

single particles were picked, classed, and averaged (Figure 5-6). The EM model was reconstructed after fit with multi-reference initial model. The EM structure reveals the overall shape of SDUF complex in a resolution of 24 Å (Figure 5-7). The 3D-reconstructed EM Structure has two-fold symmetry with the cavity in the center of the structure. The dimension of EM model is 110 Å x 80 Å x 100 Å. The width of EM complex is about 80 Å, which is relatively close to the width of 76 Å of *E.coli* IscS structure (PDB: 1P3W). Docking the known *E. coli* IscS-IscU complex (PDB: 3LVL) into the EM model seems not possible without changing the complex conformation. Notably, the structure of Isd11 is not known. It may be possible that Isd11 modifies the Nfs1 structure in some way.

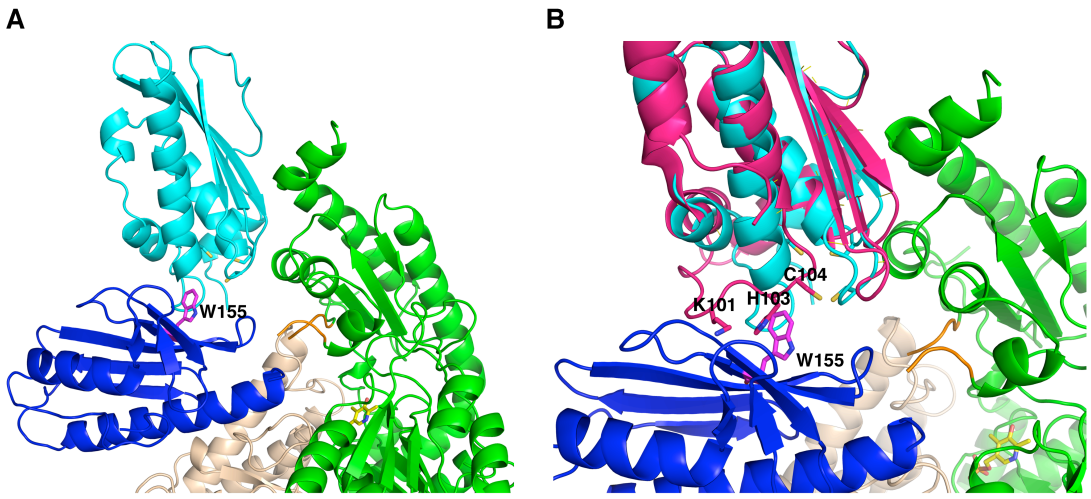

FIGURE 5-8: (A) Docking model of human Fxn with *E. coli* IscS-IscU complex (PDB: 3LVL). Fxn (blue), W155-Fxn shown in stick (magenta), IscS (green), catalytic cysteine loop on IscS (orange), PLP shown in stick (yellow), IscU (cyan), conserved cysteine residue on IscU shown in stick. (B) Alignment of *A. aerolicus* IscU to *E coli* IscU. A. aeolicus IscU (pink) structure has C-terminal coil conformation instead of helix conformation on *E. coli* IscU (cyan). K101, H103, and C104 (numbered in human Isu2) shown in stick.

Fxn Protein Docking onto IscS-IscU Complex. To better understand the interaction of Fxn with Nfs1 and Isu2. Human Fxn was docked into *E. coli* IscS-IscU crystal structure (PDB: 3LVL) with human Nfs1 and Isu2 sequence modifications. The SUF complex docking model reveals Fxn structure docks into the pocket between IscS and IscU. The conserved β-sheets of Fxn face towards to IscU (equivalent of human Isu2) and the loop between β3 and β4 sheets is near the catalytic cysteine loop of IscS (equivalent of human Nfs1) (Figure 5-8A). W155 residue is close to IscU structure near C-terminal region. N-terminal acidic patch of Fxn interacts with the other subunit of IscS, which has many positive charge arginine residues. Structure alignment of *A. aeolicus* IscU to *E. coli* IscU reveals different conformations on C-terminal region (Figure 5-8B). The coil conformation of *A. aeolicus* IscU shows K101 and H103

residues are close to W155 residue on Fxn. Together, docking model predicts Fxn interacts with IscS on N-terminal acidic patch and interacts with IscU on conserved β-sheets.

DISCUSSION

The high-resolution structure of SDUF complex is not known. Low-resolution structures of individual protein and complex were pursued to obtain the shape information. Recent studies in Isaya's group revealed full-length human Fxn (Fxn^{56-210}) oligomer can stimulate Nfs1 activity (*66*). This result was confirmed by our kinetic assay. To better understand the difference of Fxn^{56-210} and Fxn^{82-210}, low-resolution SAXS models of Fxn^{82-210} and Fxn^{56-210} were obtained to compare the non-conserved N-terminal region. The SAXS study of Fxn^{56-210} shows N-terminal region is a long disordered tail (Figure 5-1), which may either interact with other subunits to form Fxn oligomer or get cleaved to become mature Fxn (Fxn^{82-210}). Based on our previous studies, W155 residue on Fxn is critical to activate the Nfs1 activity (Figure 4-7). It may be possible that W155 residue on Fxn^{56-210} oligomer still exposes to interact with SDU complex. However, this possibility is hard to fit with our docking model (Figure 5-8A) that Fxn sits between Isu2 and Nfs1 since Fxn^{56-210} oligomer is huge (1 MDa). The other possibility is that Fxn subunit dissociates from Fxn^{56-210} oligomer and interacts with SDU complex. The association and dissociation mechanism for Fxn^{56-210} oligomer is not known. More studies on Fxn^{56-210} oligomer would be required to reconcile this dilemma.

The human Isu2 was suggested as a monomer and can bind [Fe_2S_2] cluster (*59*). We revealed Isu2 forms a four-protein complex with Nfs1, Isd11, and Fxn in a stoichiometry of $\alpha_2\beta_2\gamma_2\delta_2$ (Figure 2-6 and 2-7). The SAXS results show Isu2 forms dimer in the solution at a concentration of 2.5 mg/mL (170 μM) or above (Figure 5-3). There is no larger species has been observed at a protein concentration up to 17 mg/mL (1.2 mM). In contrast, the AUC results show Isu2 is a monomeric species at 0.5 mg/mL (34 μM) and tend to form dimer with increased concentration (Figure 5-4). The cellular level of the IscU protein has been estimated by immunoblotting methods to be about 40 μM (*53*), which is close to monomeric Isu2 concentration (34 μM) based on AUC result (Figure 5-4). This would suggest Isu2 is in monomeric state inside the cell. To further understand how Fe–S cluster bound Isu2 transfers cluster to apo target proteins. One possibility is chaperones GRP75 and HSC20 facilitate the dissociation of Isu2 from SDUF complex and assist Isu2 to transfer cluster to apo target proteins. The other possibility is another apo-Isu2 forms dimer with cluster-bound Isu2 in SDUF complex and grabs the cluster, and then dissociates. This holo-Isu2 can further transfer cluster to apo target protein under the assistance of chaperones. This possibility can be supported by our AUC and SAXS studies that Isu2 exhibits the monomer-dimer equilibrium (Figure 5-3 and 5-4).

The molecular details of interaction of Isd11 with Nfs1 and Fxn are still a mystery. Isd11 is an essential protein for Fe–S biosynthesis and only exists in eukaryotes (*51*). Isd11 maintains the function and stability of Nfs1 (*50*) and interacts with Fxn (*110*). Nfs1-Isd11 (SD) complex was crystallized as a bright yellow crystal with PLP

cofactor bound (Figure 5-5A). However, the diffraction was not high enough to determine the structure (Figure 5-5B). SD complex has molecular weight around 150 kDa based on S200 gel filtration chromatography (Figure 2-8), which was estimated as two Nfs1 and two Isd11. The sequence identity of human Nfs1 and *E. coli* IscS is about 60% and IscS structure shows strong dimer interface between two subunits. We can conclude that Nfs1 would retain the similar shape as IscS. To combine with our complex docking model (Figure 5-8A), Isd11 may sit between Nfs1 and Fxn interface. Isd11 has 14 positive arginine residues, which can interact with negative aspartate and glutamate residues on α1 helix of Fxn. However, the shape of this docking complex is difficult to fit into our EM model (Figure 5-7) unless Fxn induces SDU to different conformation.

Protein complex docking model predicts Fxn interacts between IscS (equivalent of human Nfs1) and IscU (equivalent of Isu2) (Figure 5-8A). The docking model reveals conserved β-sheet of Fxn interacts with IscU (Figure 5-8A). The position of W155 residue of Fxn could possibly interact with K101 and H103 residues of *A. aeolicus* IscU after helix-to-coli switch occurs (Figure 5-8B). The N-terminal acidic patch of Fxn, which was suggested as iron binding site (*146*), interacts with IscS. In docking model, this acidic patch may interact with positive charged arginine residues on the other subunit of IscS (Figure 5-8B), which could be the potential iron binding site. Our previous studies suggest one equivalent of ferrous iron can further stimulate the Nfs1 activity (Figure 2-1). Cowan's group suggests Isu2 interacts Fxn only in the presence of ferrous iron (*144*). Cortopassi's group suggests Fxn interacts with Isd11 is Ni-dependent (*110*). Regardless the exact iron binding site, our docking model shows the possible

interactions between Fxn and SDU complex. W155 of Fxn binds Isu2 and stabilizes the coil conformation to allow C104 on Isu2 to accept sulfur transfer from Nfs1 (Table 3-1). Docking model also supports W155 mutation would weaken the binding affinity (Table 4-1).

CHAPTER VI

CONCLUSION

Here we re-defined the role of Fxn to involve in Fe–S cluster biosynthesis. Fxn forms a complex with Nfs1, Isd11, and Isu2 and acts as an allosteric activator to initialize sulfur transfer from Nfs1 to Isu2. Fxn stabilizes the coil conformation of Isu2 and possibly interacts with K101 and H103 on Isu2 through conserved residue W155. Upon Fxn binding, the Nfs1 catalytic efficiency significantly increases from 25 to 10,100 $M^{-1}s^{-1}$. This activity stimulation is consistent with most of the published results and phenotype. There are still many unanswered questions about Fe–S cluster assembly biosynthesis such as the details of chemical mechanism of Fe–S cluster assembly, protein interactions between chaperones and Isu2, cluster transfer to apo target protein with chaperones. The fact that W155 residue of Fxn interacts with coil conformation of Isu2 suggests Fxn would lose the binding affinity to Isu2 once coil conformation switches to helix conformation for cluster bound. It indicates Fxn may leave after cluster has been made on Isu2, which allows chaperones come in and transfer cluster to apo protein. Alternatively, another apo-Isu2 comes in and grabs the cluster from holo-Isu2 on SDUF complex, followed by transferring to apo target protein under the assistance of chaperones. A larger protein complex might be also possible to become a huge Fe–S cluster assembly machine for Fe–S cluster biosynthesis. I hope these results could help other researchers further understand Fe–S cluster assembly biosynthesis.

REFERENCES

1. Arnon, D. I., Whatley, F. R., and Allen, M. B. (1957) Triphosphopyridine nucleotide as a catalyst of photosynthetic phosphorylation. *Nature 180*, 182-185.
2. Mortenson, L. E., Valentine, R. C., and Carnahan, J. E. (1962) An electron transport factor from Clostridium pasteurianum. *Biochem. Biophys. Res. Commun. 7*, 448-452.
3. Rees, D. C., and Howard, J. B. (2003) The interface between the biological and inorganic worlds: iron-sulfur metalloclusters. *Science 300*, 929-931.
4. Johnson, D. C., Dean, D. R., Smith, A. D., and Johnson, M. (2005) Structure, function, and formation of biological iron-sulfur clusters. *Annu. Rev. Biochem. 74*, 247-281.
5. Beinert, H., Holm, R. H., and Munck, E. (1997) Iron-sulfur clusters: nature's modular, multipurpose structures. *Science 277*, 653-659.
6. Frazzon, J., and Dean, D. R. (2003) Formation of iron-sulfur clusters in bacteria: an emerging field in bioinorganic chemistry. *Curr. Opin. Chem. Biol. 7*, 166-173.
7. Py, B., and Barras, F. (2010) Building Fe-S proteins: bacterial strategies. *Nat. Rev. Microbiol. 8*, 436-446.
8. Jacobson, M. R., Cash, V. L., Weiss, M. C., Laird, N. F., Newton, W. E., and Dean, D. R. (1989) Biochemical and genetic analysis of the nifUSVWZM cluster from Azotobacter vinelandii. *Mol. Gen. Genet. 219*, 49-57.

9. Zheng, L., Cash, V. L., Flint, D. H., and Dean, D. R. (1998) Assembly of iron-sulfur clusters. Identification of an iscSUA-hscBA-fdx gene cluster from Azotobacter vinelandii. *J. Biol. Chem. 273*, 13264-13272.

10. Takahashi, Y., and Tokumoto, U. (2002) A third bacterial system for the assembly of iron-sulfur clusters with homologs in archaea and plastids. *J. Biol. Chem. 277*, 28380-28383.

11. Outten, F. W., Djaman, O., and Storz, G. (2004) A suf operon requirement for Fe-S cluster assembly during iron starvation in Escherichia coli. *Mol. Microbiol. 52*, 861-872.

12. Lill, R., and Muhlenhoff, U. (2006) Iron-sulfur protein biogenesis in eukaryotes: components and mechanisms. *Annu. Rev. Cell Dev. Biol. 22*, 457-486.

13. Lill, R. (2009) Function and biogenesis of iron-sulphur proteins. *Nature 460*, 831-838.

14. Sheftel, A. D., and Lill, R. (2009) The power plant of the cell is also a smithy: the emerging role of mitochondria in cellular iron homeostasis. *Ann. Med. 41*, 82-99.

15. Zheng, L., White, R. H., Cash, V. L., and Dean, D. R. (1994) Mechanism for the desulfurization of L-cysteine catalyzed by the nifS gene product. *Biochemistry 33*, 4714-4720.

16. Yoon, T., and Cowan, J. A. (2003) Iron-sulfur cluster biosynthesis. Characterization of frataxin as an iron donor for assembly of [2Fe-2S] clusters in ISU-type proteins. *J. Am. Chem. Soc. 125*, 6078-6084.

17. Lange, H., Kaut, A., Kispal, G., and Lill, R. (2000) A mitochondrial ferredoxin is essential for biogenesis of cellular iron-sulfur proteins. *Proc. Natl. Acad. Sci. U.S.A. 97*, 1050-1055.

18. Alves, R., Herrero, E., and Sorribas, A. (2004) Predictive reconstruction of the mitochondrial iron-sulfur cluster assembly metabolism. II. Role of glutaredoxin Grx5. *Proteins 57*, 481-492.

19. Kim, K. D., Chung, W. H., Kim, H. J., Lee, K. C., and Roe, J. H. (2010) Monothiol glutaredoxin Grx5 interacts with Fe-S scaffold proteins Isa1 and Isa2 and supports Fe-S assembly and DNA integrity in mitochondria of fission yeast. *Biochem. Biophys. Res. Commun. 392*, 467-472.

20. Krebs, C., Agar, J., Smith, A. D., Frazzon, J., Dean, D. R., Huynh, B. H., and Johnson, M. (2001) IscA, an alternate scaffold for Fe-S cluster biosynthesis. *Biochemistry 40*, 14069-14080.

21. Ding, H., Clark, R. J., and Ding, B. (2004) IscA mediates iron delivery for assembly of iron-sulfur clusters in IscU under the limited accessible free iron conditions. *J. Biol. Chem. 279*, 37499-37504.

22. Tong, W.-H., Jameson, G. N. L., Huynh, B. H., and Rouault, T. (2003) Subcellular compartmentalization of human Nfu, an iron-sulfur cluster scaffold protein, and its ability to assemble a [4Fe-4S] cluster. *Proc. Natl. Acad. Sci. U.S.A. 100*, 9762-9767.

23. Liu, Y., and Cowan, J. A. (2007) Iron sulfur cluster biosynthesis. Human NFU mediates sulfide delivery to ISU in the final step of [2Fe-2S] cluster assembly. *Chem. Commun. (Cambridge, U. K.)*, 3192-3194.

24. Kispal, G., Csere, P., Prohl, C., and Lill, R. (1999) The mitochondrial proteins Atm1p and Nfs1p are essential for biogenesis of cytosolic Fe/S proteins. *EMBO J. 18*, 3981-3989.

25. Balk, J., and Lill, R. (2004) The cell's cookbook for iron--sulfur clusters: recipes for fool's gold? *Chembiochem 5*, 1044-1049.

26. Crooks, D. R., Ghosh, M. C., Haller, R. G., Tong, W.-H., and Rouault, T. A. (2009) Post-translational stability of the heme biosynthetic enzyme ferrochelatase is dependent on iron availability and intact iron-sulfur cluster assembly machinery. *Blood 115*, 860-869.

27. Jarrett, J. T. (2005) The novel structure and chemistry of iron-sulfur clusters in the adenosylmethionine-dependent radical enzyme biotin synthase. *Arch. Biochem. Biophys. 433*, 312-321.

28. Raschke, M., Burkle, L., Muller, N., Nunes-Nesi, A., Fernie, A. R., Arigoni, D., Amrhein, N., and Fitzpatrick, T. B. (2007) Vitamin B1 biosynthesis in plants requires the essential iron sulfur cluster protein, THIC. *Proc. Natl. Acad. Sci. U.S.A. 104*, 19637-19642.

29. McGoldrick, H. M., Roessner, C. A., Raux, E., Lawrence, A. D., McLean, K. J., Munro, A. W., Santabarbara, S., Rigby, S. E., Heathcote, P., Scott, A. I., and Warren, M. J. (2005) Identification and characterization of a novel vitamin B12

(cobalamin) biosynthetic enzyme (CobZ) from Rhodobacter capsulatus, containing flavin, heme, and Fe-S cofactors. *J. Biol. Chem. 280*, 1086-1094.

30. Raha, S., and Robinson, B. H. (2001) Mitochondria, oxygen free radicals, and apoptosis. *Am. J. Med. Genet. 106*, 62-70.

31. Ye, H., and Rouault, T. A. (2010) Human iron-sulfur cluster assembly, cellular iron homeostasis, and disease. *Biochemistry 49*, 4945-4956.

32. Veatch, J. R., McMurray, M. A., Nelson, Z. W., and Gottschling, D. E. (2009) Mitochondrial dysfunction leads to nuclear genome instability via an iron-sulfur cluster defect. *Cell 137*, 1247-1258.

33. Rouault, T., and Tong, W. (2008) Iron-sulfur cluster biogenesis and human disease. *Trends Genet. 24*, 398-407.

34. Olsson, A., Lind, L., Thornell, L., and Holmberg, M. (2008) Myopathy with lactic acidosis is linked to chromosome 12q23.3-24.11 and caused by an intron mutation in the ISCU gene resulting in a splicing defect. *Hum. Mol. Genet. 17*, 1666-1672.

35. Mochel, F., Knight, M. A., Tong, W.-H., Hernandez, D., Ayyad, K., Taivassalo, T., Andersen, P. M., Singleton, A., Rouault, T. A., Fischbeck, K. H., and Haller, R. G. (2008) Splice mutation in the iron-sulfur cluster scaffold protein ISCU causes myopathy with exercise intolerance. *Am. J. Hum. Genet. 82*, 652-660.

36. Kollberg, G., Tulinius, M., Melberg, A., Darin, N., Andersen, O., Holmgren, D., Oldfors, A., and Holme, E. (2009) Clinical manifestation and a new ISCU mutation in iron-sulphur cluster deficiency myopathy. *Brain 132*, 2170-2179.

37. Campuzano, V., Montermini, L., Moltè, M. D., Pianese, L., Cossee, M., Cavalcanti, F., Monros, E., Rodius, F., Duclos, F., Monticelli, A., Zara, F., Cañizares, J., Koutnikova, H., Bidichandani, S. I., Gellera, C., Brice, A., Trouillas, P., De Michele, G., Filla, A., De Frutos, R., Palau, F., Patel, P. I., Di Donato, S., Mandel, J. L., Cocozza, S., Koenig, M., and Pandolfo, M. (1996) Friedreich's ataxia: autosomal recessive disease caused by an intronic GAA triplet repeat expansion. *Science 271*, 1423-1427.

38. Schöls, L., Amoiridis, G., Przuntek, H., Frank, G., Epplen, J. T., and Epplen, C. (1997) Friedreich's ataxia. Revision of the phenotype according to molecular genetics. *Brain 120*, 2131-2140.

39. Santos, R., Lefevre, S., Sliwa, D., Seguin, A., Camadro, J. M., and Lesuisse, E. (2010) Friedreich ataxia: molecular mechanisms, redox considerations, and therapeutic opportunities. *Antioxid. Redox. Signal. 13*, 651-690.

40. Dürr, A., Cossee, M., Agid, Y., Campuzano, V., Mignard, C., Penet, C., Mandel, J. L., Brice, A., and Koenig, M. (1996) Clinical and genetic abnormalities in patients with Friedreich's ataxia. *N. Engl. J. Med. 335*, 1169-1175.

41. Kessler, D. (2006) Enzymatic activation of sulfur for incorporation into biomolecules in prokaryotes. *FEMS Microbiol. Rev. 30*, 825-840.

42. Zhang, W., Urban, A., Mihara, H., Leimkühler, S., Kurihara, T., and Esaki, N. (2010) IscS functions as a primary sulfur-donating enzyme by interacting specifically with MoeB and MoaD in the biosynthesis of molybdopterin in Escherichia coli. *J. Biol. Chem. 285*, 2302-2308.

43. Zheng, L., White, R. H., Cash, V. L., Jack, R. F., and Dean, D. R. (1993) Cysteine desulfurase activity indicates a role for NIFS in metallocluster biosynthesis. *Proc. Natl. Acad. Sci. U.S.A. 90*, 2754-2758.

44. Shi, R., Proteau, A., Villarroya, M., Moukadiri, I., Zhang, L., Trempe, J.-F., Matte, A., Armengod, M. E., and Cygler, M. (2010) Structural basis for Fe-S cluster assembly and tRNA thiolation mediated by IscS protein-protein interactions. *PLoS Biol. 8*, e1000354.

45. Behshad, E., Parkin, S. E., and Bollinger, J. M. (2004) Mechanism of cysteine desulfurase Slr0387 from Synechocystis sp. PCC 6803: kinetic analysis of cleavage of the persulfide intermediate by chemical reductants. *Biochemistry 43*, 12220-12226.

46. Cupp-Vickery, J., Urbina, H. D., and Vickery, L. (2003) Crystal structure of IscS, a cysteine desulfurase from Escherichia coli. *J. Mol. Biol. 330*, 1049-1059.

47. Land, T., and Rouault, T. (1998) Targeting of a human iron-sulfur cluster assembly enzyme, nifs, to different subcellular compartments is regulated through alternative AUG utilization. *Mol. Cell 2*, 807-815.

48. Marelja, Z., Stöcklein, W., Nimtz, M., and Leimkühler, S. (2008) A novel role for human Nfs1 in the cytoplasm: Nfs1 acts as a sulfur donor for MOCS3, a protein involved in molybdenum cofactor biosynthesis. *J. Biol. Chem. 283*, 25178-25185.

49. Wiedemann, N., Urzica, E., Guiard, B., Müller, H., Lohaus, C., Meyer, H. E., Ryan, M. T., Meisinger, C., Muhlenhoff, U., Lill, R., and Pfanner, N. (2006)

Essential role of Isd11 in mitochondrial iron-sulfur cluster synthesis on Isu scaffold proteins. *EMBO J. 25*, 184-195.

50. Adam, A. C., Bornhövd, C., Prokisch, H., Neupert, W., and Hell, K. (2006) The Nfs1 interacting protein Isd11 has an essential role in Fe/S cluster biogenesis in mitochondria. *EMBO J. 25*, 174-183.

51. Richards, T. A., and van der Giezen, M. (2006) Evolution of the Isd11-IscS complex reveals a single alpha-proteobacterial endosymbiosis for all eukaryotes. *Mol. Biol. Evol. 23*, 1341-1344.

52. Tsai, C. L., and Barondeau, D. P. (2010) Human frataxin is an allosteric switch that activates the Fe-S cluster biosynthetic complex. *Biochemistry 49*, 9132-9139.

53. Hoff, K. G., Silberg, J. J., and Vickery, L. (2000) Interaction of the iron-sulfur cluster assembly protein IscU with the Hsc66/Hsc20 molecular chaperone system of Escherichia coli. *Proc. Natl. Acad. Sci. U.S.A. 97*, 7790-7795.

54. Kim, J. H., Fuzery, A. K., Tonelli, M., Ta, D. T., Westler, W. M., Vickery, L. E., and Markley, J. L. (2009) Structure and dynamics of the iron-sulfur cluster assembly scaffold protein IscU and its interaction with the cochaperone HscB. *Biochemistry 48*, 6062-6071.

55. Hwang, D. M., Dempsey, A., Tan, K. T., and Liew, C. C. (1996) A modular domain of NifU, a nitrogen fixation cluster protein, is highly conserved in evolution. *J. Mol. Evol. 43*, 536-540.

56. Tong, W.-H., and Rouault, T. (2000) Distinct iron-sulfur cluster assembly complexes exist in the cytosol and mitochondria of human cells. *EMBO J. 19*, 5692-5700.

57. Huang, J., and Cowan, J. A. (2009) Iron-sulfur cluster biosynthesis: role of a semi-conserved histidine. *Chem. Commun. (Cambridge, U. K.) 21*, 3071-3073.

58. Shimomura, Y., Wada, K., Fukuyama, K., and Takahashi, Y. (2008) The asymmetric trimeric architecture of [2Fe-2S] IscU: implications for its scaffolding during iron-sulfur cluster biosynthesis. *J. Mol. Biol. 383*, 133-143.

59. Foster, M. W., Mansy, S. S., Hwang, J., Penner-Hahn, J. E., Surerus, K. K., and Cowan, J. A. (2000) A mutant human IscU protein contains a stable [2Fe2S]2+ center of possible functional significance. *J. Am. Chem. Soc. 122*, 6805-6806.

60. Agar, J., Zheng, L., Cash, V. L., Dean, D. R., and Johnson, M. K. (2000) Role of the IscU protein in iron-sulfur cluster biosynthesis: IscS-mediated assembly of a [Fe2S2] cluster in IscU. *J. Am. Chem. Soc. 122*, 2136-2137.

61. Bertini, I., Cowan, J. A., Del Bianco, C., Luchinat, C., and Mansy, S. S. (2003) Thermotoga maritima IscU. Structural characterization and dynamics of a new class of metallochaperone. *J. Mol. Biol. 331*, 907-924.

62. Mansy, S. S., Wu, S.-p., and Cowan, J. A. (2004) Iron-sulfur cluster biosynthesis: biochemical characterization of the conformational dynamics of Thermotoga maritima IscU and the relevance for cellular cluster assembly. *J. Biol. Chem. 279*, 10469-10475.

63. Hoff, K. G., Ta, D. T., Tapley, T. L., Silberg, J. J., and Vickery, L. (2002) Hsc66 substrate specificity is directed toward a discrete region of the iron-sulfur cluster template protein IscU. *J. Biol. Chem. 277*, 27353-27359.

64. Schmucker, S., and Puccio, H. (2010) Understanding the molecular mechanisms of Friedreich's ataxia to develop therapeutic approaches. *Hum. Mol. Genet. 19*, R103-110.

65. Schmucker, S., Argentini, M., Carelle-Calmels, N., Martelli, A., and Puccio, H. (2008) The in vivo mitochondrial two-step maturation of human frataxin. *Hum. Mol. Genet. 17*, 3521-3531.

66. Gakh, O., Bedekovics, T., Duncan, S. F., Smith, D. Y. t., Berkholz, D. S., and Isaya, G. (2010) Normal and Friedreich ataxia cells express different isoforms of frataxin with complementary roles in iron-sulfur cluster assembly. *J. Biol. Chem. 285*, 38486-38501.

67. Karlberg, T., Schagerlöf, U., Gakh, O., Park, S., Ryde, U., Lindahl, M., Leath, K., Garman, E., Isaya, G., and Al-Karadaghi, S. (2006) The structures of frataxin oligomers reveal the mechanism for the delivery and detoxification of iron. *Structure 14*, 1535-1546.

68. Lewin, A., Moore, G. R., and Le Brun, N. E. (2005) Formation of protein-coated iron minerals. *Dalton transactions (Cambridge, England : 2003)*, 3597-3610.

69. Schagerlof, U., Elmlund, H., Gakh, O., Nordlund, G., Hebert, H., Lindahl, M., Isaya, G., and Al-Karadaghi, S. (2008) Structural basis of the iron storage

function of frataxin from single-particle reconstruction of the iron-loaded oligomer. *Biochemistry 47*, 4948-4954.

70. Nichol, H., Gakh, O., O'Neill, H. A., Pickering, I. J., Isaya, G., and George, G. N. (2003) Structure of frataxin iron cores: an X-ray absorption spectroscopic study. *Biochemistry 42*, 5971-5976.

71. Park, S., Gakh, O., O'Neill, H. A., Mangravita, A., Nichol, H., Ferreira, G. C., and Isaya, G. (2003) Yeast frataxin sequentially chaperones and stores iron by coupling protein assembly with iron oxidation. *J. Biol. Chem. 278*, 31340-31351.

72. Adinolfi, S., Trifuoggi, M., Politou, A., Martin, S. R., and Pastore, A. (2002) A structural approach to understanding the iron-binding properties of phylogenetically different frataxins. *Hum. Mol. Genet. 11*, 1865-1877.

73. O'Neill, H. A., Gakh, O., and Isaya, G. (2005) Supramolecular assemblies of human frataxin are formed via subunit-subunit interactions mediated by a non-conserved amino-terminal region. *J. Mol. Biol. 345*, 433-439.

74. Aloria, K., Schilke, B., Andrew, A. J., and Craig, E. (2004) Iron-induced oligomerization of yeast frataxin homologue Yfh1 is dispensable in vivo. *EMBO Rep. 5*, 1096-1101.

75. Lane, D. J. R., and Richardson, D. R. (2010) Frataxin, a molecule of mystery: trading stability for function in its iron-binding site. *Biochem. J. 426*, e1-3.

76. Gakh, O., Park, S., Liu, G., Macomber, L., Imlay, J. A., Ferreira, G. C., and Isaya, G. (2006) Mitochondrial iron detoxification is a primary function of

frataxin that limits oxidative damage and preserves cell longevity. *Hum. Mol. Genet. 15*, 467-479.

77. Bulteau, A.-L., O'Neill, H. A., Kennedy, M. C., Ikeda-Saito, M., Isaya, G., and Szweda, L. I. (2004) Frataxin acts as an iron chaperone protein to modulate mitochondrial aconitase activity. *Science 305*, 242-245.

78. Yoon, T., and Cowan, J. A. (2004) Frataxin-mediated iron delivery to ferrochelatase in the final step of heme biosynthesis. *J. Biol. Chem. 279*, 25943-25946.

79. Gallivan, J. P., and Dougherty, D. A. (1999) Cation-pi interactions in structural biology. *Proc. Natl. Acad. Sci. U.S.A. 96*, 9459-9464.

80. Adinolfi, S., Iannuzzi, C., Prischi, F., Pastore, C., Iametti, S., Martin, S. R., Bonomi, F., and Pastore, A. (2009) Bacterial frataxin CyaY is the gatekeeper of iron-sulfur cluster formation catalyzed by IscS. *Nat. Struct. Mol. Biol. 16*, 390-396.

81. Li, K., Besse, E. K., Ha, D., Kovtunovych, G., and Rouault, T. A. (2008) Iron-dependent regulation of frataxin expression: implications for treatment of Friedreich ataxia. *Hum. Mol. Genet. 17*, 2265-2273.

82. Li, K., Singh, A., Crooks, D. R., Dai, X., Cong, Z., Pan, L., Ha, D., and Rouault, T. A. (2010) Expression of human frataxin is regulated by transcription factors SRF and TFAP2. *PLoS ONE 5*, e12286.

83. Cossee, M., Dürr, A., Schmitt, M., Dahl, N., Trouillas, P., Allinson, P., Kostrzewa, M., Nivelon-Chevallier, A., Gustavson, K. H., Kohlschütter, A.,

Müller, U., Mandel, J. L., Brice, A., Koenig, M., Cavalcanti, F., Tammaro, A., De Michele, G., Filla, A., Cocozza, S., Labuda, M., Montermini, L., Poirier, J., and Pandolfo, M. (1999) Friedreich's ataxia: point mutations and clinical presentation of compound heterozygotes. *Ann. Neurol. 45*, 200-206.

84. Deutsch, E. C., Santani, A. B., Perlman, S. L., Farmer, J. M., Stolle, C. A., Marusich, M. F., and Lynch, D. R. (2010) A rapid, noninvasive immunoassay for frataxin: utility in assessment of Friedreich ataxia. *Mol. Genet. Metab. 101*, 238-245.

85. Correia, A., Pastore, C., Adinolfi, S., Pastore, A., and Gomes, C. (2008) Dynamics, stability and iron-binding activity of frataxin clinical mutants. *FEBS J. 275*, 3680-3690.

86. Correia, A. R., Ow, S. Y., Wright, P. C., and Gomes, C. M. (2009) The conserved Trp155 in human frataxin as a hotspot for oxidative stress related chemical modifications. *Biochem. Biophys. Res. Commun. 390*, 1007-1011.

87. Correia, A. R., Wang, T., Craig, E. A., and Gomes, C. M. (2010) Iron-binding activity in yeast frataxin entails a trade off with stability in the alpha1/beta1 acidic ridge region. *Biochem. J. 426*, 197-203.

88. Leidgens, S., De Smet, S., and Foury, F. (2010) Frataxin interacts with Isu1 through a conserved tryptophan in its beta-sheet. *Hum. Mol. Genet. 19*, 276-286.

89. Kato, S.-I., Mihara, H., Kurihara, T., Takahashi, Y., Tokumoto, U., Yoshimura, T., and Esaki, N. (2002) Cys-328 of IscS and Cys-63 of IscU are the sites of disulfide bridge formation in a covalently bound IscS/IscU complex: implications

for the mechanism of iron-sulfur cluster assembly. *Proc. Natl. Acad. Sci. U.S.A. 99*, 5948-5952.

90. Smith, A. D., Frazzon, J., Dean, D. R., and Johnson, M. (2005) Role of conserved cysteines in mediating sulfur transfer from IscS to IscU. *FEBS Lett. 579*, 5236-5240.

91. Fontecave, M., Choudens, S. O. d., Py, B., and Barras, F. (2005) Mechanisms of iron-sulfur cluster assembly: the SUF machinery. *J. Biol. Inorg. Chem. 10*, 713-721.

92. Layer, G., Gaddam, S. A., Ayala-Castro, C. N., Ollagnier de Choudens, S., Lascoux, D., Fontecave, M., and Outten, F. W. (2007) SufE transfers sulfur from SufS to SufB for iron-sulfur cluster assembly. *J. Biol. Chem. 282*, 13342-13350.

93. Ollagnier de Choudens, S., Lascoux, D., Loiseau, L., Barras, F., Forest, E., and Fontecave, M. (2003) Mechanistic studies of the SufS-SufE cysteine desulfurase: evidence for sulfur transfer from SufS to SufE. *FEBS Lett. 555*, 263-267.

94. Smith, A. D., Agar, J., Johnson, K. A., Frazzon, J., Amster, I. J., Dean, D. R., and Johnson, M. (2001) Sulfur transfer from IscS to IscU: the first step in iron-sulfur cluster biosynthesis. *J. Am. Chem. Soc. 123*, 11103-11104.

95. Adinolfi, S., Rizzo, F., Masino, L., Nair, M., Martin, S. R., Pastore, A., and Temussi, P. A. (2004) Bacterial IscU is a well folded and functional single domain protein. *Eur. J. Biochem. 271*, 2093-2100.

96. Mansy, S. S., Wu, G., Surerus, K. K., and Cowan, J. A. (2002) Iron-sulfur cluster biosynthesis. Thermatoga maritima IscU is a structured iron-sulfur cluster assembly protein. *J. Biol. Chem. 277*, 21397-21404.

97. Urbina, H. D., Silberg, J. J., Hoff, K. G., and Vickery, L. (2001) Transfer of sulfur from IscS to IscU during Fe/S cluster assembly. *J. Biol. Chem. 276*, 44521-44526.

98. Beinert, H., Holm, R. H., and Münck, E. (1997) Iron-sulfur clusters: nature's modular, multipurpose structures. *Science 277*, 653-659.

99. Layer, G., Ollagnier de Choudens, S., Sanakis, Y., and Fontecave, M. (2006) Iron-sulfur cluster biosynthesis: characterization of Escherichia coli CYaY as an iron donor for the assembly of [2Fe-2S] clusters in the scaffold IscU. *J. Biol. Chem. 281*, 16256-16263.

100. Cook, J. D., Bencze, K. Z., Jankovic, A. D., Crater, A. K., Busch, C. N., Bradley, P. B., Stemmler, A. J., Spaller, M. R., and Stemmler, T. L. (2006) Monomeric yeast frataxin is an iron-binding protein. *Biochemistry 45*, 7767-7777.

101. Sheftel, A. D., Stehling, O., Pierik, A. J., Elsasser, H. P., Muhlenhoff, U., Webert, H., Hobler, A., Hannemann, F., Bernhardt, R., and Lill, R. (2010) Humans possess two mitochondrial ferredoxins, Fdx1 and Fdx2, with distinct roles in steroidogenesis, heme, and Fe/S cluster biosynthesis. *Proc. Natl. Acad. Sci. U.S.A. 107*, 11775-11780.

102. Amutha, B., Gordon, D., Gu, Y., Lyver, E., Dancis, A., and Pain, D. (2008) GTP is required for iron-sulfur cluster biogenesis in mitochondria. *J. Biol. Chem. 283*, 1362-1371.

103. Muhlenhoff, U., Richhardt, N., Ristow, M., Kispal, G., and Lill, R. (2002) The yeast frataxin homolog Yfh1p plays a specific role in the maturation of cellular Fe/S proteins. *Hum. Mol. Genet. 11*, 2025-2036.

104. Stehling, O., Elsässer, H.-P., Brückel, B., Muhlenhoff, U., and Lill, R. (2004) Iron-sulfur protein maturation in human cells: evidence for a function of frataxin. *Hum. Mol. Genet. 13*, 3007-3015.

105. Cavadini, P., O'Neill, H. A., Benada, O., and Isaya, G. (2002) Assembly and iron-binding properties of human frataxin, the protein deficient in Friedreich ataxia. *Hum. Mol. Genet. 11*, 217-227.

106. Seguin, A., Sutak, R., Bulteau, A. L., Garcia-Serres, R., Oddou, J. L., Lefevre, S., Santos, R., Dancis, A., Camadro, J. M., Latour, J. M., and Lesuisse, E. (2010) Evidence that yeast frataxin is not an iron storage protein in vivo. *Biochim. Biophys. Acta 1802*, 531-538.

107. Duby, G., Foury, F., Ramazzotti, A., Herrmann, J., and Lutz, T. (2002) A non-essential function for yeast frataxin in iron-sulfur cluster assembly. *Hum. Mol. Genet. 11*, 2635-2643.

108. Gerber, J., Muhlenhoff, U., and Lill, R. (2003) An interaction between frataxin and Isu1/Nfs1 that is crucial for Fe/S cluster synthesis on Isu1. *EMBO Rep. 4*, 906-911.

109. Tokumoto, U., Nomura, S., Minami, Y., Mihara, H., Kato, S.-I., Kurihara, T., Esaki, N., Kanazawa, H., Matsubara, H., and Takahashi, Y. (2002) Network of protein-protein interactions among iron-sulfur cluster assembly proteins in Escherichia coli. *J. Biochem. 131*, 713-719.

110. Shan, Y., Napoli, E., and Cortopassi, G. A. (2007) Mitochondrial frataxin interacts with ISD11 of the NFS1/ISCU complex and multiple mitochondrial chaperones. *Hum. Mol. Genet. 16*, 929-941.

111. Ramazzotti, A., Vanmansart, V., and Foury, F. (2004) Mitochondrial functional interactions between frataxin and Isu1p, the iron-sulfur cluster scaffold protein, in Saccharomyces cerevisiae. *FEBS Lett. 557*, 215-220.

112. Shi, Y., Ghosh, M. C., Tong, W. H., and Rouault, T. A. (2009) Human ISD11 is essential for both iron-sulfur cluster assembly and maintenance of normal cellular iron homeostasis. *Hum. Mol. Genet. 18*, 3014-3025.

113. Muhlenhoff, U., Gerber, J., Richhardt, N., and Lill, R. (2003) Components involved in assembly and dislocation of iron-sulfur clusters on the scaffold protein Isu1p. *EMBO J. 22*, 4815-4825.

114. Bradford, M. M. (1976) A rapid and sensitive method for the quantitation of microgram quantities of protein utilizing the principle of protein-dye binding. *Anal. Biochem. 72*, 248-254.

115. Gill, S. C., and von Hippel, P. H. (1989) Calculation of protein extinction coefficients from amino acid sequence data. *Anal. Biochem. 182*, 319-326.

116. Siegel, L. M. (1965) A direct microdetermination for sulfide. *Anal. Biochem. 11*, 126-132.

117. Agar, J., Krebs, C., Frazzon, J., Huynh, B. H., Dean, D. R., and Johnson, M. (2000) IscU as a scaffold for iron-sulfur cluster biosynthesis: sequential assembly of [2Fe-2S] and [4Fe-4S] clusters in IscU. *Biochemistry 39*, 7856-7862.

118. Schagger, H. (2001) Blue-native gels to isolate protein complexes from mitochondria. *Methods Cell Biol. 65*, 231-244.

119. Furne, J., Saeed, A., and Levitt, M. D. (2008) Whole tissue hydrogen sulfide concentrations are orders of magnitude lower than presently accepted values. *Am. J. Physiol. Regul. Integr. Comp. Physiol. 295*, R1479-1485.

120. Ohmori, S., Nawata, Y., Kiyono, K., Murata, H., Tsuboi, S., Ikeda, M., Akagi, R., Morohashi, K. I., and Ono, B. (1999) Saccharomyces cerevisiae cultured under aerobic and anaerobic conditions: air-level oxygen stress and protection against stress. *Biochim. Biophys. Acta 1472*, 587-594.

121. Ross-Inta, C., Tsai, C. Y., and Giulivi, C. (2008) The mitochondrial pool of free amino acids reflects the composition of mitochondrial DNA-encoded proteins: indication of a post- translational quality control for protein synthesis. *Biosci. Rep. 28*, 239-249.

122. Kondapalli, K. C., Kok, N. M., Dancis, A., and Stemmler, T. L. (2008) Drosophila frataxin: An iron chaperone during cellular Fe-S cluster bioassembly. *Biochemistry 47*, 6917-6927.

123. Li, H., Gakh, O., Smith, D. Y. t., and Isaya, G. (2009) Oligomeric yeast frataxin drives assembly of core machinery for mitochondrial iron-sulfur cluster synthesis. *J. Biol. Chem. 284*, 21971-21980.

124. Truman, D. E., and Korner, A. (1962) Incorporation of amino acids into the protein of isolated mitochondria. A search for optimum conditions and a relationship to oxidative phosphorylation. *Biochem. J. 83*, 588-596.

125. Baird, G. D. (1964) The release of amino acids from rat-liver mitochondrial extract. *Biochim. Biophys. Acta 93*, 293-303.

126. Loiseau, L., Ollagnier de Choudens, S., Nachin, L., Fontecave, M., and Barras, F. (2003) Biogenesis of Fe-S cluster by the bacterial Suf system: SufS and SufE form a new type of cysteine desulfurase. *J. Biol. Chem. 278*, 38352-38359.

127. Goldsmith-Fischman, S., Kuzin, A., Edstrom, W. C., Benach, J., Shastry, R., Xiao, R., Acton, T. B., Honig, B., Montelione, G. T., and Hunt, J. F. (2004) The SufE sulfur-acceptor protein contains a conserved core structure that mediates interdomain interactions in a variety of redox protein complexes. *J. Mol. Biol. 344*, 549-565.

128. Albrecht, A. G., Netz, D. J. A., Miethke, M., Pierik, A. J., Burghaus, O., Peuckert, F., Lill, R., and Marahiel, M. A. (2010) SufU is an essential iron-sulfur cluster scaffold protein in Bacillus subtilis. *J. Bacteriol. 192*, 1643-1651.

129. Dutkiewicz, R., Marszalek, J., Schilke, B., Craig, E., Lill, R., and Muhlenhoff, U. (2006) The Hsp70 chaperone Ssq1p is dispensable for iron-sulfur cluster formation on the scaffold protein Isu1p. *J. Biol. Chem. 281*, 7801-7808.

130. Kambampati, R., and Lauhon, C. T. (1999) IscS is a sulfurtransferase for the in vitro biosynthesis of 4-thiouridine in Escherichia coli tRNA. *Biochemistry 38*, 16561-16568.

131. Boehm, T., Scheiber-Mojdehkar, B., Kluge, B., Goldenberg, H., Laccone, F., and Sturm, B. (2010) Variations of frataxin protein levels in normal individuals. *Neurol. Sci.*, [Epub ahead of print].

132. Mueller, E. G. (2006) Trafficking in persulfides: delivering sulfur in biosynthetic pathways. *Nat. Chem. Biol. 2*, 185-194.

133. Cavadini, P., Adamec, J., Taroni, F., Gakh, O., and Isaya, G. (2000) Two-step processing of human frataxin by mitochondrial processing peptidase. Precursor and intermediate forms are cleaved at different rates. *J. Biol. Chem. 275*, 41469-41475.

134. Long, S., Jirku, M., Ayala, F. J., and Lukes, J. (2008) Mitochondrial localization of human frataxin is necessary but processing is not for rescuing frataxin deficiency in Trypanosoma brucei. *Proc. Natl. Acad. Sci. U.S.A. 105*, 13468-13473.

135. Koutnikova, H., Campuzano, V., and Koenig, M. (1998) Maturation of wild-type and mutated frataxin by the mitochondrial processing peptidase. *Hum. Mol. Genet. 7*, 1485-1489.

136. Branda, S. S., Cavadini, P., Adamec, J., Kalousek, F., Taroni, F., and Isaya, G. (1999) Yeast and human frataxin are processed to mature form in two sequential

steps by the mitochondrial processing peptidase. *J. Biol. Chem. 274*, 22763-22769.

137. Condo, I., Ventura, N., Malisan, F., Rufini, A., Tomassini, B., and Testi, R. (2007) In vivo maturation of human frataxin. *Hum. Mol. Genet. 16*, 1534-1540.

138. Yoon, T., Dizin, E., and Cowan, J. A. (2007) N-terminal iron-mediated self-cleavage of human frataxin: regulation of iron binding and complex formation with target proteins. *J. Biol. Inorg. Chem. 12*, 535-542.

139. Stemmler, T. L., Lesuisse, E., Pain, D., and Dancis, A. (2010) Frataxin and mitochondrial FeS cluster biogenesis. *J. Biol. Chem. 285*, 26737-26743.

140. Calmels, N., Schmucker, S., Wattenhofer-Donzé, M., Martelli, A., Vaucamps, N., Reutenauer, L., Messaddeq, N., Bouton, C., Koenig, M., and Puccio, H. (2009) The first cellular models based on frataxin missense mutations that reproduce spontaneously the defects associated with Friedreich ataxia. *PLoS ONE 4*, e6379.

141. Di Cera, E. (2009) Kinetics of Allosteric Activation. *Methods Enzymol. 466*, 259-271.

142. Heine, A., DeSantis, G., Luz, J. G., Mitchell, M., Wong, C. H., and Wilson, I. A. (2001) Observation of covalent intermediates in an enzyme mechanism at atomic resolution. *Science 294*, 369-374.

143. Dhe-Paganon, S., Shigeta, R., Chi, Y. I., Ristow, M., and Shoelson, S. E. (2000) Crystal structure of human frataxin. *J. Biol. Chem. 275*, 30753-30756.

144. Huang, J., Dizin, E., and Cowan, J. A. (2008) Mapping iron binding sites on human frataxin: implications for cluster assembly on the ISU Fe-S cluster scaffold protein. *J. Biol. Inorg. Chem. 13*, 825-836.

145. Cook, J. D., Bencze, K. Z., Jankovic, A. D., Crater, A. K., Busch, C. N., Bradley, P. B., Stemmler, A. J., Spaller, M. R., and Stemmler, T. (2006) Monomeric yeast frataxin is an iron-binding protein. *Biochemistry 45*, 7767-7777.

146. Foury, F., Pastore, A., and Trincal, M. (2007) Acidic residues of yeast frataxin have an essential role in Fe-S cluster assembly. *EMBO Rep. 8*, 194-199.

147. Riboldi, G. P., Verli, H., and Frazzon, J. (2009) Structural studies of the Enterococcus faecalis SufU [Fe-S] cluster protein. *BMC Biochem. 10*, 3.

148. Fu, W., Jack, R. F., Morgan, T. V., Dean, D. R., and Johnson, M. (1994) nifU gene product from Azotobacter vinelandii is a homodimer that contains two identical [2Fe-2S] clusters. *Biochemistry 33*, 13455-13463.

149. Bandyopadhyay, S., Chandramouli, K., and Johnson, M. (2008) Iron-sulfur cluster biosynthesis. *Biochem. Soc. Trans. 36*, 1112-1119.

APPENDIX A

MECHANISTIC AND STRUCTURAL STUDIES OF H373Q FLAVO-CYTOCHROME B2: EFFECTS OF MUTANTING THE ACTIVE SITE BASE*

ABSTRACT

His373 in flavocytochrome b_2 has been proposed to act as an active site base during the oxidation of lactate to pyruvate, most likely by removing the lactate hydroxyl proton. The effects of mutating this residue to glutamine have been determined to provide further insight into its role. The k_{cat} and $k_{cat}/K_{lactate}$ values for the mutant protein are 3 to 4 orders of magnitude smaller than the wild-type values, consistent with a critical role for H373. Similar effects are seen when the mutation is incorporated into the isolated flavin domain of the enzyme, narrowing the effects to lactate oxidation rather than subsequent electron transfers. The decrease of 3500-fold in the rate constant for reduction of the enzyme-bound FMN by lactate confirms this part of the reaction as that most effected by the mutation. The primary deuterium and solvent kinetic isotope effects for the mutant enzyme are significantly smaller than the wild-type values, establishing that bond cleavage steps are less rate-limiting in H373Q flavocytochrome b_2 than in the wild-type enzyme. The structure of the mutant enzyme with pyruvate bound, determined

*This appendix is reprinted with permission from "Mechanistic and Structural Studies of H373Q Flavocytochrome b_2: Effects of Mutating the Active Site Base" by Tsai, C.-L., Gokulan, K., Sobrado, P., Sacchettini, J.C., Fitzpatrick, P.F. (2007). *Biochemistry, 46*, 7844-7851, Copyright [2007] by American Chemical Society.

at 2.8 Å, provides a rationale for these effects. The orientation of pyruvate in the active site is altered from that seen in the wild-type enzyme. In addition, the active site residues R289, D292, and L286 have altered positions in the mutant protein. The combination of an altered active site and the small kinetic isotope effects is consistent with the slowest step in turnover being a conformational change involving a conformation in which lactate is bound unproductively.

INTRODUCTION

Flavocytochrome b_2 from *Saccharomyces cerevisae* is a lactate dehydrogenase that catalyzes the transfer of a hydride equivalent from its hydroxy acid substrate to the enzymebound flavin and thence to proteins of the mitochondrial electron transport chain via a bound cytochrome (*1*). This enzyme is the paradigm for the flavoproteins that catalyze the oxidation of α-hydroxy acids, a family of enzymes with conserved three-dimensional and active site structures found in plants, animals, and bacteria (*2–8*). The two cofactors of flavocytochrome b_2 are in different domains of the protein (*9*). Residues 1–99 make up the heme binding domain and resemble cytochrome b_5 in structure. Residues 100–486 contain the FMN in a TIM barrel. This flavin domain is homologous to the other α-hydroxy acid-oxidizing flavoproteins (*6*) and can catalyze lactate oxidation in the absence of the heme domain (*10*). Figure A-1 shows the arrangements of amino acids in the active site of flavocytochrome b_2 in relation to the FMN cofactor and bound pyruvate product (*9*). Of the seven amino acid residues in Figure A-1, six are conserved in all members of the family to date, whereas Y143 is conserved in most

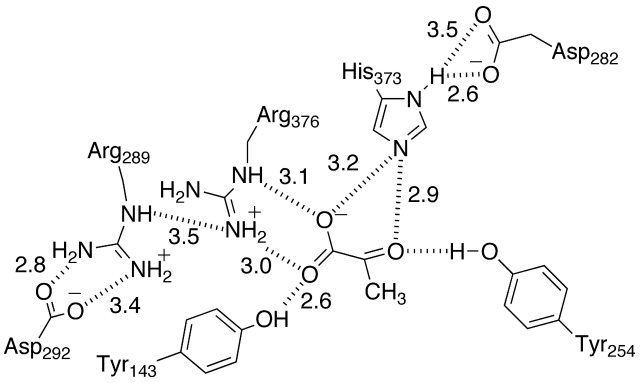

FIGURE A-1: Interactions between active site residues in wild-type flavocytochrome b_2 and pyruvate, on the basis of pdb file 1KBI (*39*).

flavocytochrome b_2	A**Y**YSSGAND	YQL**Y**VN	V**D**APSLGQ**R**	GVVLSN**H**GG**R**QLD
hydroxy acid oxidase	DFIEGEADD	FQL**Y**MK	I**D**TPVLGN**R**	GIVVSN**H**GG**R**QLD
glycolate oxidase	D**Y**YASGAED	FQL**Y**VY	V**D**TPRLGR**R**	GIIVSN**H**GA**R**QLD
mandelate dehydrogenase	D**Y**LEGGAED	FQL**Y**VI	T**D**VAVNGY**R**	GVILSN**H**GG**R**QLD
lactate monooxygenase	S**Y**VAGGSGD	FQL**Y**YP	L**D**TWIFGW**R**	GIYCSN**H**GG**R**QAN
	143	254	282 289	373

FIGURE A-2: Alignment of sequences of flavoprotein hydroxy acid oxidases and dehydrogenases, showing conservation of active site residues. The residue numbering is for flavocytochrome b_2.

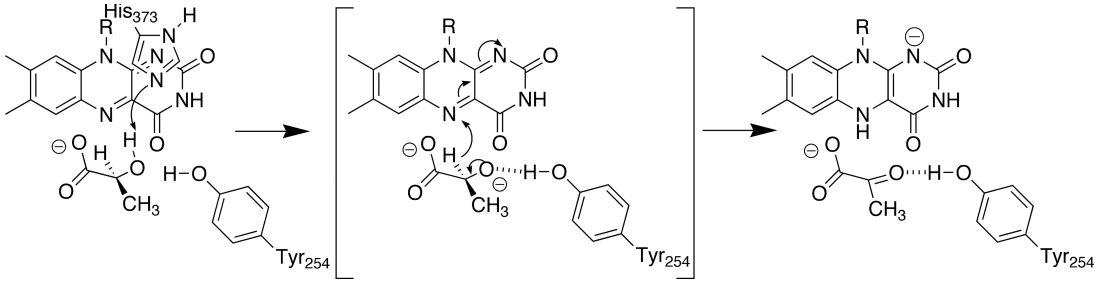

FIGURE A-3: Proposed mechanism for oxidation of lactate by flavocytochrome b_2 (*19*).

(Figure A-2). Site-directed mutagenesis has confirmed the importance of several of these residues for substrate oxidation by this family of flavoproteins (*11–21*).

The details of the mechanism by which these enzymes transfer a hydride equivalent from the α-hydroxy acid substrate to the flavin have been controversial (*22–24*). Results of mechanistic studies have been interpreted as evidence for removal of the α-hydrogen both as a proton, followed by subsequent transfer of electrons, and as a hydride so that the proton and two electrons are simultaneously transferred to the flavin. A similar controversy exists for the related flavoprotein amine oxidases, for which there is accumulating support for a hydride transfer mechanism (*24–27*). Recently, deuterium and solvent kinetic isotope effects on wild-type flavocytochrome *b*2 and the Y254F mutant enzyme led to a variation on a mechanism involving hydride transfer (Figure A-3) (*19*). In this mechanism, H373 acts as a base to remove the hydroxyl proton of the substrate and form an alkoxide. The α-hydrogen is then transferred to the FMN as a hydride. The previous results could not distinguish whether the alkoxide is a true intermediate or whether the reaction is highly asynchronous with proton transfer essentially complete in the transition state for CH bond cleavage. The role of H373 in this proposal is different from that in which the α-hydrogen is removed as a proton to form a carbanion, where this residue is the base that abstracts the α-proton (*28*).

Site-directed mutagenesis of H373 in flavocytochrome b_2 or of the corresponding residue in other members of this family of flavoproteins results in a large decrease in activity. In the case of flavocytochrome b_2, the k_{cat} and k_{cat}/K_m values of the mutant

enzyme have been reported to be 8000- and 3500-fold lower than the wild-type values (*16*). Because the K_m value for lactate only changed 2- to 3-fold in the mutant protein, the low residual activity was attributed to contamination with wild-type enzyme, leading to the conclusion that the mutant enzyme is at least 10,000-fold less active than the wild-type enzyme. In the case of lactate monooxygenase from *Mycobacterium smegmatis*, the H290Q enzyme cannot be reduced by lactate, consistent with a decrease of 7 to 8 orders of magnitude in activity (*14*). Similarly, mutation of H274 in mandelate dehydrogenase from *Pseudomonas putida* to glycine, alanine, or asparagine yields enzyme with no detectable activity, consistent with decreases of at least 100,000-fold (*18*). Decreases in activity of this magnitude would be unexpected for the mechanism of Figure A-3, where the histidine is not involved in a rate-limiting bond cleavage. Although large decreases in the activities of the mutant proteins would be more consistent with a mechanism in which the base removes a proton from carbon in a ratelimiting step, the effects are quite large even for such a role. Consequently, we have re-examined H373Q flavocytochrome b_2, using a combination of kinetic and structural approaches. The results of these analyses are described here.

EXPERIMENTAL PROCEDURES

Materials. Lithium L-lactate and D,L-lactate were from Sigma (St. Louis, MO). Sodium L-[2-^{2}H]-lactate (98%) and deuterium oxide (99.9%) were purchased from Cambridge Isotope Co., (Andover, MA). Hydroxyapatite was from Bio-Rad Laboratories (Hercules, CA).

Enzyme Preparation. Site-directed mutagenesis of H373 to glutamine was performed following the QuikChange protocol (Stratagene) with the primers 5'-GGTGGTTCTATCCAATCAAGGTGGTAGACAATTAGA-3' and 5'-TCTAATTGT-CTACCACCTTGATTGGATAGAACCACC-3'. The H373Q mutation was introduced into the genes for the wild-type enzyme in pET21d and for the flavin domain in $pDSb_2$ (*29*). The expression and purification of the wild-type enzyme and mutant enzymes were as described previously (*19*, *29*). Enzyme concentrations were determined using an ε_{423} value of 183 mM^{-1} cm^{-1} and an ε_{413} value of 129.5 mM^{-1} cm^{-1} for the reduced and oxidized full length enzymes, respectively (*30*), and an ε_{453} value of 11.1 mM^{-1} cm^{-1} for the flavin domain (*31*). Purified enzymes were stored in 100 mM potassium phosphate, 1 mM EDTA, and 20 mM D,L-lactate at pH 7.5, at –70 °C. To remove the lactate used for storage, the day of use an aliquot was precipitated with 70% ammonium sulfate in 100 mM potassium phosphate, 1 mM EDTA at pH 7.5, at 4 °C. The pellet obtained by centrifugation at 15,000*g* for 5 min was resuspended in 100 mM potassium phosphate and 1 mM EDTA at pH 7.5. This procedure was repeated twice. The final enzyme concentration was about 3 μM. This treatment also resulted in oxidation of the cofactors. For stopped-flow experiments, enzyme was passed through a Sephadex G-25 column in

100 mM potassium phosphate and 1 mM EDTA at pH 7.5 to remove the lactate.

Enzyme Assays. Initial rate assays were performed in 100 mM potassium phosphate, 5 mM EDTA, and 1 mM potassium ferricyanide at pH 7.5 and 25 °C, with varied concentrations of L-lactate or L-[2-^{2}H]lactate, following the decrease in absorbance at 420 nm and using an ε_{420} value for ferricyanide of 1.04 mM^{-1} cm^{-1}. For the flavin domain, 3 mM potassium ferricyanide was used. Concentrations of lactate were determined by end-point assay with wild-type flavocytochrome b_2. For pH studies, the buffers were 50 mM Bis-Tris at pH 5.5–7.0, 150 mM HEPES at pH 7.0–8.5, and 50 mM ethanolamine at pH 8.5-10.0. All assays were done in the presence of 1 mM potassium ferricyanide at 25 °C. Solvent isotope effects were determined in 100 mM phosphate, 1 mM EDTA at pH 7.5 or pD 8.0, with 1 mM potassium ferricyanide at 25 °C. Assays were initiated by the addition of 5 μL of enzyme in H_2O to a final volume of 1 mL.

Rapid Reaction Kinetics. Rapid reaction kinetic measurements were performed with a Applied Photophysics SX.18MV stopped-flow spectrophotometer. Enzyme in 100 mM potassium phosphate and 1 mM EDTA at pH 7.5 was mixed with an equal volume of the same buffer containing 10 mM lactate at 25 °C. Enzyme reduction was monitored at 438 nm. *Data Analysis*. Kinetic data were analyzed using the programs KaleidaGraph (Adelbeck Software, Reading, PA) and Igor (Wavemetrics, Lake Oswego, OR). Initial rate data were fit to the Michaelis-Menten equation to obtain k_{cat}, $k_{cat}/K_{lactate}$, and $K_{lactate}$ values. Primary deuterium and solvent isotope effects were calculated using eqs A.1–A.3. Equation A.1 describes separate isotope effects on the k_{cat} and $k_{cat}/K_{lactate}$ values; eq A.2 describes an isotope effect on the k_{cat} value only; and eq A.3 describes an isotope

effect on the $k_{cat}/K_{lactate}$ value only. Here, F_i is the fraction of heavy atom substitution in the substrate, E_v is the isotope effect on the k_{cat} value minus 1, and E_{vk} is the isotope effect on the $k_{cat}/K_{lactate}$ value minus 1. Stopped-flow traces were fit to eq A.4, which describes a single-exponential decay: A is the absorbance at time t, A_∞ is the final absorbance, and k is the first-order rate constant.

$$v/e = k_{cat} A/[K_m (1 + F_i(E_{vk})) + A(1 + F_i(E_k))] \quad (A.1)$$

$$v/e = k_{cat} A/[K_m + A(1 + F_i(E_v))] \quad (A.2)$$

$$v/e = k_{cat} A/[K_m(1 + F(E_{vk}) + A] \quad (A.3)$$

$$A_t = A_\infty + Ae^{-kt} \quad (A.4)$$

Crystallization. Initial crystallization of H373Q flavocytochrome b_2 (7 mg mL^{-1} plus 50 mM pyruvate) was carried out at 18 °C by vapor diffusion with the hanging drop method (*32*) using a sparse matrix kit (Crystal Screen I and II, Hampton Research, CA). Well-diffracting crystals were obtained in 4–8 days at 18 °C from 4 μL hanging drops consisting of a 1:1 mixture of H373Q flavocytochrome b_2 and a crystallization buffer containing 100 mM sodium citrate at pH 4.6, 17% polyethylene glycol 3000, and 0.2 mM sucrose monolaurate.

Data Collection. Crystals mounted in cryo loops were flash-cooled in a N_2 stream (120 K) after brief soaks in 2 µL of the mother liquor plus 2 μL of 50% glycerol. The data from the H373Q crystals were recorded on Advanced Photon Source beam line 23ID using a CCD detector. The diffraction data were reduced using DENZO, and intensities were scaled with SCALEPACK (*33*). The reflections were indexed as primitive tetragonal ($a = b$ = 163.68 Å, c = 112.01 Å) with Laue symmetry 3m1.

Examination of the integrated and scaled data indicated the trigonal space group $P3_221$. Solvent content calculations (*34*) indicated the presence of the homodimer in the asymmetric unit. The crystallographic data collection, statistics and refinement parameters are summarized in Table A-1.

Table A-1: Data Collection and Refinement Statistics for H373Q Flavocytochrome b_2	
Data collection	
resolution, Å	2.80 to 30.00
total no. of reflections	69,254
no. of unique reflections	36,191
completeness	88%
$I/[(I)]$	14.5
$I/[(I)]$ in outer shell	1.9
R merge	0.26%
refinement	
R-factor	0.21
R-free	0.27
number of protein atoms	7,077
number of water molecules	18
rmsd from ideal values	
bond lengths (Å)	0.005
bond angels (deg)	2.02
Ramachandran analysis	
most favored (%)	74%
additionally allowed (%)	24.3%

Structure Determination and Refinement. The three-dimensional structure of H373Q flavocytochrome b_2 complexed with pyruvate was solved by molecular replacement using EPMR (*35*) with the wild-type structure file 1FCB as the search model for the data extending from 25 to 3.5 Å. After model building and fitting, bias minimized electron density maps were obtained using the Shake and Warp protocol (*36*). The

refinement continued with structure factors measuring 1.0 sigma or better within the resolution range 30 to 2.8 Å to reduce the effects of poorly measured reflections. After repeated cycles of refinement and manual model building, water molecules were added to the structure using Xfit (*37*). The final model consists of two protein molecules, subunit A and subunit B. Subunit A contains the ordered heme domain as well as the flavin domain. Subunit B shows no interpretable density for the heme domain; therefore, it has been omitted from the model. In both subunits, no electron density was observed for residues 298–317, suggesting that they are highly disordered.

RESULTS

Kinetic Characterization of H373Q Flavocytochrome b_2. To determine the effects of mutating H373 flavocytochrome b_2 to glutamine, the steady-state kinetic parameters of the mutant protein were determined. The results of these analyses are summarized in Table A-2. Ferricyanide was used as the electron acceptor because lactate oxidation is rate-limiting with this substrate, unlike the situation with cytochrome *c* as substrate (*1*). The mutant protein still has some activity as a lactate dehydrogenase, although there is a substantial decrease in activity compared to that of the wild-type enzyme. With the intact protein, the k_{cat}/K_m value for lactate is 48,000-fold lower than the wild-type value, while the k_{cat} value is 12,000-fold lower. In addition, the K_m values are altered slightly. The K_m value for ferricyanide increases to 0.11 ± 0.01 mM (results not shown) from a reported value of less than 0.1 mM for the wild-type enzyme (*38*). The k_{cat} and $k_{cat}/K_{lactate}$ values for the mutant protein are comparable to those previously

reported by Gaume *et al.* (*16*) with dichlorophenol indophenol as the electron acceptor. The mutation does not significantly affect the K_m value for cytochrome *c*, in that the mutant protein has a K_{cytc} value of 210 ± 42 μM compared to a value of 180 μM for the wild-type enzyme (*1*), but the k_{cat} value of the mutant protein is only one-half as large with cytochrome *c* as the acceptor compared to the value with ferricyanide (results not shown).

The complete reaction catalyzed by flavocytochrome b_2 includes lactate oxidation and electron-transfer steps. To determine if the effects of the mutation were due to a decrease in the rate constants for electron transfer from the flavin to the heme, the mutation was also incorporated into the isolated flavin domain of the enzyme. With this protein, electrons must be transferred directly from the reduced flavin to the exogenous electron acceptor rather than being passed through the bound cytochrome. The kinetic

Table A-2: Steady-state Kinetic Parameters for Wild-type and Mutant Flavocytochrome b_2

Kinetic parameter	Intact protein				Flavin protein			
		H373Q				H373Q		
	Wild-type		eq	χ^2	Wild-type		eq	χ^2
k_{cat}, s^{-1}	372 ± 12	0.031 ± 0.001			200 ± 7	0.057 ± 0.001		
$k_{cat}/K_{lactate}$, $mM^{-1}s^{-1}$	2300 ± 220	0.048 ± 0.003			543 ± 32	0.23 ± 0.02		±
$K_{lactate}$, mM	0.16 ± 0.02	0.65 ± 0.06			0.36 ± 0.03	0.25 ± 0.03		
$^{D}k_{cat}$	2.9 ± 0.1	1.71 ± 0.07	B.1	0.000204	3.7 ± 0.3	1.42 ± 0.08	B.1	0.000152
		1.78 ± 0.05	B.2	0.000208		1.47 ± 0.06	B.2	0.000158
$^{D}(k_{cat}/K_{lactate})$	3.0 ± 0.3	1.16 ± 0.14	B.1		3.5 ± 0.2	1.18 ± 0.25	B.1	
		3.2 ± 0.4	B.3	0.000591		2.80 ± 0.65	B.3	0.000454
$^{D2O}k_{cat}$	1.38 ± 0.07	0.99 ± 0.05	B.1	0.000576	1.18 ± 0.05	nd[b]		
		1.04 ± 0.04	B.2	0.000589				
$^{D2O}(k_{cat}/K_{lactate})$	0.90 ± 0.04	1.21 ± 0.16	B.1		0.44 ± 0.05	nd		
		1.18 ± 0.10	B.2	0.00578				

[a] Data from ref *29*. [b] nd, not determined

parameters for the flavin domain of the mutant protein are slightly higher than those of the intact protein (Table A-2), but the k_{cat} and $k_{cat}/K_{lactate}$ values are still several thousand-fold less than the wild-type values. Thus, the effects of the mutation are primarily in steps for lactate oxidation.

As a more direct measure of the effect of the mutation on the rate constant for lactate oxidation, the mutant enzyme was mixed with 5 mM lactate in the stopped-flow spectrophotometer in the absence of an electron acceptor. The resulting spectral change was monophasic, with the reduction of both the flavin and the heme occurring with the same rate constant of 0.15 ± 0.04 s^{-1}. This is a decrease of 3500-fold from the wild-type value of 520 s^{-1} (*29*). Comparable results were obtained for the isolated flavin domain, with a rate constant for reduction by 5 mM lactate of 0.09 ± 0.02 s^{-1}. Thus, the effect of the mutation can be attributed to a substantial decrease in the rate constant for flavin reduction. The simultaneous reduction of both cofactors in the intact mutant protein is consistent with electron transfer from reduced flavin to heme being much more rapid than the reduction of the flavin by lactate.

With wild-type flavocytochrome b_2, there is no solvent isotope effect on lactate oxidation, but there is a significant primary deuterium isotope effect (*29*). This is consistent with the rapid and reversible removal of the hydroxyl proton followed by much slower cleavage of the carbon-hydrogen bond of lactate. If the role of H373 is to abstract the hydroxyl proton as shown in Figure A-3, there should be a significant solvent isotope effect in the mutant protein as this step becomes rate-limiting; the magnitude of the primary isotope effect may also be altered, depending on the relative

magnitudes of the rate constants for OH and CH bond cleavage. Consequently, primary and solvent isotope effects were determined for H373Q flavocytochrome b_2. Primary deuterium isotope effects were determined for both the intact mutant protein and for the flavin domain. In both cases, there was a slightly better fit of the data to eq A.1, which applies for significant and nonidentical isotope effects on both the k_{cat} and the $k_{cat}/K_{lactate}$ values, than to either eq A.2, which describes an effect on k_{cat} only, or eq A.3, which describes an effect on $k_{cat}/K_{lactate}$ only. The resulting isotope effects on the k_{cat} values are significantly smaller than the effects seen for the wild-type enzyme but still substantially greater than unity. The primary isotope effect on the $k_{cat}/K_{lactate}$ value is also significantly smaller than the wild-type value. For both the intact protein and the flavin domain, the $^{D}(k_{cat}/K_{lactate})$ value is statistically only marginally greater than unity. However, when the data are analyzed using eq A.2, which applies when there is only an isotope effect on the k_{cat} value, the resulting χ^2 values are slightly larger than is the case with eq A.1.

Prior to measurement of the solvent isotope effects, the pH dependence of the k_{cat} and $k_{cat}/K_{lactate}$ values of the mutant protein were determined. Both kinetic parameters are independent of pH over the pH range 5.5-10 (results not shown). Solvent isotope effects were then determined at pH 7. With wild-type flavocytochrome b_2, there is a small solvent isotope effect on the k_{cat} value due to effects on the oxidative half-reaction and a slightly inverse effect on the $k_{cat}/K_{lactate}$ value, attributed to a conformational change (*29*). In contrast, H373Q flavocytochrome b_2 exhibits no significant solvent isotope effect on the k_{cat} value and a very small normal effect on the $k_{cat}/K_{lactate}$ value (Table A-2). Taken together, the isotope effects suggest that both hydrogen abstraction steps have become

less rate-limiting in the mutant protein.

Structural Characterization of H373Q Flavocytochrome b_2. To obtain further insight into the effects of the mutation on the properties of the enzyme, the crystal structure of H373Q flavocytochrome b_2 was determined at 2.8 Å. The two subunits in the asymmetric unit are not equivalent in the structure of the mutant protein. The electron density map clearly shows the absence of the heme domain in subunit B and the presence of bound pyruvate at the active site of subunit B only (Figure A-4A). This asymmetry is also observed in structures of the wild-type enzyme (*9*, *39*). The mutation of H373 to glutamine does not result in any change in the overall protein structure from that seen for the wild-type enzyme. The mutant protein shows the largest divergence

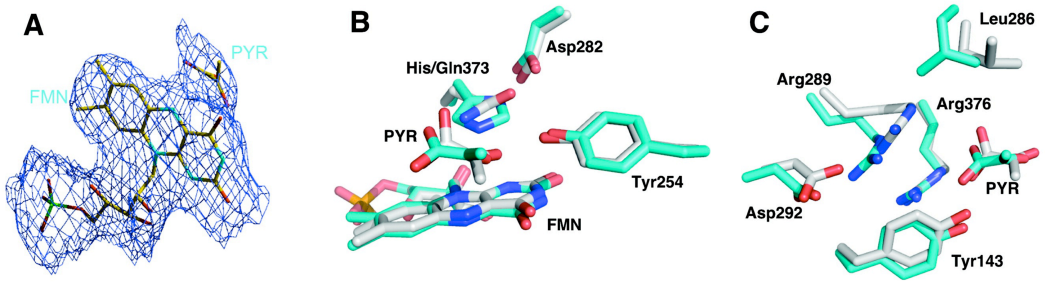

FIGURE A-4: (A) Electron density of ligands complexed with H373Q flavocytochrome b_2. The electron density of Snw omit maps is contoured at the 1σ level. (B and C) Comparison of the active sites of wild-type and H373Q flavocytochrome b_2. The residues and pyruvate (PYR) with carbons in cyan represent the wild-type enzyme structure, whereas the carbon atoms for the mutant structure are in gray. The wild-type enzyme structure is from pdb file 1KBI (*39*).

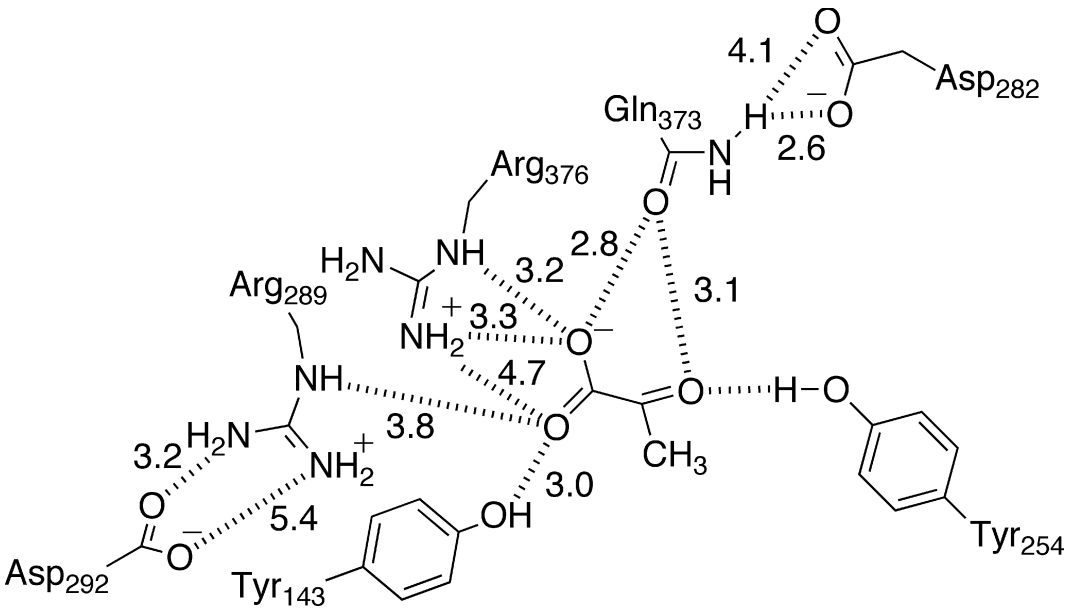

FIGURE A-5: Interactions between active site residues in H373Q flavocytochrome b_2 and pyruvate.

from the wild-type structure for residues 292–298 and 317–324 (rmsd 1.78 and 1.70 Å, respectively), residues adjacent to a surface loop that is not seen in any available structure, and residues 100–114 of subunit B, which connect to the missing heme domain in that subunit.

Figure A-4 compares the active site chain B of H373Q flavocytochrome b_2 with that of the wild-type enzyme, whereas Figure A-5 illustrates the interactions between the active site of the mutant protein and the bound pyruvate. Omit electron density (*36*) maps of the mutant protein show clear electron density for the side chain of Gln373 in the mutant protein. The glutaminyl side chain of the mutant protein overlaps with the

side chain of H373 in the wild-type enzyme (Figure A-4B). However, the heteroatoms of the side chains of the glutamine in the mutant protein are twisted by 90° relative to the imidazole nitrogens in H373, and this results in altered interactions with D282 and pyruvate. In the mutant enzyme, the distance from the glutaminyl side chain to OD1 in D282 is comparable to the distance to the histidinyl side chain in the wild-type protein at 2.6 Å. In contrast, the distance to OD2 in D282 has increased from 3.5 Å in the wild-type enzyme to 4.1 Å in the mutant protein due to the different relative positions of the heteroatoms in the histidinyl and glutaminyl side chains (Figure A-5). In addition, in the wild-type enzyme, the NE2 of H373 is 2.9 Å from the carbonyl oxygen of pyruvate and 3.2 Å from one of the pyruvate carboxylate oxygens; in the mutant enzyme, the corresponding atom of the glutaminyl side chain is closer to the pyruvate carboxylate oxygen (2.8 Å) than the carbonyl (3.1 Å) (Figure A-1). The different positions of the heteroatoms involved in this interaction in the wild-type and mutant proteins shift the pyruvate 0.7 Å relative to its position in the wild-type enzyme. The pyruvate is also twisted in the mutant enzyme relative to its position in the wild-type protein so that the interactions of the carboxylate with R376 and Y143 are altered, even though the positions of these residues are not (Figure A-4C). In the wild-type enzyme, pyruvate CO1 interacts with the NE of R376, while CO2 interacts with R376 NH2 and the phenolic oxygen of Y143 (Figure A-1). The interaction of R376 with Y143 is only slightly longer in the mutant enzyme, but the distance from the pyruvate carboxylate CO2 to R376 has increased from 3.0 to 4.7 Å so that the primary interaction of this oxygen is now with Y143 (Figure A-5).

More dramatic changes are seen in the positions of other active site residues in the mutant protein, most notably R289, L286, and D292 (Figure A-4C). In the wild-type structure, NE of R289 is too far from the pyruvate carboxylate for an electrostatic interaction; in contrast, in the mutant protein, the position of the side chain of R289 has shifted by 2 Å so that NE of R289 is close enough (3.8 Å) to exert some electrostatic influence on the pyruvate carboxylate CO2. This movement of R289 also results in a displacement of the side chain of L286 by over 2 Å. Finally, in the wild-type structure, the guanidinium nitrogens of R289 are at appropriate distances (2.8 and 3.4 Å) from the carboxylate oxygens of D292 for ionic interactions (Figure A-1). In H373Q flavocytochrome b_2, both NH1 and NH2 of R289 are farther from the carboxylate oxygens of D292, 3.4 and 5.4 Å, respectively, so that only one oxygen of D292 is close enough to interact (Figure A-5). As a result, the electropotential surface of the active site is altered so that the acidic charge of D292 is neutralized by R289 in the wild-type enzyme but not in the mutant protein (Figure A-6).

Similar changes are seen in the active site of chain A, although there is no pyruvate in the active site in this case. The glutamine at position 373 occupies the same position as H373 of the wild-type enzyme, as does D282. As is the case in subunit A, the side chains of L286, R289, and D292 are displaced. As a result, the interactions of R289 with both D292 and R376 are also weaker in this subunit.

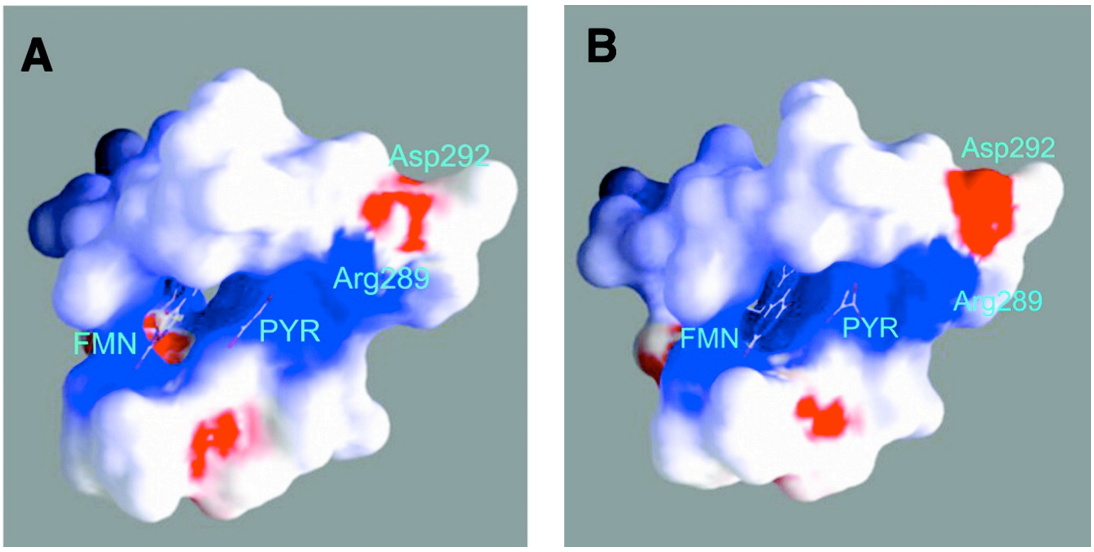

FIGURE A-6: Eletrostatics of the substrate binding pockets of wild-type (A) and H373Q (B) flavocytochrome b_2 (red, -9.8 KT/e; white, neutral; and blue, +3.4 KTe).

DISCUSSION

The effects of the mutation of H373 to glutamine are fully consistent with this residue having an important role in the flavocytochrome b_2 reaction. Both the k_{cat} and $k_{cat}/ K_{lactate}$ values decrease by 3 to 4 orders of magnitude, in line with the expectations for the mutation of an active site base. The steady-state kinetic properties of the intact enzyme with ferricyanide as the electron acceptor agree with a previous study of this mutant by Gaume *et al.* (*16*). However, the additional kinetic data presented here do not support the previous conclusion that the residual activity seen with preparations of the mutant protein is due to small amounts of the wild-type enzyme produced by ribosomal incorporation of histidine at position 373. If that were the case, the isotope effects on the mutant enzyme would be identical to those on the wild-type enzyme, and the rate constant for flavin reduction would not show a similar decrease. Instead, the kinetic parameters in Table A-2 directly reflect the effects of the mutation on the enzyme. The kinetic data establish that mutation of H373 to glutamine primarily alters flavin reduction. The effects of the mutation on the intact protein are mirrored in the effects on the isolated flavin domain, for which the k_{cat} value clearly does not include electron transfer to the heme. Even more explicitly, the decrease of 3,500-fold in the rate constant for flavin reduction measured in single-turnover analyses directly identifies the decrease in this kinetic parameter as the critical effect of the mutation.

Although there has been substantial controversy regarding the mechanism of lactate oxidation by flavocytochrome b_2 and the other flavoprotein hydroxy acid oxidases (*22*, *24*), the mechanism shown in Figure A-3 accommodates the vast majority

of kinetic and structural studies to date. Here, the role of H373 is to abstract the lactate hydroxyl proton prior to hydride transfer; the negative charge that develops on the oxygen is stabilized by Y254. The effects of mutating Y254 to phenylalanine (*19*) provide a benchmark for the expected effects of mutating H373. In the Y254F enzyme, the rate constant for flavin reduction decreases 35-fold. More informatively, in terms of insight into the catalytic details, that mutant enzyme exhibits a primary deuterium isotope effect on k_{cat} of 4.5 and a solvent isotope effect of 1.4, whereas there is no effect of D_2O on flavin reduction in the wild-type enzyme (*19*). These results were previously interpreted as resulting from a change in mechanism in the mutant enzyme to a more synchronous cleavage of the OH and CH bonds, as the loss of the interaction stabilizing the alkoxide results in a delay in OH bond cleavage until hydride transfer is initiated. Mutagenesis of the base responsible for abstracting the lactate hydroxyl proton would be anticipated to qualitatively have the same effect on the reaction, in that loss of the lactate hydroxyl proton would not occur until the decreasing electron density at the α carbon due to transfer of the hydride sufficiently decreased the p*K*a of the oxygen for deprotonation to occur in the absence of the histidine. This synchronous cleavage of the two bonds should be reflected in solvent and primary kinetic isotope effects with values close to those seen with the Y254F enzyme. Indeed, this is the result upon mutagenesis of the histidine in choline oxidase, which abstracts the substrate hydroxyl proton prior to hydride transfer (*40*). However, the isotope effects summarized in Table A-2 do not agree with this prediction. The primary isotope effects on both the intact mutant protein and on the flavin domain are significantly smaller than the wild-type values, whereas the

solvent isotope effects are very close to unity.

The isotope effects suggest that the greatest effect of the mutation is not on a bond cleavage step. The structure of the mutant enzyme provides an explanation for the altered activity. Although the glutamine occupies the same space in the mutant protein that the histidine does in the wild-type enzyme, the mutation has significant effects on the active site structure. The binding of pyruvate is altered in the mutant protein, suggesting that the binding of the substrate lactate is also altered. The mutation results in a change in the interaction between D282 and the glutamine at position 373 that is propagated down the polypeptide backbone such that several active site residues have altered positions in the mutant protein. Of the residues showing altered positions in the mutant protein, R289 is probably the most critical. This residue is conserved throughout the family of flavoproteins that oxidize α-hydroxy acids. The side chain of R289 interacts with that of R376, the key residue for binding the carboxylate of the substrate (*21*). The conservative mutation of R289 to lysine has been described previously and provides a measure of the effect on activity that any change in this residue will have. The R289K mutation results in a decrease in the k_{cat} value of about 30-fold and a decrease in the $k_{cat}/K_{lactate}$ value of about 90-fold. On the basis of the structure of the mutant, the decrease in activity in the mutant protein was attributed to altered electrostatic interactions in the active site (*21*). The H373Q enzyme described here also shows altered electrostatics in the active site (Figure A-6).

A straightforward explanation activity of the H373Q enzyme is that there are two contributions to the decrease in activity. The mutation of the activity site base that

removes the hydroxyl proton would be expected to decrease the rate constant for lactate oxidation by 1 to 2 orders of magnitude, on the basis of the properties of the Y254F enzyme. The altered binding of the substrate and the altered electrostatics in the active site result in a further decrease in activity. However, the kinetic data are not compatible with the minimal model in which these changes simply result in a decreased rate constant for lactate oxidation. In such a case, this step would become rate-limiting, resulting in expression of the intrinsic isotope effects for CH and OH bond cleavage. Instead, the primary and solvent isotope effects are much smaller than those seen with the Y254F enzyme. The data can be explained by a model in which the binding mode seen in the structure is not the reactive form. Instead, the substrate binds to this unreactive form, and a conformational change is required to yield a reactive conformation. This introduces an internal commitment that suppresses the isotope effect. The rate constant for the reversal of the conformational change must be at least 10-fold faster than CH bond cleavage to decrease the $^{D}(k_{cat}/K_{m})$ from the intrinsic value of 5 to the observed value. Similarly, the forward rate constant for the conformational change must be about 7-fold slower than CH bond cleavage to reduce the $^{D}k_{cat}$ value of the flavin domain to 1.5. H373Q flavocytochrome b_2 thus provides an example of a mutation in which the structural effects of the mutation on catalysis are comparable to the effects on chemical steps. This observation raises the possibility that the larger effects of mutating this residue in other members of this family of flavoproteins are due primarily to structural perturbations.

REFERENCES

1. Lederer, F. (1991) Flavocytochrome b_2, in *Chemistry and Biochemistry of Flavoenzymes* (Muller, F., Ed.) Vol. II, pp 153-242, CRC Press, Boca Raton, FL.
2. Urban, P., Chirat, I., and Lederer, F. (1988) Rat kidney L-2-hydroxyacid oxidase. Structural and mechanistic comparison with flavocytochrome b_2 from Baker's yeast, *Biochemistry 27*, 7365-7371.
3. Tsou, A. Y., Ransom, S. C., Gerlt, J. A., Buechter, D. D., Babbitt, P. C., and Kenyon, G. L. (1990) Mandelate pathway of *Pseudomonas putida*: Sequence relationships involving mandelate racemase, (*S*)-mandelate dehydrogenase, and benzoylformate decarboxylase and expression of benzoylformate decarboxylase in *Escherichia coli, Biochemistry 29*, 9856-9862.
4. Ghisla, S., and Massey, V. (1991) L-Lactate Oxidase, in *Chemistry and Biochemistry of Flavoenzymes, Vol. II* (Muller, F., Ed.) pp 243-289, CRC Press, Boca Raton.
5. Giegel, D. A., Williams, C. H., Jr., and Massey, V. (1990) L-Lactate 2-monooxygenase from *Mycobacterium smegmatis*. Cloning, nucleotide sequence, and primary structure homology within an enzyme family, *J. Biol. Chem. 265*, 6626-6632.
6. Lindqvist, Y., Brändén, C.-I., Mathews, R., and Lederer, F. (1991) Spinach glycolate oxidase and yeast flavocytochrome b_2 are structurally homologous and evolutionarily related enzymes with distinctly different function and flavin

mononucleotide binding, *J. Biol. Chem. 266*, 3198-3207.

7. Maeda-Yorita, K., Aki, K., Sagai, H., Misaki, H., and Massey, V. (1995) L-Lactate oxidase and L-lactate monooxygenase: mechanistic variations on a common structural theme, *Biochimie 77*, 631-642.

8. Cunane, L. M., Barton, J. D., Chen, Z. W., Le, K. H., Amar, D., Lederer, F., and Mathews, F. S. (2005) Crystal structure analysis of recombinant rat kidney long chain hydroxy acid oxidase, *Biochemistry 44*, 1521-1531.

9. Xia, Z.-X., and Mathews, F. S. (1990) Molecular structure of flavocytochrome b_2 at 2.4 Å resolution, *J. Mol. Biol. 212*, 837-863.

10. Balme, A., Brunt, C. E., Pallister, R. L., Chapman, S. K., and Reid, G. A. (1995) Isolation and characterization of the flavinbinding domain of flavocytochrome b_2 expressed independently in *Escherichia coli*, *Biochem. J. 309*, 601-605.

11. Reid, G. A., White, S., Black, M. T., Lederer, F., Mathews, F. S., and Chapman, S. K. (1988) Probing the active site of flavocytochrome b_2 by site-directed mutagenesis, *Eur. J. Biochem. 178*, 329-333.

12. Macheroux, P., Kieweg, V., Massey, V., Soderlind, E., Stenberg, K., and Lindqvist, Y. (1993) Role of tyrosine 129 in the active site of spinach glycolate oxidase, *Eur. J. Biochem. 213*, 1047-1054.

13. Rouviere-Fourmy, N., Capeillere-Blandin, C., and Lederer, F. (1994) Role of tyrosine 143 in lactate dehydrogenation by flavocytochrome b_2. Primary kinetic isotope effect studies with a phenylalanine mutant, *Biochemistry 33*, 798-806.

14. Müh, U., Williams, C. H., Jr., and Massey, V. (1994) Lactate monooxygenase II.

Site-directed mutagenesis of the postulated active site base histidine 290, *J. Biol. Chem. 269*, 7989-7993.

15. Müh, U., Williams, C. H., Jr., and Massey, V. (1994) Lactate monooxygenase III. Additive contributions of active site residues to catalytic efficiency and stabilization of an anionic transition state, *J. Biol. Chem. 269*, 7994-8000.

16. Gaume, B., Sharp, R. E., Manson, F. D. C., Chapman, S. K., Reid, G. A., and Lederer, F. (1995) Mutation to glutamine of histidine 373, the catalytic base of flavocytochrome b_2 (L-lactate dehydrogenase), *Biochimie 77*, 621-630.

17. Lehoux, I. E., and Mitra, B. (2000) Role of arginine 277 in (*S*)-mandelate dehydrogenase from *Pseudomonas putida* in substrate binding and transition state stabilization, *Biochemistry 39*, 10055-10065.

18. Lehoux, I. E., and Mitra, B. (1999) (*S*)-Mandelate dehydrogenase from *Pseudomonas putida*: Mutation of the catalytic base histidine-274 and chemical rescue of activity, *Biochemistry 38*, 9948-9955.

19. Sobrado, P., and Fitzpatrick, P. F. (2003) Solvent and primary deuterium isotope effects show that lactate CH and OH bond cleavages are concerted in Y254F flavocytochrome b_2, consistent with a hydride transfer mechanism, *Biochemistry 42*, 15208-15214.

20. Sanders, S. A., Williams, C. H., Jr., and Massey, V. (1999) The roles of two amino acid residues in the active site of L-lactate monooxygenase, *J. Biol. Chem. 274*, 22289-22295.

21. Mowat, C. G., Beaudoin, I., Durley, R. C. E., Barton, J. D., Pike, A. D., Chen,

Z.-W., Reid, G. A., Chapman, S. K., Mathews, F. S., and Lederer, F. (2000) Kinetic and crystallographic studies on the active site Arg289Lys mutant of flavocytochrome b_2 (yeast L-lactate dehydrogenase), *Biochemistry 39*, 3266-3275.

22. Lederer, F. (1996) The Mechanism of Flavoprotein-Catalyzed Alpha-hydroxy Acid Dehydrogenation, Revisited, in *Flavins and Flavoproteins 1996* (Stevenson, K. J., Massey, V., and Williams, C. H., Eds.) pp 545-553, University of Calgary Press, Alberta Canada.

23. Fitzpatrick, P. F. (2001) Substrate dehydrogenation by flavoproteins, *Acc. Chem. Res. 34*, 299-307.

24. Fitzpatrick, P. F. (2004) Carbanion versus hydride transfer mechanisms in flavoprotein-catalyzed dehydrogenations, *Bioorg. Chem. 32*, 125-139.

25. Kurtz, K. A., Rishavy, M. A., Cleland, W. W., and Fitzpatrick, P. F. (2000) Nitrogen isotope effects as probes of the mechanism of D-amino acid oxidase, *J. Am. Chem. Soc. 122*, 12896-12897.

26. Ralph, E. C., Anderson, M. A., Cleland, W. W., and Fitzpatrick, P. F. (2006) Mechanistic studies of the flavoenzyme tryptophan 2-monooxygenase: deuterium and 15N kinetic isotope effects on alanine oxidation by an L-amino acid oxidase, *Biochemistry 45*, 15844-15852.

27. Ralph, E. C., and Fitzpatrick, P. F. (2005) pH and kinetic isotope effects on sarcosine oxidation by N-methyltryptophan oxidase, *Biochemistry 44*, 3074-3081.

28. Dubois, J., Chapman, S. K., Mathews, F. S., Reid, G. A., and Lederer, F. (1990) Substitution of Tyr254 with Phe at the active site of flavocytochrome b_2: consequences on catalysis of lactate dehydrogenation, *Biochemistry 29*, 6393-6400.

29. Sobrado, P., Daubner, S. C., and Fitzpatrick, P. F. (2001) Probing the relative timing of hydrogen abstraction steps in the flavocytochrome b_2 reaction with primary and solvent deuterium isotope effects and mutant enzymes, *Biochemistry 40*, 994-1001.

30. Labeyrie, F., Baudras, A., and Lederer, F. (1978) Flavocytochrome b_2 or L-lactate cytochrome c reductase from yeast, *Methods Enzymol. 53*, 238-256.

31. Iwatsubo, I., Mevel-Ninio, M., and Labeyrie, F. (1977) Rapid kinetic studies of partial reactions in the heme free derivative of L-lactate cytochrome c oxidoreductase (flavocytochrome b_2); the flavodehydrogenase function, *Biochemistry 16*, 3558-3566.

32. McPherson, A. (1982) *Preparation and Analysis of Protein Crystals*, John Wiley, New York.

33. Otwinowski, Z., and Minor, W. (1997) Processing of X-ray diffraction data collected in oscillation mode, *Methods Enzymol. 276*, 307-326.

34. Matthews, B. W. (1968) Solvent content of protein crystals, *J. Mol. Biol. 33*, 491-497.

35. Kissinger, C. R., Gehlhaar, D. K., and Fogel, D. B. (1999) Rapid automated molecular replacement by evolutionary search, *Acta Crystallogr., Sect. D 55*,

484-491.

36. Kantardjieff, K. A., Hochtl, P., Segelke, B. W., Tao, F. M., and Rupp, B. (2002) Concanavalin A in a dimeric crystal form: revisiting structural accuracy and molecular flexibility, *Acta Crystallogr., Sect. D 58*, 735-743.

37. McRee, D. E. (1999) XtalView/Xfit-A versatile program for manipulating atomic coordinates and electron density, *J. Struct. Biol. 125*, 156-165.

38. Miles, C. S., Rouviere-Fourmy, N., Lederer, F., Mathews, F. S., Reid, G. A., Black, M. T., and Chapman, S. K. (1992) Tyr-143 facilitates interdomain electron transfer in flavocytochrome b_2, *Biochem. J. 285*, 187-192.

39. Cunane, L. M., Barton, J. D., Chen, Z. W., Welsh, F. E., Chapman, S. K., Reid, G. A., and Mathews, F. S. (2002) Crystallographic study of the recombinant flavin-binding domain of baker's yeast flavocytochrome b_2: comparison with the intact wild-type enzyme, *Biochemistry 41*, 4264-4272.

40. Ghanem, M., and Gadda, G. (2005) On the catalytic role of the conserved active site residue His466 of choline oxidase, *Biochemistry 44*, 893-904.

VITA

Name: Chi-Lin Tsai

Address: 301 Old Main Dr., ILSB Rm. 1196
College Station, TX 77843

Department of Chemistry
M.S. 3255
c/o Dr. David Barondeau

Email Address: cltsai70@yahoo.com.tw

Education: B.S., Chemistry, National Chung Hsing University, 1998
M.S., Chemistry, National Taiwan University, 2000
Ph.D., Chemistry, Texas A&M University, 2011